



Durham E-Theses

Characterisation of a hyperbranched polyesterin solution

Luca, Edoardo De

How to cite:

Luca, Edoardo De (2001) *Characterisation of a hyperbranched polyesterin solution*, Durham theses, Durham University. Available at Durham E-Theses Online: <http://etheses.dur.ac.uk/4273/>

Use policy

The full-text may be used and/or reproduced, and given to third parties in any format or medium, without prior permission or charge, for personal research or study, educational, or not-for-profit purposes provided that:

- a full bibliographic reference is made to the original source
- a [link](#) is made to the metadata record in Durham E-Theses
- the full-text is not changed in any way

The full-text must not be sold in any format or medium without the formal permission of the copyright holders.

Please consult the [full Durham E-Theses policy](#) for further details.

Characterisation of a hyperbranched polyester in solution

Edoardo De Luca

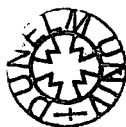
The copyright of this thesis rests with the author. No quotation from it should be published in any form, including Electronic and the Internet, without the author's prior written consent. All information derived from this thesis must be acknowledged appropriately.

A thesis submitted to the university of Durham in partial fulfilment of the regulations
for the degree of Doctor in Philosophy

University of Durham

Department of Chemistry

2001



22 MAR 2002

Contents

<i>Declaration</i>	iii
<i>Statement of copyright</i>	iii
<i>Acknowledgements</i>	iv
<i>Abstract</i>	v
<i>Chapter 1: Introduction</i>	1
1.1 Aim and objectives	6
References	6
<i>Chapter 2: Theory and basis of methods used</i>	7
2.1 Branching in polyesters	7
2.2 Dendrimers and hyperbranched polymers	13
2.3 Thermodynamics of polymer solutions	18
2.4 Size exclusion chromatography	23
2.5 NMR and branching	25
2.6 Viscometry	29
2.7 Light scattering	36
2.7.1 Static light scattering	36
2.7.2 Dynamic light scattering	43
2.8 Small angle neutron scattering	46
References	53
<i>Chapter 3: Experimental results</i>	54
3.1 Materials	54
3.2 Syntheses	55
3.3 Fractionation	63
3.4 SEC data	66
3.5 Degree of branching	74
3.6 Viscometry data	78
3.7 Static light scattering data	81

3.8 Dynamic light scattering data	87
3.9 SANS data	92
References	98
<i>Chapter 4: Analysis and discussion</i>	99
4.1 Dilute solutions	99
References	140
4.2 Semi-dilute solutions	141
References	169
<i>Chapter 5: Conclusions and future work</i>	170
References	175
<i>Glossary of symbols</i>	176
<i>Appendices</i>	179
Appendix A. NMR, IR, MS spectra for methyl 3-(4-acetoxybutoxy) benzoate	179
Appendix B. NMR, IR, MS spectra for methyl 3-(4-hydroxybutoxy) benzoate	182
Appendix C. Dynamic light scattering data	185
Appendix SANS	188

Declaration

The work reported in this thesis has been carried out at Durham site of the Interdisciplinary Research Centre in Polymer Science and Technology. The small-angle neutron scattering experiments have been carried out at the Rutherford Appleton Laboratory, Chilton, Oxon and the Institut Laue Langevin, Grenoble, France.

This work has not been submitted for any other degree either in Durham or elsewhere and is the original work of the author except where otherwise stated.

Statement of copyright

The copyright of this thesis rest with the author. No quotation from it should be published without his prior written consent and information derived from it should be acknowledged.

Acknowledgments

I would like to acknowledge the IRC and EPSRC, which funded this project and also provided for my living maintenance. In particular, I would like to thank Professor Randal Richards for his constant and continuous supervision and Professor Jim Feast for his support in synthetic work.

I would also like to remember in my acknowledgments Steve King, Richard Heenan and Isabel Grillo for the SANS experiments in the Rutherford Appleton Laboratory and Institut Laue Langevin; Lian Hutchings and Douglas Carswell for the SEC and thermal analysis and Alan Kenwright for the NMR characterisation.

A huge thank you to the people working in the Chemistry Department of Durham University for their big effort in making my work easier and to my colleagues and friends who have, in these three years, shared with me the exciting and discouraging aspects of research in polymer science, which is still one of the most amazing toys in my life.

Abstract

The hyperbranched polyester based on poly dimethyl 5-(4 hydroxybutoxy) isophthalate has been successfully fractionated and a complete analysis of the solution properties has been carried out. Fractions with an average polydispersity of 1.8 over a range of molecular weight from $5 \times 10^3 \text{ g mol}^{-1}$ to $4 \times 10^5 \text{ g mol}^{-1}$ were produced starting from an initial polymer with an approximate polydispersity of 7 and average molecular weight of $1.3 \times 10^5 \text{ g mol}^{-1}$.

A linear analogue of the hyperbranched polyester has been also synthesised and different molecular weight samples were obtained by the use of a transesterification reaction.

The hyperbranched fractions were investigated in the dilute regime by size exclusion chromatography, viscometry and light scattering techniques, while the semi-dilute regime has been studied by small-angle neutron scattering. Dilute solution properties in chloroform and in THF have been investigated, whilst D-THF was the solvent for the semi-dilute regime. In the dilute solution regime a whole range of physical parameters have been determined for the hyperbranched fractions and compared, where possible, with the linear analogues. From these results it is concluded that chloroform is a good solvent and THF a poor solvent for the hyperbranched polyester.

The molar mass dependence of the radii of gyration has been interpreted by fractal dimension analysis and for the hyperbranched polyester the exponents obtained gave a fractal dimension $d_f = 2.5 \pm 0.3$ in both the solvents.

The exponents obtained by the molar mass dependence of the radius of gyration in the semi-dilute regime have confirmed these values. These exponents also fit with those obtained from analysis of the intermediate Q -range of the small-angle neutron scattering cross sections, where an average slope 2.5 ± 0.1 was obtained. The values suggested the hyperbranched polymer is a mass fractal object with a rough surface.

Chapter 1

Introduction

In recent years there has been significant interest in highly branched polymer species and in the unusual characteristics that arise in these materials as a consequence of their novel topologies and molecular structures.

The different possibilities of molecular branching in polymers can lead to very complex structure, in fact any unit on a linear chain can be, in theory, replaced with a branched point from where another chain can grow and branch at a more or less defined position. For a better understanding of the effect of branching it is useful to begin the examination of these polymer structures with simple models and continue to more complex shapes¹. The comprehension of regular structures seems to be much easier, however, their chemical realisation has given great difficulties. This approach does not represent the historical development, in fact, the study of branched polymers started with the random polycondensation of f -functional monomer units that represent a very complex system. The simplest structure is that of f linear chains of exactly the same length attached to an f -functional central unit² (Figure 1(1.1)).

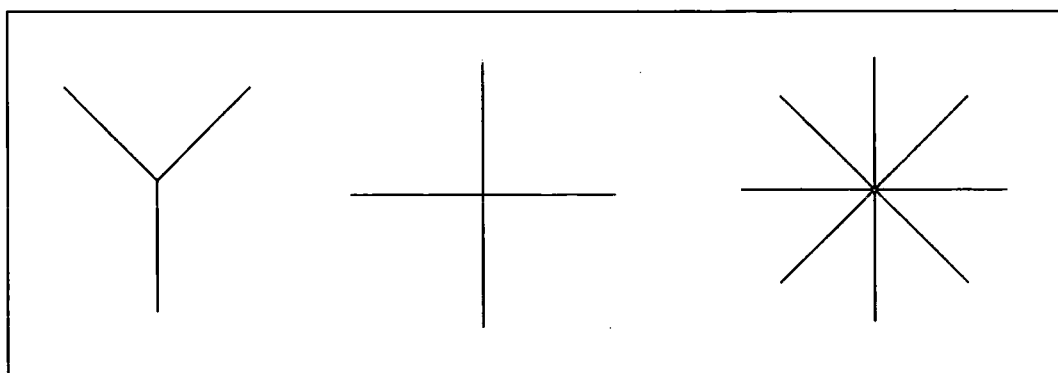
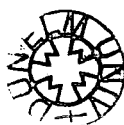


Figure 1(1.1). Schematic structure of star polymers.

In this model the f linear chains, consisting of m repeating units, become the rays of a star molecule and can be considered like stiff or flexible rods and described in a first approximation by the Gaussian chain statistics. A star polymer has only one branching unit among the $f \times m$ units, which belong to the linear chains.



The next higher complexity structures are obtained with flexible regular comb molecules (Figure 2(1.1)). They consist of a linear flexible chain of defined length and f flexible side chains of uniform length which are grafted at a regular distances onto the main chain.

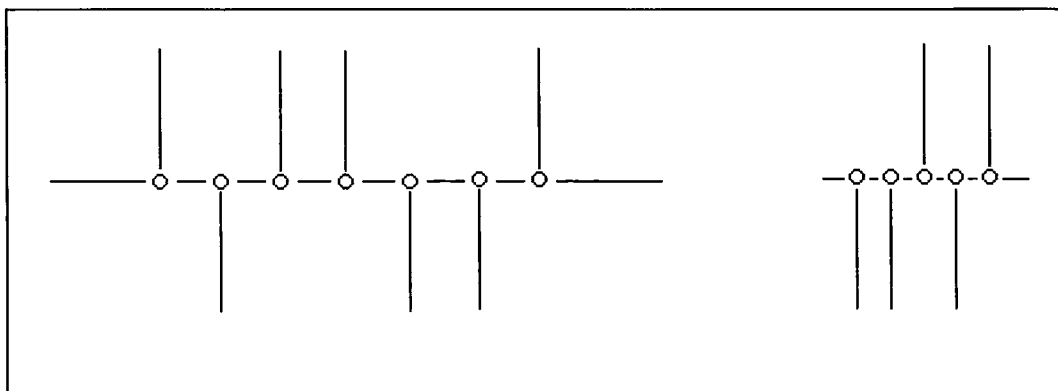


Figure 2(1.1). *Schematic structure of comb polymers.*

The comb like structure resembles a linear chain when the side chains are much shorter than the backbone chain and will approach the structure of star molecules if it has a short backbone compared to the side chains. The chemical realisation of a complete regular comb is rarely possible and imperfections in the side chains spacing are often the result of the synthesis.

Increasing the complexity of the structure, the next group to be considered is dendrimers. They can be represented, in a generalised form, by terminating each ray of a star molecule with a f -functional branched unit from which rays of the same length can emanate³(Figure 3(1.1)). A next generation is possible when other branched units terminate these rays and further branching can originate. This model reduces to dendrimers, in the strict sense, when no spacer chains between the branching units are present. In recent years the chemistry of preparing dendrimers has become very successful although time consuming, but because of space filling effect it has not been possible to prepare more than 5 generations and the reaction to higher generations stops completely or the outermost shells develop imperfections.

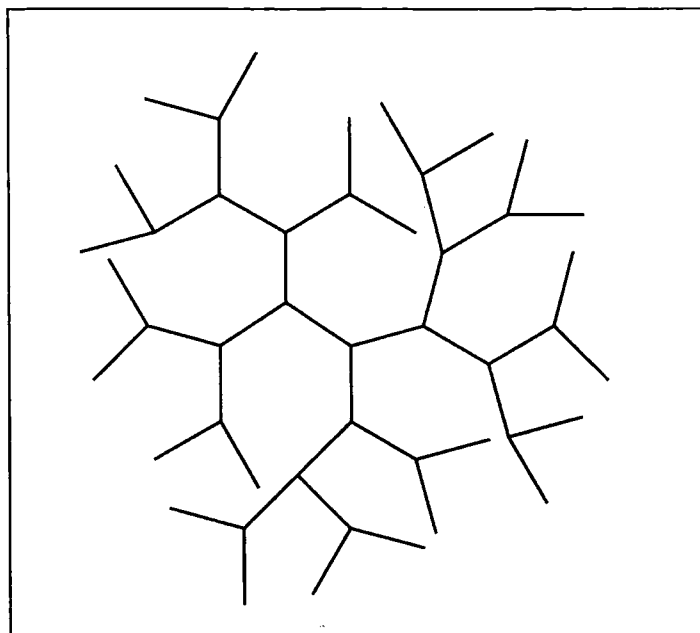


Figure 3(1.1). *Schematic picture of a dendrimer.*

In some polymerisations the achievement of regularity in the structure is not particularly important and, as in the case of A_f monomer units, they are mixed in the reaction vessel giving a randomly branched polymer. In these systems all functional groups have the same reactivity independent of whether they are connected to a monomer or to macromolecular species. Such fully random systems can be adequately treated analytically by theories of random statistics and rooted tree models, where every branching point represents a generation (Figure 4(1.1)). For these particular polymerisations Flory⁴ predicted a critical point where gelation takes place and proposed the first statistical treatment of the random branching.

The most relevant characteristic of the randomly branched systems is the effect of the finite volume of the monomer units limiting the distance between the polymer segments and excluding a certain volume to other repeating units. The excluded volume also causes a change in the expected topological architecture because in a densely branched system the reaction of various functional groups on a monomer will be influenced by the position of the f -functions that have already reacted.

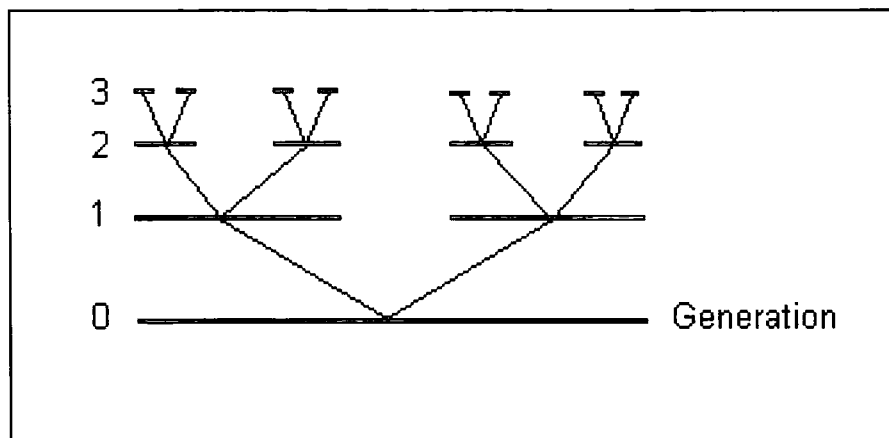


Figure 4 (1.1). *Schematic structure of rooted tree.*

Hyperbranched systems are a special group of branched structure that can be described by statistical models. This situation occurs when a monomer has two types of functional groups, A and B where the A group can only react with one of the $(f-1)$ B groups of another monomer unit (Figure 5(1.1)). This chemical constraint reduces the number of possible reactions considerably and consequently leads to a much narrower molar mass distribution compared to the randomly branched systems.

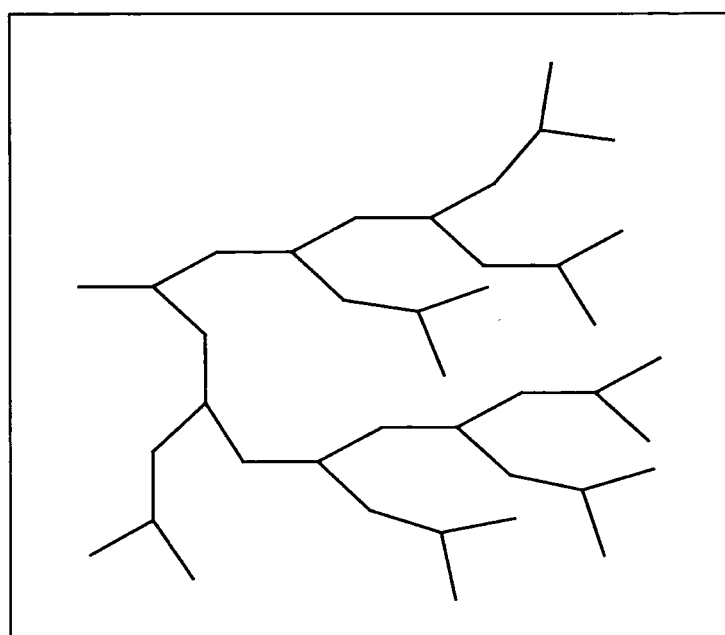


Figure 5(1.1). *Schematic structure of hyperbranched polymer.*

The extent of reaction, α , of the A-group can cover all values from zero to unity, but the extent of reaction of the equally reactive B-group cannot be larger than $\alpha/(f-1)$. As a consequence, gelation can never occur and a higher branching density compared to random polycondensation can be achieved.

Because of their more compact structure, branched polymers always have smaller dimensions than a linear macromolecule of the same molecular weight. The pervaded space and not the molar mass of the macromolecule determines the properties in solution as well as in the condensed state and this relation becomes more complex in the case of branched macromolecules, a linear and a branched macromolecule of the same molar mass have different hydrodynamic volumes. The effect of branching is to increase the segment density within the molecular coil and thus a branched molecule occupies a smaller volume and has a lower intrinsic viscosity than a linear analogue. Another characteristic feature of branched polymers is the broad molecular weight distribution that strongly influences the polymer behaviour in solution.

A significant effort has been invested in determining the size and shape of branched polymers in solution and comparing with those of analogous linear chains because hypotheses about molecular structure can be made from such comparison.

In most cases, polymerisation processes are conducted either in the melt or in fairly concentrated solution and under such conditions a complex interplay between the structure of the individual macromolecules and the intermolecular interactions take place. To disentangle this complexity it is helpful to derive a precise picture of the structure and behaviour of individual macromolecules by investigation of solutions in the dilute regime where intermolecular interactions have a very weak effect. Once the dilute solution characteristics are known, the data can be used to give scaling parameters for the description of more concentrated regimes.

1.1 Aim and objectives

Hyperbranched polymers are a relatively new class of branched macromolecules and because of their highly branched structure they have potential applications in many technological fields like coating, paints, medicine and agro-chemistry.

Hyperbranched and dendritic systems represent a continuing field of investigation in the IRC laboratories and a project on the synthesis and properties of series of AB₂ monomer based on dimethyl 5-(n-hydroxyalkoxy) isophthalates is in progress. Poly dimethyl 5-(4 hydroxybutoxy) isophthalate hyperbranched polyester is the polymer of interest in the research reported here. It is generally believed that the important properties that characterise these types of polymers are their high branching density, the large number of terminal groups and the globular structure. Under these assumptions, the intrinsic large molecular weight polydispersity of the hyperbranched polymer is not a real problem for some applications, but for many others the possibility of having narrower molecular weight distribution could open new fields of research. Therefore, obtaining fractions with narrower polydispersity was a first objective and the solution fractionation was the procedure settled to reach this aim.

In all the processes in which a solubilisation procedure is involved, knowledge of the polymer behaviour in solution is of fundamental importance and the solution characterisation of hyperbranched fractions using modern techniques was another important objective.

The classical method of comparison with a linear polymer analogue has been used and the different samples have been characterised by a combination of size exclusion chromatography, viscometry, static and dynamic light scattering and small-angle neutron scattering. The final goal is to describe and promote a predictive capability of the polymer behaviour in solution with the possibility of some insight into bulk behaviour.

References

1. Burchard, W., *Adv. Polym. Sci.* 1999. **143**: p. 113.
2. Huang, J., N. Hadjichristidis, and M. Lin, *Macromolecules*, 1994. **27**: p. 3821.
3. Frechet, J., *Science*, 1994. **263**: p. 1710.
4. Flory, P., *Principles of polymer chemistry*. 1953: Cornell University Press, Ithaca, NY.

Chapter 2

Theory and basis of methods used

2.1 Branching in polyesters

Polyesters are macromolecular materials characterised by the presence of carboxylate ester groups in the repeating units of the main chain. The rational study of polyesters dates from 1920s with Kienle's investigations¹, which led to the development of alkyd resin technology, and later with the research of Carothers² the basis of the step-polymerisation chemistry and the relationship between molar mass and polymer properties. The properties of linear polyesters are determined by the amount of carboxylate ester group in their structure and by the geometry, polarity, segmental mobility of their repeating units and since their intermolecular interactions are not particularly strong, polyester properties are more sensitive to the structure variations.

If a multifunctional monomer is introduced in the reaction mixture the opportunity of branching has to be taken into account and the characteristic properties of the related polymer will be strongly different from the analogous linear chain.

The presence of polyfunctional units introduces the possibility of forming structures with macroscopic dimensions termed infinite networks. Since solvent cannot disperse these essentially infinite sized molecules, their production in the course of a solution polymerisation is physically evident as the appearance of a solvent swollen highly viscous gel. The first appearance of gel as the polymerisation proceeds is called the gel point. To understand their possible structure and configuration Flory³ developed the first statistical approach to the problem of the branching in polycondensation and following his treatment, it is convenient to define a branching coefficient, α_b , that represents the probability that, from a given branch point, a selected chain continues with another branch point rather than terminating in a loose end. In this way, it is possible to trace an indefinitely long path to reach a selected branch point and there are $f-1$ choices for continuing on the path, where f is the branch point functionality. If α_b is the probability of successfully proceeding to the next branch point, then $(f-1)\alpha_b$ is the probability of reaching another branch by any of the $f-1$ available paths. If the

connected series of i monomers for a continuous path is taken into account, the probability that a new branching point will be successfully created is defined as in equation 1(2.1)

$$1(2.1) \quad [(f-1) \cdot \alpha_b]^i$$

Since equation 1(2.1) must be finite as the exponent i increases, consequently the relationship $(f-1) \times \alpha_b \leq 1$ must apply for the formation of very large molecules and gel in the case of equality.

Branched polyester can be synthesised, for example, using a three-functional alcohol like glycerol, therefore, for the statistical treatment of branching, the step polymerisation of a three-functional A_3 monomer with two bi-functional monomers A-A, B-B schematically represented in figure 2(2.1) is first considered.

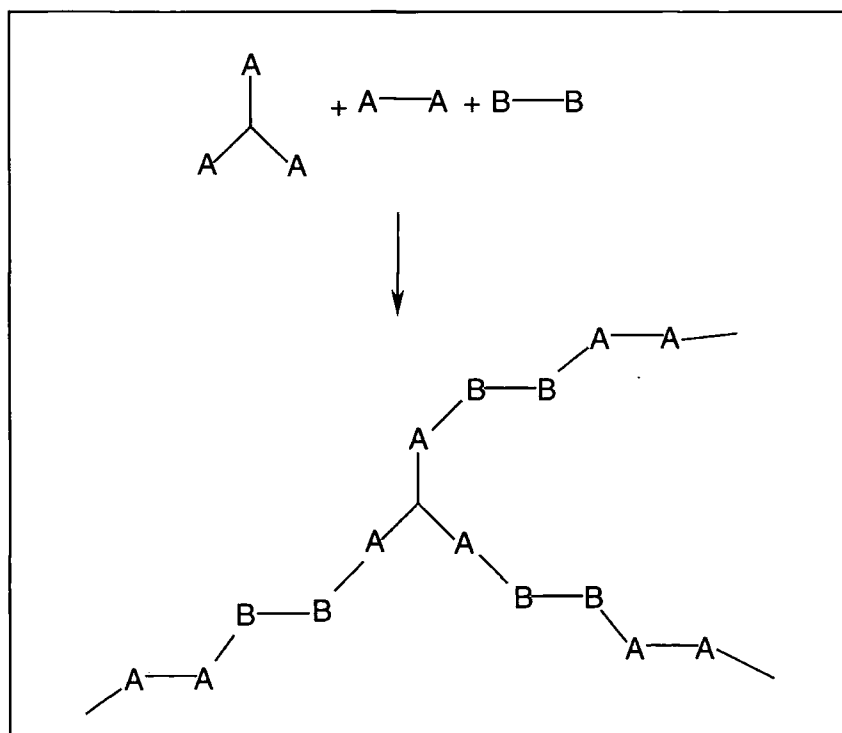


Figure 2(2.1). Schematic reaction of an A_3 unit and two bi-functional units.

C_A is the concentration of A groups, $C_A(0)$ is the initial amount and $r \times C_A(0)$ the initial concentration of A in the tri-functional monomer, whilst $(1-r) \times C_A(0)$ in the bi-

functional monomer, r being the monomer fraction. It is assumed that the all A groups have the same reactivity, the concentration of $r \times C_A$ and $(1-r) \times C_A$ is the same at any time during the polymerisation and there are C_B bi-functional groups, with the initial concentration $C_B(0)$.

The probability P_A and P_B that an A or a B group has reacted respectively is then defined by the equations 2(2.1).

$$2(2.1) \quad \begin{aligned} P_A &= 1 - \frac{C_A}{C_A(0)} \\ P_B &= 1 - \frac{C_B}{C_B(0)} \end{aligned}$$

In general the probability that $n-1$ A-A and n B-B monomers provide a connection between a selected branch point and another branch point can be defined by the equation 3(2.1).

$$3(2.1) \quad [(1-r)P_A P_B]^{n-1} \cdot r P_A P_B$$

The probability α_b that a sequence connects the selected branch point with another one regardless of length is the sum of the single probability as defined in 4(2.1).

$$4(2.1) \quad \alpha_b = \sum_n [(1-r)P_A P_B]^{n-1} \cdot r P_A P_B$$

It is now possible to calculate the number average degree of polymerisation for the system A₃, A-A, B-B considering first the total number of units $N(0)$.

$$5(2.1) \quad N(0) = \frac{rN_A(0)}{f} + \frac{(1-r) \cdot N_A(0)}{2} + \frac{N_B(0)}{2}$$

Where $N_A(0)$ and $N_B(0)$ are the starting number of A and B groups and then defining the total number of chains N as the total number of unit subtracted by the number of bonds formed during the polymerisation.

$$6 (2.1) \quad N = N(0) - N_A(0) \cdot P_A = N(0) - P_B N_B(0)$$

By the equation 5(2.1) and 6(2.1), the number average degree of polymerisation X_N in the case of $f=3$ and $r=1$ is obtained in 7(2.1).

$$7 (2.1) \quad X_N = \frac{N(0)}{N} = \frac{1}{1 - \frac{6 \times P_A}{5}}$$

A special case is presented by the AB_2 monomer polycondensation, where A may react with B but reactions between similar functional group are forbidden. The branched polymers derived from this monomer type occupy an intermediate position between linear polymers and network-forming polyfunctional types as shown in figure 3(2.1). Flory⁴ studied the problem of weight average degree of polymerisation under certain approximations. In this study, the $f-1$ B groups of a unit are considered to be distinguishable from one other but identical in reactivity and intramolecular reactions are neglected. Any given molecular structure may be specified by stipulating which of the B groups of each successive unit have reacted, starting with the one bearing the unreacted A unit. The probability that an unreacted A group joins n -mer of the specified structure is the same that of a particular sequence of $n-1$ B groups have reacted while the $(f n - 2n + 1)$ have not.

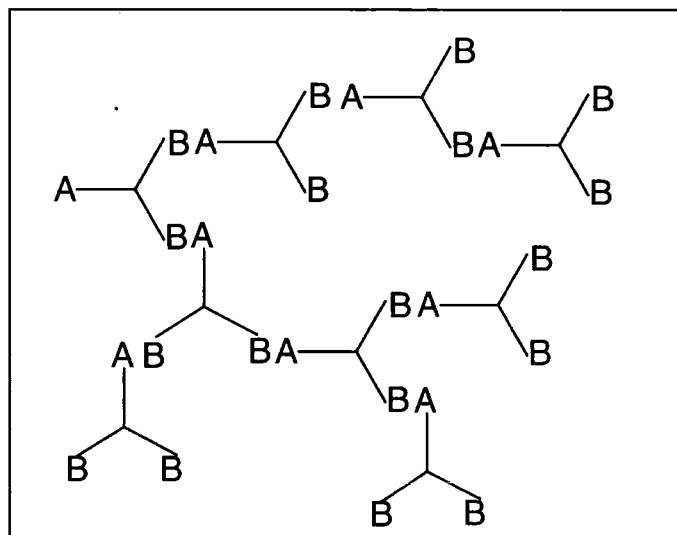


Figure 3(2.1). Schematic picture of AB_2 system.

Under the assumption that B groups are equally reactive, the probability α_b equals P_B , where P_B is the fraction of B groups that have reacted and since the number of A and B groups reacted must be the same, the relationship 8(2.1) applies.

$$8(2.1) \quad P_B(f-1) = P_A$$

Where P_A is the extent of reaction for the A group. The probability α_b in this case is the probability that a given functional group of a branched unit is connected to another branch unit and is define as follows;

$$9(2.1) \quad \alpha_b = \frac{P_A}{(f-1)}$$

The maximum value which α_b may approach is $1/(f-1)$ and corresponds to the critical condition in f -functional system. In this case the degree of polymerisation is that given in equation 10 (2.1).

$$10(2.1) \quad X_N = \frac{1}{(1-P_A)} = \frac{1}{[1-\alpha_b(f-1)]}$$

The classical Flory⁵ approach is based on the structural model of tree-like molecules and the assumption of equal probability of reaction of an unreacted A group with another B group could be a possible limitation. On the other hand, a probability of reaction that varies according to the local environment looks much more realistic. There are two other features of the classical approach that have motivated the investigation of alternative models, the first is the neglect of loops and the second is the neglect of excluded volume effect.

A well-known approach to the modelling of AB_f monomer polymerisation is percolation theory. This model allows the reaction to take place on a lattice and contrary to the classical method, completely analytical statistics are not obtained, but numerical simulations produce approximate results sensitive to the change of the properties in the vicinity of the gel point. As presented by Stauffer⁶ the weight average

degree of polymerisation, which diverges at the gel point, is expressed as function of reaction probability p as in equation 11(2.1).

$$11(2.1) \quad X_p = \frac{P}{(p - p^*)^{\gamma_c}} \quad \text{with } p \rightarrow p^*$$

Where γ_c is a critical exponent, p^* is the reaction probability at the gel point and P is a proportionality constant. Since loops are included, critical exponents from percolation are presumed to be superior to values obtained by classical theory, but these results are confined to the vicinity of the gelation point whilst the classical model covers the entire range of extent of reaction.

2.2 Dendrimers and hyperbranched polymers

The end of the 1970s was characterised by interest in developing areas of host-guest⁷ and supramolecular chemistry⁸. Several research groups became interested in the synthesis of 'tentacle'⁹ and 'octopus' macromolecular structures^{10,11}, where long branches radiate from a central core and polymer chemists started to address efforts to the synthesis and study of highly branched macromolecules.

Newkome¹² developed a series of very highly branched macromolecules built up in layers or generations with different structure that were called 'arborols' and characterised as covalently linked micelle analogues.

Tomalia's research group¹³ developed synthetic routes by which highly branched polymers with extremely low molecular weight polydispersity were created. The most famous product was the polyamidoamine, PAMAM, also called 'dendrimer', after the Greek word 'dendra' for a tree. After PAMAM, the term 'dendrimer' was almost universally used to describe regular highly branched monodisperse polymers.

The synthesis of dendrimers involves the repetitive alternation of a growth and activation reactions performed on many sites of the same molecule simultaneously.

The synthetic method used establishes the way in which branching is introduced into the dendrimer. The early dendrimer syntheses were known as the 'divergent' approach because the dendrimer grows outwards from the core, diverging in the outer space. Starting from a reactive core, a generation is grown, then the new periphery of the molecule is activated by the reaction with more monomers and these two steps can be repeated. The divergent approach was successful for the synthesis of high molecular weight dendrimers because in each generation step the molar mass of the dendrimer is doubled, but it also gave non-perfectly branched molecules, so another synthetic method, called 'convergent' was proposed as a response to this limitations¹⁷.

Convergent synthesis begins with the preparation of what will be the surface of the dendrimer, proceeds inwards by linking together surface units with more monomers and when the growing 'wedges' are large enough, they are attached to a suitable core to give a complete dendrimer. The main advantages of convergent growth are the obtaining perfect dendritic structure and the possibility of introducing different functional groups into the dendrimer, but typically lower yields compared to the divergent method are obtained.

Although many investigations for technological applications of dendrimers have been studied, the repetitive and time-consuming synthesis procedures seem to reduce their widespread use. If the potentially useful properties of dendrimers arise from their highly branched and globular structure rather than their monodisperse molecular weight distribution, it may be possible to reproduce these properties by polydisperse hyperbranched analogues.

Hyperbranched polymers show much similarity with the conventional linear polymers from the synthetic point of view in fact they are typically prepared by polymerisation of AB_f -type monomers, where f is 2 or higher, but the intrinsic globular structure, the high branching density and the large number of terminal groups are their unique characteristics. Unlike dendrimers, hyperbranched polymers have elements of conventional polymers like molecular weight polydispersity and isomerism. Flory¹⁸ predicted that AB_f monomers containing one reactive group A and f reactive group of type B would polymerise readily to give soluble three dimensional structures free of cross links. Normally, the functional groups A and B should only react with each other in the presence of a catalyst, or after a suitable activation step. Whereas both hyperbranched polymers and dendrimers are prepared by AB_f monomers, the significant difference between them is the one step synthetic method used to prepare the hyperbranched macromolecules. The reactivity of the two B groups, while initially equal, could change as soon as one of the two reacts because of the increasing steric hindrance in the immediate vicinity of the remaining B function. The result is a complex product in which some of the B functionalities do not react giving linear-like segments.

The concept of degree of branching, Db , was introduced to define better the structure of the hyperbranched systems and make possible a comparison with analogous linear or dendrimer polymers. The degree of branching can be simply defined as $Db = (1-x)$ where x is the fraction of sub-unit linked with one of their B groups only, but specific formulae for the degree of branching will be discussed in section 2.5.

The most common monomers for the synthesis of hyperbranched polymers are the AB_2 systems but highly functionalised monomers like AB_3 and AB_4 have also been used leading to highly compact and globular hyperbranched polymers but lower degrees of polymerisation compared with the AB_2 monomers are obtained because of the dense packing phenomenon.

Cyclisation as an intra-molecular branch is a side reaction that can be considered in the polymerisation of AB_2 monomers. In one of his early papers Flory neglected the occurrence of this reaction because of the complexity introduced in the statistical calculation, but the research of Kienle¹⁹ showed that in the glycerol-dibasic polymerisation, the deviation of the experimental molecular weight data from the statistical calculation was a strong indication that other molecular species were formed and the intra-esterification reaction was suggested. Gooden²⁰ has recently demonstrated by the use of MALDI-TOF spectrometry that the formation of macrocycles during the polymerisation of AB_2 monomers can be experimentally quantified.

Hyperbranched macromolecules have irregular globular shape affected both by the flexibility of their components and the degree of branching. They normally show low viscosity both in solution and in the molten state, enhanced solubility when compared with their linear analogues and a good compatibility with other polymers.

Only regular dendrimers do not obey the Mark-Houwink relationship, whilst hyperbranched polymers follow the relationship, with lower values of the exponent $a_{[\eta]}$ when compared to linear polymers as described by Turner et al²¹.

Kim and Webster²² reported that hyperbranched polyphenylenes have very good solubility in various solvents as compared to the analogous linear polymer. This improvement in the solubility depends mainly on the structure and polarity of the end groups.

Hyperbranched materials, normally, have good chemical reactivity and this property is particularly important with regards to the chemical modification of their chain ends, although this reactivity is poorer if compared to that of regular dendrimers.

The investigations on possible hyperbranched systems cover a wide range of functionalities. Polyesters are an important class of condensation polymers and the availability of AB_2 dihydroxy carboxylic monomers has encouraged many research groups to investigate the hyperbranched polyesters in more detail and considerable attention has been given to the aromatic hyperbranched polyesters derived from 3,5-dihydroxybenzoic acid. Frechet et al.²³ carried out a systematic investigation of hyperbranched polyesters derived from 3,5-bis (trimethylsiloxy) benzoyl chloride. The polymers obtained have a degree of branching close to 0.55.

Kricheldorf²⁴ compared the polycondensation of silylated and non-silylated 5-acetoxyisophthalic acids obtaining a degree of branching close to 0.6.

Feast and Stainton²⁵ reported the synthesis of aromatic hyperbranched polyester based on 5-(2-hydroxyethoxy) isophthalate with a degree of branching 0.6 as determined by ¹³C-NMR. The use of aliphatic AB₂ monomers for the synthesis of hyperbranched polymers has not been as successful because these molecules under normal reaction conditions undergo thermal degradation reactions such as decarboxylation and dehydration. However, Hult et al²⁶ described the synthesis of 2,2-bis (methylol) propionic acid with a four functional polyol resulting in hyperbranched polyester with a degree of branching close to 0.45. The highly branched structure normally implies that crystallisation cannot occur, but interestingly in this specific copolymer a sufficiently long alkyl chain resulted in the presence of a melt transition as determined by differential scanning calorimetry.

Since hyperbranched polymers are almost exclusively amorphous materials, the glass transition temperature, T_g, is one of the most important features of their thermal properties. The classical explanation for T_g is related to the large motions in the polymer chain segments and the fact that the role of the end groups diminishes above a certain molecular weight. This is more difficult to appreciate in the case of hyperbranched polymers because the large number of branching points and the presence of numerous end groups affect the segmental motions, but Kim²² proposed that the T_g for hyperbranched systems is a translation movement of the entire molecule instead of a segmental movement. Voit et al²⁷ compared the glass transition of a series of aromatic polyesters and they found a shift of about 100° C on going from carboxylic acid to acetate end groups, proving that the thermal behaviour of hyperbranched polymers is related to the chemical structure in the same way as linear polymers.

From the rheological point of view,²⁸ hyperbranched polymers are normally brittle materials and this characteristic limits their use as thermoplastics to applications where the mechanical properties are of minor importance.

The properties of the hyperbranched polymers and dendrimers have suggested applications in a wide range of technological fields and examples will be briefly discussed here. An application of hyperbranched polymers in the control of metal surfaces corrosion is represented by the study of Bergbreiter²⁹ et al. where a fluorinated hyperbranched polyacrylic acid film was found able to stop these corrosion reactions. Hyperbranched polyphenylenes have been demonstrated to act successfully as rheology modifiers in linear thermoplastic polymers processing, in fact, a small amount added to

polystyrene resulted in lower melt viscosity²². Manson et al.²⁸ showed how the use of epoxy-modified hyperbranched polyester as a toughener improved the critical energy release rate of carbon fibre reinforced epoxy resins and verified a combination of enhanced reactivity and reduced viscosity by the use of hyperbranched polyesters in coating applications. An important application of polymers in medicine is drug delivery, where the polymer acts as an absorbing material for concentrating and delivery control of drugs. Roberts³⁰ carried out a study on the effect of dendrimers size inside the human body and found that dendrimers with a molecular weight higher than about $90 \times 10^3 \text{ g mol}^{-1}$ were excreted within two days but smaller macromolecules with molecular weight of about $5 \times 10^3 \text{ g mol}^{-1}$ accumulated in the liver and kidneys. This type of applications can be extended to hyperbranched polymers if the possibility of having defined molecular weight with narrow polydispersity is implemented.

2.3 Thermodynamics of polymer solutions

A polymer solution is a uniform molecular dispersion of a macromolecular solute in a solvent usually of much lower molecular weight and the dilute regime has a central position in the understanding of polymer structure and behaviour in solution. The term dilute solution in polymer science refers to solutions with concentration below a critical value, c^* , where chains begin to overlap. In dilute regime chains interact via hydrodynamic interaction with the solvent and theoretically there is no possibility of interactions between chains. In this regime, the centres of mass of the individual macromolecules are excluded from the domains of the other macromolecules and the local concentration is not uniform throughout the system.

A thermodynamic approach to the solubilisation process of a polymer species considers the variation in the free energy when two pure substances at a given temperature are mixed together. The Flory-Huggins³ theory is basic to the comprehension of the possible interactions between polymer chains in dilute solution and subsequent interpretation of experimental results. It is possible to write an equation for the free energy of mixing, ΔG^M as follows:

$$1(2.3) \quad \Delta G^M = kT [N_1 \ln \phi_1 + N_2 \ln \phi_2 + \chi \phi_2 N_1]$$

Where k is Boltzmann's constant, T is the temperature, N_1 and N_2 are the number of solvent molecules and the number of polymer molecules; ϕ_1 , ϕ_2 are the volume fraction of solvent and volume fraction of polymer respectively; χ is the interaction parameter. The same quantity can be expressed in a more useful form by the chemical potential and this is obtained by differentiating equation 1(2.3) with respect to the number of solvent molecules N_1 . This operation is shown in equation 2(2.3) where the relationship $rN_2\phi_1 = N_1\phi_2$ applies and r is the degree of polymerisation.

$$2(2.3) \quad \frac{\partial \Delta G^M}{\partial N_1} = RT \cdot \left[\ln(1 - \phi_2) + \left(1 - \frac{1}{r}\right) \phi_2 + \chi_1 \cdot \phi_2^2 \right]$$

By expanding the logarithmic terms in a Taylor series, a more useful form of the free energy of mixing, which includes information about the deviation from ideal behaviour, is obtained. In the equation 3(2.3) the first two terms of the expansion are shown.

$$3(2.3) \quad \frac{\partial \Delta G^M}{\partial N_1} = (\mu_1 - \mu_1^0) = -RT \cdot \left[\frac{c \cdot V_1}{M} + v^2 \left(\frac{1}{2} - \chi_1 \right) \cdot c^2 \right]$$

Where μ_1^0 and μ_1 are the chemical potential of the pure solvent and the solvent in solution respectively, $v = (V/M)$ and $(\phi_2/r) = c V_1/M_2$. It is now possible to link the equation 3(2.3) with a measurable parameter like the osmotic pressure, π , defined as follows.

$$4(2.3) \quad (\mu_1 - \mu_1^0) = -V_1 \pi$$

Substituting equation 4(2.3) in 3(2.3) the osmotic pressure is given by 5(2.3).

$$5(2.3) \quad \frac{\pi}{c} = \frac{RT}{M} + A_2 c$$

Where

$$6(2.3) \quad A_2 = \frac{v^2}{V_1} \left(\frac{1}{2} - \chi_1 \right)$$

A_2 is the second virial coefficient and its value is related to the polymer-solvent interaction. Polymer chains cannot interpenetrate in solvent where the mean forces between polymer segments are repulsive and in such solvents a correlation between the relative position and the conformation of segments appears.

The second virial coefficient is a measure of this interpenetration and depends on the strength of the segment-segment interaction and the chain length of the polymer. For linear polymers in good and poor solvents A_2 is a decreasing function of molar mass.

For a better understanding of the temperature effect on the solution equilibrium it is pertinent to study a two-component system. As the temperature is increased the limit of two-phase coexistence contracts, until they coalesce to produce a homogenous phase at T_c , the critical solution temperature. This is an important quantity that can be defined in terms of chemical potential and represents the point where the first, second and third

derivatives of the free energy of mixing with respect of mole fraction are zero (equation 7(2.3)).

$$7(2.3) \quad \frac{\partial \mu_1}{\partial \phi_2} = \frac{\partial^2 \mu_1}{\partial \phi_1^2} = \frac{\partial^3 \mu_1}{\partial \phi_1^3} = 0$$

It is possible to define the critical composition for phase separation as in equation 8(2.3) and a useful expression for the interaction parameter at T_c is given in 9(2.3) where x_n is the chain length.

$$8(2.3) \quad \phi_{2,c} = \frac{1}{\left(1 + x_n^{1/2}\right)} \approx \frac{1}{x_n^{1/2}}$$

$$9(2.3) \quad \chi_{1,c} = \frac{1}{2} + \frac{1}{x_n^{1/2}} + \frac{1}{2x_n}$$

Equation 9(2.3) establishes a strong relation between the solvent power and also tells that $\chi_{1,c} = 0,5$ for an infinite chain length.

Another treatment for the dissolution process of polymers in a solvent is proposed in Flory-Krigbaum theory. Here a parameter κ is defined for the enthalpy and a parameter ψ for the entropy of dilution at equilibrium. The free energy of solubilisation is given by equation 10(2.3).

$$10(2.3) \quad \Delta G^M = RT \phi_2^2 (\kappa - \psi)$$

Comparing the second terms of equations 5(2.3) and 10(2.3), it is possible to have a fundamental relationship for the non-ideal behaviour of the solution.

$$11(2.3) \quad \left(\frac{1}{2} - \chi_1\right) = (\psi - \kappa)$$

When the interaction parameter, χ , is equal 0.5, the entropic and enthalpic contributions for the mixing process are equal.

$$12(2.3) \quad \Delta H_1^E = T\Delta S_1^E$$

The temperature at which this condition is obtained is the theta temperature, θ , defined as:

$$14(2.3) \quad \theta = \frac{\kappa_1}{\psi_1} T$$

The θ temperature identifies the critical miscibility in the limit of infinite molecular weight. From the experimental point of view there will be a combination of solvent and temperature to give a theta condition, but this also means that there are critical conditions at which the solubility strongly depends on the polymer length.

Fractionation

The interaction parameter is a quantitative measure of the solvent power and since it can be manipulated, by adjusting temperature and solvent conditions, it can be also used for the solution fractionation of some molecular species that can be precipitated out, leaving other molecules in solution. The precipitation process is more appropriately regarded as a separation of the system into two liquid phases³; one relatively rich in polymer, called the precipitate, and the other called the supernatant. Each polymer species is partitioned between these two phases and is more soluble in the more concentrated or precipitated phase.

The smaller polymer species will be distributed at nearly equal concentration in the two phases and this is explained by the fact that they have less units per molecule to interact with the unfavourable environment of the supernatant phase and so they are less discriminating in the choice of their surroundings.

For a given amount of polymer transported from the supernatant to the precipitated phase, there is a decrease in the entropy of solubilisation directly proportional to the number of particles transported.

Solution fractionation is normally carried out by the addition of a non-solvent to a polymer solution. A new solvent is formed in this way, where it is easier to manipulate

the temperature and obtain a critical point analogous to the θ condition where separation into two phases is possible. Because of this addition, the interaction parameter increases gradually until the critical value is reached for larger molecules, which precipitate and can be separated from the smaller.

The interaction parameters are the thermodynamical quantities involved in the process. If the two polymer-solvent interaction parameters are equal and the one between the two solvents is zero, it is possible to say that the mixed solvents behave as a single solvent and we are in the single liquid approximation.

An important issue involved in fractionation is the efficiency of partitioning the species between the two phases and in order to make the fractionation process efficient, the ratio of the volumes of the supernatant and the precipitated phases should be as large as possible. The separation, although never sharp, becomes more efficient as the ratio between the volume added and the solution is increased.

2.4 Size exclusion chromatography

Size exclusion chromatography (SEC) separates molecules according to their size in solution. When the polymer solution is eluted through a column containing porous packing, the molecules that are too large to penetrate the pores of the packing materials are excluded and remain in the interstitial volume; these molecules are eluted first from the column. In the opposite situation, small molecules that can permeate all the pores elute at the solvent front in the zone of total permeation. Molecules of intermediate size will penetrate some of the pores and spend a fraction of their time within the pores and the interstitial volume. This is the region of selective permeation, represents the pore volume of the packing medium and is usually a small range of single columns, but can be extended by connecting several columns each containing a gel of different pore size. Generally a SEC chromatogram shows a polymer molecular weight distribution, but to associate a particular elution volume to a molecular weight a calibration is needed and the retention volumes of solutions of polymer standards with narrow molecular weight distribution are determined. A polymer can have different sizes in different solvents and molecules of different polymers might have the same size in the same solvent despite their different molecular weight. Thus the calibration curve is valid only if the standards are of the same nature as the unknown sample and the eluent is identical.

Molecular weight distribution can be obtained using the refractive index detector. The main advantage of the differential refractive index detector is its universality, in fact, almost any polymer solution will give a response. The two main disadvantages are the low sensitivity and the high dependence on pressure, flow, and temperature fluctuations.

Another common detector involved in the size exclusion chromatography analysis is the online viscometer. In this apparatus a pressure transducer monitors the pressure changes as the polymer solution passes through the detector and gives a response proportional to the intrinsic viscosity and concentration

A third detector commonly employed is laser light scattering. This is based on the experimental fact that the intensity of light scattered from small particles in solution, expressed in terms of the Rayleigh ratio does not depend on the observation angle and so can be measured at a single angle that is usually 90° . The application of a light scattering detector allows the absolute determination of the molecular weight.

Viscotek coined the term Tri-SEC to describe not only the three detectors but also the three dimensions created by the addition of these detectors to the SEC technique. The

first dimension is the chromatographic process that separates polymer molecules according to molecular size, the second is the light-scattering detector response that yields molecular weight and the third dimension comes from the viscometry detector. Together, these variables present a more complete picture of the molecular weight distribution and the shape in solution.

Universal calibration based on the hydrodynamic volume of linear polymers is not valid for polymers with branches longer than a certain length. This is because such branched species are more compact than linear macromolecules with the same molecular weight. Because of their more compact structure, branched polymers always have smaller dimensions than a linear macromolecule with the same molecular weight.

The effect of branching is to increase the segment density within the molecular coil, thus a branched molecule occupies a smaller volume and has a lower intrinsic viscosity than its linear analogue. This suggests that the comparison of molecular dimensions of branched and linear polymers is an appropriate method for the characterisation of branched polymers and the amount of branching is often characterised in terms of the branching factors.

Zimm and Stockmayer³¹ introduced the branching factors defined as the ratio of the radius of gyration of the branched polymer to the linear analogue with the same molecular weight.

A branching factor that uses the dynamical properties in solution is the ratio of the intrinsic viscosity of the branched polymer to the linear analogues with the same molecular weight. To calculate this branching factor it is necessary to measure the intrinsic viscosity and molecular weight of the branched polymer fraction, and to know the Mark-Houwink-Sakurada relationship for the linear polymer so that the intrinsic viscosity of the linear polymer can be calculated.

In 1970, Drott and Mendelson³² developed a method for the evaluation of the short and long chain branching in polymer molecules by SEC. The method was semi-empirical and essentially based on the calculation of calibration curves for the branched polymer derived from the universal calibration of the linear analogues.

The use of the Zimm-Stockmayer statistical equation for the branching factor in the case of three-functional branching units will be discussed in detail in section 4.1.

2.5 NMR and branching

The archetypical example of a branched polymer is low-density polyethylene (LDPE)³³ produced by radical polymerisation at high temperature and pressure. In this polymer significant branching³⁴ was suspected because of the influence of the polymerisation conditions upon the crystallinity of the polymer. The development of high-resolution ¹³C-NMR³⁵ allowed the study of branching in LDPE. The spectrum of the polymer recorded for a molten material or close to its melting point displayed two different signals for the methylene carbon, a methyl signal, a signal for methine and even a quaternary carbon signal and the quantitative analysis of the different signals gives 18.9 branches per 1000 backbone carbons in a typical LDPE.

Branching occurs in the reactions of aldehydes, such as formaldehyde, with polyfunctional amines and amides such as urea and melamine. NMR has been extensively used to study systems of this type with the aim of identifying various linear and branched structures and the effect of reaction conditions. In these cases ¹³C-NMR provides more detailed information than ¹H-NMR because of the wider range of chemical shifts accessible.

Hyperbranched macromolecules are structurally different from both linear and dendritic polymers because of their three-dimensional highly branched structure and their random branching. A closer examination of the structure shows that the complex structure can be simplified at the building block level and since hyperbranched polymers are derived from AB₂ monomers, three types of sub-units, linear, branched and terminal are evident. Because of the necessity of having a general parameter that could better define hyperbranched polymers and allow their comparison with linear and dendritic polymers, the degree of branching (*Db*) has been introduced. Intuitively, a linear polymer would have a degree of branching of zero, while a perfectly branched dendritic would have a *Db* of one and hyperbranched polymers have degree of branching ranging between 0 and 1.

Two methods have been developed for the determination of the degree of branching in hyperbranched polymers. One relies on a two-step process involving modification of the chain end followed by cleavage of the bond between the repeat units. The modification of the chain ends allows the differentiation of the different sub-units and the chemical cleavage produces fragment that can be correlated with the specific sub-unit structure. The relative percentage of these sub-units can be determined by chromatographic techniques and then used to calculate the degree of branching.

Another method to calculate the degree of branching of a hyperbranched polymer is based on NMR spectroscopy and relies on the ability to differentiate the discrete resonance for the three sub-units (terminal T , linear L and branched B) in the macromolecule (Figure 1(2.5)).

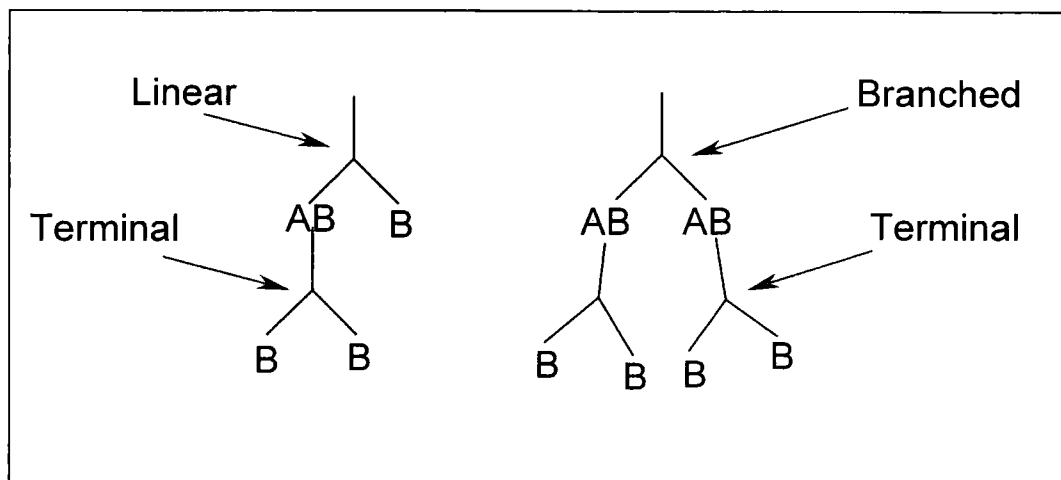


Figure 1(2.5). Schematic of the sub-units in the hyperbranched polymer structure.

Hawker and Frechet³⁶ in 1991 introduced the first formula for the degree of branching as in equation 1(2.5).

$$1(2.5) \quad Db = \frac{B+T}{B+T+L}$$

Holter and Frey³⁷ developed another approach for the calculation of the degree of branching by defining the overall number of monomer units incorporated in one hyperbranched molecule, DP , as the sum of the terminal, linear and branched units.

$$2(2.5) \quad DP = T + L + B$$

Evidently any terminal unit may become a linear one by the addition of one AB_2 monomer and a branched one by the addition of two AB_2 monomers and for every branched unit formed from a linear unit, a new terminal group is formed. Thus the number of terminal and branched units is related by the following relationship:

$$3(2.5) \quad T = B + 1$$

For high conversions of the hyperbranched polymerisation, the number of terminal and branched units becomes practically identical. Therefore, the number of linear units is independent of the number of the other two units and constitutes the key factor that determines the degree of branching. In this method the degree of branching is defined as the actual number of growth directions, B , compared to the maximum number of possible growth directions, B_{max} . Since in the case of AB_2 systems every branched sub-unit will introduce a new branch the degree of branching is redefined as follows.

$$4(2.5) \quad Db = \frac{B}{B_{max}}$$

Since two linear sub-units can be transformed into one branched and one terminal sub-unit, one can define:

$$5(2.5) \quad B_{max} = B + \frac{1}{2}L$$

And thus the degree of branching is equal to:

$$6(2.5) \quad Db = \frac{2 \times B}{2 \times B + L}$$

This formula is universally applicable for the Db of small and large hyperbranched macromolecules. In the statistics of polymerisation of an AB_2 monomer, equal reactivity of the A and B groups is normally assumed regardless of their presence in the different sub-units and the formation of a loop in the same macromolecule is neglected. The most probable final situation after the reaction of all monomer molecules will be characterised by an equal number of unreacted B functions at the linear and terminal sub-units. In this case the ratio of terminal to linear sub-units is 1/2, so a large hyperbranched molecule must contain the same number of terminal and branched sub-units and the degree of branching will be 0.5. Generally the degree of branching obtained experimentally is somewhat lower than 0.5 because complete conversion of all

A groups is not obtained. Furthermore linear units formed during the polymerisation process are normally less accessible than the terminal units leading to a higher linear fraction than statistically expected. Details of the experimental calculation of the degree of branching are given in section 3.5.

2.6 Viscometry

Poiseuille's law gives the viscosity of a liquid flowing through a capillary³⁸ and is summarized by the equation 1(2.6).

$$1(2.6) \quad \frac{dV}{dt} = \frac{\pi \times p_h \times r^4}{8 \times \eta \times l_c}$$

Where dV/dt is the volume of the liquid flowing through the capillary per unit time; p_h is the hydrostatic pressure head; r is the radius of the capillary; l_c is the length of the capillary and η is the viscosity of the liquid. If the volume of liquid per unit time is constant it is possible to rewrite the formula as 2(2.6).

$$2(2.6) \quad \frac{V}{t} = \frac{\pi \times p_h^* \times r^4}{8 \times \eta \times l_c}$$

Where p_h^* is the average hydrostatic pressure under which the liquid is flowing and it is defined as follows;

$$3(2.6) \quad p_h^* = \delta \times a_g \times h$$

Where δ is the density of the liquid, a_g is the acceleration due to gravity and h is the average value of the liquid head. Substituting equation 3(2.6) in equation 2(2.6) an expression for the viscosity is obtained.

$$4(2.6) \quad \eta = \frac{a_g \times h \times r^4 \times \pi}{8 \times V \times l_c} \times t \cdot \delta = S \times t \times \delta$$

Where S is a constant characteristic of the specific viscometer and can be evaluated by the use of liquids with a known viscosity. The equation 4(2.6) is valid where the potential energy of the liquid column does not give kinetic energy to the flux, so for the experimental situations one should consider an additional term that takes into account the kinetic energy and write the equation as follows.

$$5(2.6) \quad \frac{\eta}{\delta \times t} = S - \frac{D}{t^2}$$

The factor D corrects for the kinetic energy contribution and its value decreases with decreasing capillary length and can be calculate from plot of known viscosity liquids as a function of the flow time

Equations 4(2.6) and 5(2.6) are related to what is normally called the actual viscosity of the solution, but in the case of polymer solution the interest is in the increase of the solvent viscosity by the presence of the macromolecules.

A typical characteristic of dilute solutions of polymers is that their viscosity is considerably higher than that of the pure solvent because of the big differences in the molecular size of the solvent and the polymer. Dilute solution viscometry is concerned with the quantitative measurement of the increase in viscosity and this physical parameter gives indications about the size, molecular weight and the structure of the macromolecules in solution.

Absolute measurements of viscosity are not essential in dilute solution viscometry since it is only important to determine the viscosity of a polymer solution relative to that of the pure solvent. A simple viscosity measurement uses a capillary viscometer and the relative viscosity is obtained as the ratio of the solution and pure solvent flow times as in equation 6(2.6).

$$6(2.6) \quad \eta_{rel} = \frac{t}{t_0}$$

This ratio is a dimensionless number greater than 1, the specific viscosity is then defined as;

$$7(2.6) \quad \eta_{sp} = \eta_{rel} - 1 = \frac{\eta - \eta_0}{\eta_0}$$

The reduced specific viscosity (η_{sp}/c) extrapolated to infinite dilution is known as intrinsic viscosity and is defined in equation 8(2.6).

$$8(2.6) \quad [\eta] = \lim_{c \rightarrow 0} \frac{\eta_{sp}}{c} = \lim_{c \rightarrow 0} \frac{(\eta_{rel} - 1)}{c}$$

In experimental practice the Huggins equation 9(2.6) is normally used.

$$9(2.6) \quad \frac{\eta_{sp}}{c} = [\eta] + k_H [\eta]^2 c$$

By plotting η_{sp}/c against c , the intrinsic viscosity, $[\eta]$, is obtained from the intercept and the Huggins coefficient k_H as a slope. The intrinsic viscosity value depends on the particular polymer-solvent system. Usually the value of intrinsic viscosity increases as the concentration of the solution increases, reflecting the increasing entanglement of polymer chains with one other. This is a general behaviour for linear polymers, but branched and hyperbranched polymers as well as dendrimers have a very different behaviour because of their different interaction with the solvent.

The viscosity of an isolated coil macromolecule in solution can be rationalised on the basis of its behaving like a suspended sphere in a continuous solvent. The shear field³⁹ of the solvent flow in the viscosity measurements causes rotation of the effective spherical polymer coil and this leads to an additional frictional loss and increases the viscosity of the solvent-polymer system.

Two extreme cases can be taken into account for the response of the solvent that penetrate the coil. The free-draining case is the one in which the solvent in the coil experiences the same shear field as the bulk solvent. In the opposite situation, the solvent in the coil could be considered as completely trapped, riding along with the rotating coil. The latter model is called non-draining or impermeable coil. The viscosity can be attributed to a suspension of impenetrable rotating spheres as formalised by the Einstein equation 10 (2.6).

$$10(2.6) \quad \eta = \eta_0 \left(1 + \frac{5}{2} \phi_2 \right)$$

Where ϕ_2 is the volume fraction of the suspended spheres and is a parameter related to the effective radius, R_E , of the coil by equation 11 (2.6).

$$11 (2.6) \quad \phi_2 = \frac{N \cdot 4\pi}{3 \cdot V} R_E^3$$

Where N is the number of spheres, V is the solution volume. So the intrinsic viscosity can be written in the following form:

$$12 (2.6) \quad \frac{\eta}{\eta_0} - 1 = [\eta] = \frac{5 \times 4\pi}{2 \times 3} \times \frac{N_A}{100} \times \frac{R_E^3}{M} \times c$$

where the relation $c = 100NM/N_A V$ applies for the concentration in g/dl and N_A is the Avogadro's number. The effective radius of the average sphere can be determined by calculation of the frictional properties of the segment distribution. If the mean squared end-to-end distance, $\langle r^2 \rangle$, is used in the calculation of the effective radius then the following equation applies.

$$13(2.6) \quad R_E = \gamma \langle r^2 \rangle^{1/2}$$

Where γ is a proportionality constant. Hence:

$$14(2.6) \quad [\eta] = \Phi_0 \frac{\langle r^2 \rangle^{3/2}}{M}$$

Where the constant, Φ_0 , is defined in equation 15(2.6).

$$15(2.6) \quad \Phi_0 = \frac{5}{2} \times \frac{4\pi}{3} \times \frac{N_A}{100} \times \gamma^3$$

As proposed by Flory, Φ_0 should be independent of the particular structure of polymer molecules and be a universal constant.

In poor solvents, polymer-polymer interaction are more favoured than polymer-solvent contacts and so the tendency is to have polymer segment self-association and the coil would be smaller than in good solvents.

There is a specific condition in which polymer-solvent contacts are balanced by segment-segment interaction at a particular temperature and the solvent becomes a better solvent as the temperature increases and poorer as it decreases. This is the θ solvent and the temperature θ as mentioned in section 2.3. The average end-to end distance of a polymer coil at the θ temperature can be described by equation 16(2.6).

$$16(2.6) \quad \langle r^2 \rangle = C_{\infty} N \times l^2$$

where N is the number of bonds, l is the bond length and C_{∞} is the characteristic ratio that depends on the flexibility of the chain. Since the mean squared end-to-end distance depends on the molecular weight it is possible to write an equation (equation 17(2.6)) under the θ condition;

$$17(2.6) \quad \langle r^2 \rangle = \frac{C_{\infty} \times l^2 \times M}{M_0}$$

where M_0 is the monomer molecular weight. Combining equation 17 (2.6) with the 14 (2.6) the typical relationship with the molecular weight is obtained.

$$18 (2.6) \quad [\eta] = K_{[\eta]} M^{1/2}$$

where

$$19(2.6) \quad K_{[\eta]} = \left(\gamma^2 \cdot l^2 \cdot \frac{C_{\infty}}{M_0} \right)^{3/2} \times \frac{5}{2} \times \frac{4\pi}{3} \times \frac{N_A}{100}$$

The main difference between the branched and the linear polymer lies in the smaller spacial extension of the former at a given molecular weight⁴⁰. The segment density within the occupied volume by a branched macromolecule is larger than the linear one with the same number of monomer units.

The effect of branching is usually expressed by the branching factor g' , defined as the ratio of the intrinsic viscosity of the branched polymer to that of a linear polymer of the same molecular weight

$$20(2.6) \quad g' = \frac{[\eta_b]}{[\eta_l]}$$

where the subscript b is for branched and l for linear. Writing again the equations for the intrinsic viscosity considering the mean squared radius of gyration, $\langle s^2 \rangle$, equation 21(2.6) and 22(2.6) are obtained.

$$21(2.6) \quad [\eta_b] = \phi_b \times \left(\frac{\langle s_b^2 \rangle_0}{M} \right)^{3/2} \times M^{1/2} \times \alpha_{\eta,b}^3$$

$$22(2.6) \quad [\eta_l] = \phi_l \times \left(\frac{\langle s_l^2 \rangle_0}{M} \right)^{3/2} \times M^{1/2} \times \alpha_{\eta,l}^3$$

Where ϕ is the volume fraction of the polymer and $\alpha_{\eta,l}$ and $\alpha_{\eta,b}$ are the viscosity expansion factors for the linear and branched polymer respectively; they are defined as the ratio between the intrinsic viscosity in the real and ideal situation and they take into account the excluded volume effects. A more useful form of the g' factor is;

$$23(2.6) \quad g' = \left(\frac{\phi_{0,b}}{\phi_{0,l}} \right) \times g_0^{3/2} \times \left(\frac{\alpha_{\eta,b}^3}{\alpha_{\eta,l}^3} \right)$$

Where g_0 is defined as the ratio of the mean squared radius of gyration of the branched polymer to that of the linear in the ideal conditions as indicated by the subscript 0 .

The intrinsic viscosity of a polymer-solvent system has an empirical relationship to the molecular weight expressed by the Mark-Houwink-Sakurada equation 24(2.6).

$$24(2.6) \quad [\eta] = K_{[\eta]} M^{a_{[\eta]}}$$

Where $K_{[\eta]}$ is a constant and the exponent $a_{[\eta]}$ is a scalar related to the stiffness of the polymer chains. In general for flexible polymers the value has been found in the range $0.5 < a_{[\eta]} < 0.8$; however higher values have been observed for less flexible polymer chains like celluloses and polyelectrolytes. The value of $a_{[\eta]}$ provides indications on the polymer conformation in solution and for a particular polymer-solvent system at a certain temperature $K_{[\eta]}$ and $a_{[\eta]}$ are effectively constant.

2.7 Light scattering

This section introduces the basic principles of light scattering, the specific application of this technique to dilute solution of polymers and data analysis methods.

2.7.1 Static light scattering

When electromagnetic radiation interacts with molecules, a dipole moment is produced and its magnitude is proportional to the electromagnetic field and to the specific polarizability α_p of the molecule (equation 1(2.7.1)).

$$1 \text{ (2.7.1)} \quad \alpha_p = \frac{c \times \left(\frac{\partial n}{\partial c}\right) \times n_0}{2\pi \times N}$$

Where c is the concentration; N is the number of particles; n_0 is the refractive index of the solvent and $\left(\frac{\partial n}{\partial c}\right)$ is the differential refractive index⁴¹.

As in other scattering techniques, when carrying out a light scattering experiment the size of the particle under investigation must be considered in relation to the wavelength of the incident light. It is in fact possible to distinguish between small particles in which the size is much smaller than the wavelength λ (typical by $\lambda/20$) and large particles in which the size is comparable to the wavelength of the incident light. Small particles behave like point masses with respect to the light wavelength and this particular situation simplify the treatment of the scattering experiment. Typical synthetic polymers with molecular weight lower than $250 \times 10^3 \text{ g mol}^{-1}$ usually have dimensions of few tens of nanometres and therefore can be treated as small particles in solution.

For a qualitative point of view, when vertically polarised monochromatic light beam interacts with small isotropic molecules, the oscillation of the electric vector of the electromagnetic field induces the same oscillation frequency in the electrons of the molecule and they emit the same wavelength. The molecules irradiate in the plane of oscillation of the electric vector and emit the same amount of energy in all directions perpendicular to the direction of oscillation. From a general quantitative treatment of the scattering phenomenon of isotropic ideal gas molecules the intensity of light is;

$$2(2.7.1) \quad I = \frac{8 \times \pi^4 \times \alpha^2}{r^2 \times \lambda_0^4} \times I_0 (1 + \cos^2 \theta)$$

Where I is the intensity scattered from a unit volume; θ is the angle between the propagation direction of the incident wave and the direction of observation; I_0 is the intensity of the light beam; α is the polarisability of the molecule; λ_0 is the wavelength of the light in vacuum and r is the distance of the scatterer and the detector. The factor $(1 + \cos^2 \theta)$ takes into account the angular dependence of the light scattering due to the polarised component of the primary light beam. In the case of vertically polarised light, the intensity of the scattered radiation is;

$$3(2.7.1) \quad I_{90} = \frac{4 \times \pi^2 \times \alpha^2}{r^2 \times \lambda_0^4} \times I_0$$

Other phenomena happen at the same time, in fact, a certain spectral distribution of the scattered light occurs due to the translation motion of the particle in solution, this is quasi-elastic or dynamic light scattering and the basics of the dynamic light scattering experiment will be explained in section 2.7.2.

Dealing with dilute solution of macromolecules, we are considering a system of mutually independent particles. In this situation there are two main contributions to the scattering intensity; the density fluctuations in the solvent and the scattering from the polymer particles. In dilute regime the density fluctuation of the solvent molecules is virtually not affected by the macromolecules in solution and therefore the subtraction of the scattering intensity of the solvent from the overall scattering of the solution gives the scattering contribution of the macromolecules;

$$4(2.7.1) \quad I_{90} = \frac{4 \times \pi^2 \times n_0^2}{r \times \lambda_0^4 \times N_A} \times I_0 \left(\frac{dn}{dc} \right)^2 \times M \times c$$

The refractive index increment describes the change of the refractive index in the solution by a change in the solute concentration and it is typical of specific polymer-solvent system at a certain temperature.

At the microscopic level, equal volumes of the solution do not contain the same amount of solute because of the concentration fluctuations and these concentration variations are able to produce excess scattering in addition to that of the solvent. The solute concentration fluctuation creates changes in the free energy and by the use of the Boltzmann's law the average of the concentration fluctuation, $(\delta c)^2$, is inversely proportional to the second derivative of the free energy with respect to the concentration.

$$5(2.7.1) \quad \left(\frac{\partial^2 G}{\partial c^2} \right)_{T,P} \approx \frac{1}{(\delta c)^2}$$

The same second derivative of the Gibbs energy can be written in terms of change of solvent chemical potential with the solute concentration and expressed as in equation 6(2.7.1) in the form a power series (virial expansion) of the concentration expanded in the vicinity of $c=0$.

$$6(2.7.1) \quad \left(\frac{\partial \mu_1}{\partial c} \right)_{T,P} = \left(\frac{\partial^2 G}{\partial c^2} \right)_{T,P} = \text{Const} \times \left(\frac{1}{M} + 2A_2c + 3A_3c + \dots \right)$$

The first term of the virial expansion applies in infinitely dilute solution and the other terms are the corrections for the non-ideal behaviour in more concentrated solutions. Since the concentration fluctuation are related to the fluctuation of the scattering and proportional to $(\delta c)^2$ it is possible to write the scattering intensity in the case of vertically polarised incident light as in equation 7(2.7.1):

$$7(2.7.1) \quad I_{90} = \frac{4 \times \pi^2 \times n_0^2}{r^2 \times \lambda_0^4 \times N_A} \times I_0 \times \left(\frac{dn}{dc} \right)^2 \times c \times \frac{1}{M^{-1} + 2A_2c + 3A_3c^2 + \dots}$$

The equation 7(2.7.1) is historically written by the Rayleigh ratio, R_θ , form 8(2.7.1).

$$8(2.7.1) \quad R_\theta = \frac{I_{90} \times r^2}{I_0} = \frac{K \times c}{M^{-1} + 2A_2c + 3A_3c^2 + \dots}$$

Where K is defined as;

$$9(2.7.1) \quad K = \frac{4 \times \pi^2 \times n_0^2}{\lambda_0^4 \times N_A} \left(\frac{dn}{dc} \right)^2$$

For small isotropic particles and polymer dimensions small compared to the wavelength, the corresponding Rayleigh ratio is independent of the angle of observation and if the reciprocal Kc/R_θ is plotted versus the concentration the typical equation for the classical light scattering is obtained⁴².

$$10(2.7.1) \quad \frac{Kc}{R_\theta} = \frac{1}{M} + 2A_2c + 3A_3c^2 + \dots$$

If the scattering particles are larger than $\lambda/20$, there will be phase difference that increases as the observation angle increases. The reduction of the scattering intensity caused by this phenomenon is described by the particle scattering factor $P(\theta)$.

$$11(2.7.1) \quad P(\theta) = \frac{R_\theta}{R_0}$$

Where R_θ is the Rayleigh ratio at angle θ and R_0 is the Rayleigh ratio at zero angle.

In solution of finite concentration, light scattering from different solute particle can interfere, causing a scattering intensity smaller than the sum of the single particles scattering intensity. This phenomenon is determined by the polymer-solvent interaction and depends on the specific system under investigation.

It is possible to define the particle scattering factor by taking into account some considerations. The contributions of all scattering points are summed and the total field strength is converted into the scattered intensity. The result depends on the orientation of the scattering particles with respect to incident beam. For a randomly oriented particle consisting of σ identical scattering point the general form of particle scattering function is defined by the Debye equation as in 12(2.7.1).

$$12(2.7.1) \quad P(\theta) = \frac{1}{\sigma^2} \sum_{i=1}^{\sigma} \sum_{j=1}^{\sigma} \left\langle \frac{\sin Qh_{ij}}{Qh_{ij}} \right\rangle \quad Q = \frac{4\pi n_0}{\lambda_0} \sin\left(\frac{\theta}{2}\right)$$

Where h_{ij} is the distance between the i -th and j -th mass points; Q is the scattering vector; n_0 is the refractive index of the solvent, λ_0 is the wavelength and θ is the angle between the primary beam and the observation direction.

It is also possible to define the mean square radius of gyration on the basis of the distances between all pairs of mass elements within the particle.

$$13(2.7.1) \quad \langle s^2 \rangle = \frac{1}{2\sigma} \sum_{i=1}^{\sigma} \sum_{j=1}^{\sigma} \langle h_{ij}^2 \rangle$$

So one can explain the relationship between the particle scattering factor and the mean square radius of gyration by the limit in 14(2.7.1).

$$14(2.7.1) \quad \lim_{\theta \rightarrow 0} P(\theta) = 1 - \frac{Q^2 \langle s^2 \rangle}{3}$$

This relationship is of fundamental importance because it shows that the angular dependence of the intensity of scattered light represented by the particle scattering function, in the small angle area, enables the determination of the radius of gyration of macromolecules.

The Zimm plot

Zimm plot is a general method developed for the determination of the molar mass, radius of gyration and second virial coefficient by the measurement of the angular and concentration dependence of the intensity of light scattered from dilute solutions of polymers. The basic equation 10(2.7.1) for light scattering from dilute solution of both large and small polymers is the same if the scattering angle is equal to zero, because there is no influence of the intramolecular interference in the limit of zero concentration. Introducing the particle form factor we have;

$$15(2.7.1) \quad \lim_{c \rightarrow 0} \frac{Kc}{R_\theta} = \frac{1}{M \times P(\theta)}$$

The last equation shows that in the case of large particles, the zero concentration extrapolation of Kc/R_θ is not only dependent on the molecular weight but also on the size and shape of the particle under investigation.

From the equations 10(2.7.1) and 15(2.7.1) it is possible to understand that extrapolation of the scattering intensity to infinite dilution eliminates the intermolecular interference and the extrapolation to zero angle can eliminate the intramolecular interference. The initial slope of the concentration dependence of Kc/R_θ is then proportional to the second virial coefficient of the polymer-solvent system and the initial slope of the angular dependence of $[Kc/R_\theta]_{c=0}$ is proportional to the mean square radius of gyration. These relationships are general and hold for any particle shape. To obtain the value of the radius of gyration in the limit of infinite dilution equation 16(2.7.1) is considered.

$$16(2.7.1) \quad \left[\frac{Kc}{R_\theta} \right]_{c=0} = \frac{1}{M_w} + \frac{16\pi^2}{3 \cdot \lambda_0^2} \times \frac{1}{M_w} \times \langle s^2 \rangle \times \sin^2\left(\frac{\theta}{2}\right)$$

The slope of this angular dependence is thus defined as in equation 17(2.7.1), from which it is possible to extract the mean squared radius of gyration.

$$17(2.7.1.2) \quad k_t = \frac{16 \cdot \pi^2}{3 \cdot \lambda_0^4} \times \frac{1}{M_w} \times \langle s^2 \rangle$$

The virial coefficients are important parameters characterising the thermodynamic interaction between the solvent and polymer molecules at a given temperature. In the dilute solution regime normally the third and higher terms are negligibly small compared to the second virial coefficient. If A_2 is positive this corresponds to a large change in the chemical potential and this also means that the affinity between the solvent molecules and the polymer is large. In this situation solvation reduces the free volume available for concentration fluctuations and since the polymer-solvent interaction is energetically favoured the solvent is considered a good solvent.

When A_2 is equal to zero at a specific temperature, the polymer-polymer interactions are energetically equivalent to the polymer-solvent interactions, the mixture is defined as ideal solution and the solvent is a θ solvent. If the second virial coefficient is negative the polymer-polymer interaction are favoured with respect to the polymer-solvent interaction and the solvent is a poor one.

The radius of gyration normally decreases with the degree of branching. Highly branched macromolecules can be seen as spherical particles and the transition from the linear coils to spheres is characterised by upward curvature of the reciprocal particle scattering function as a function of θ . It is also expected that the particle scattering function for branched polymers have shapes intermediate between those for linear coils and homogeneous spheres.

Branched systems are polydisperse not only in molecular weight but also in molecular shape because molecules of the same molecular weight may differ in the number of branching points and molecules with a definite number of branching points differ in structure and also in particle scattering function. Polydispersity changes the dependence of the particle scattering function on $\sin^2(\theta/2)$, so the combined effect of branching and polydispersity more or less compensate each other and the experimental particle scattering function are not interpretable in terms of degree of branching. The comparison of the radii of gyration of linear and branched polymers of the same molecular weight can give accurate information on the degree of branching only with relatively monodisperse samples.

The radius of gyration in a polydisperse branched polymer is thus the result of two counteracting factors, the diminishing effect of the branching and the broadening distribution of the polydispersity. Because of this compensation, the quantification of branching from the radii of gyration is not possible in many experimental situations. Due to their smaller dimensions, branched polymers have a higher segment density within the domain occupied by the macromolecule in dilute solution than a linear polymer of the same molecular weight and the segmental density influences the thermodynamics of the polymer interaction and hence the value of the second virial coefficient. Experimentally, the second virial coefficient decreases with the increasing degree of branching, but a quantitative theory that describe the effects of branching on the second virial coefficient does not exist.

2.7.2 Dynamic light scattering

Dynamic or quasi-elastic light scattering technique allows the study of the dynamics of the polymer particles in solution. The idea on which the technique is based relies on the fact that at equilibrium, solutions are macroscopically homogeneous but this situation does not apply on the microscopic view. In a polymer solution the macromolecules are in irregular motion caused by the thermal energy imparted to them by the collisions with the solvent molecules. This Brownian collisions cause the particles to undergo translational and rotational motions⁴³. The speed of the movement is inversely proportional to particle size and the velocity can be detected by analysing the time dependency of light intensity fluctuations scattered by the particles when they are illuminated with a monochromatic light beam. The variation of the probability, $P(\rho, t)$, of finding a molecule at the position ρ at the time t , is given by equation 1(2.7.2).

$$1 (2.7.2) \quad \frac{\partial P(\rho, t)}{\partial t} = D_t \nabla^2 P(\rho, t)$$

Where D_t is the translational diffusion coefficient, ∇ is the spatial derivative.

Moving particles will scatter light in a way that is quantitatively related to their motion and light scattering measurements provide a method to determine diffusion coefficients. The light scattered by a solution has a frequency spectrum characteristic of time dependent fluctuations and particle motion. Since the frequency difference between the scattered light and the incident light is small, this scattering is called quasi-elastic light scattering.

In the determination of the correlation function, the scattering is homodyne if only the light from the scattering volume is used in the detection system and heterodyne if light from a local oscillator is mixed with the scattered light. The following discussion is confined to homodyne scattering because this was method used.

Correlation functions provide a concise method expressing the degree by which two dynamical properties are correlated over a period of time⁴⁴. Formally a time correlation function between two signals A and B is given by equation 2(2.7.2).

$$2(2.7.2) \quad F(\tau) = \lim_{T \rightarrow \infty} \frac{1}{T} \int_0^{t_0+T} A(t)B(t-\tau)dt$$

Where t is a delay time, t_0 is the starting time, T the averaging time and τ is a time increment. If B is a delayed form of A then the relationship between the two signals is called autocorrelation. In the case of an ensemble of hard non-interacting spheres moving by Brownian motion in a fluid the correlation function can be expressed as an exponential function as defined in equation 3(2.7.2).

$$3(2.7.2) \quad F(\tau) = A_0 + A \times e^{(-\Gamma\tau)}$$

Where

$$4(2.7.2) \quad \Gamma = D_t \times Q^2$$

Where D_t is the translational diffusion coefficient and Q is the scattering vector. The value of Γ can be obtained by appropriate fitting of the experimental correlation data and the diffusion coefficient thus calculated.

A digital correlator records the correlation functions. This is able to store successive samples of the signal, multiplies each old sample by the current signal as it is measured and accumulates the products in store channels. The change in value of the correlator coefficients measured by each channel is a characteristic of the fluctuation in the signal. In the case of polymer solutions where interactions with the solvent are present, the effect of concentration has to be taken into account by extrapolating the value of the translational diffusion coefficient to infinite dilution by equation 5(2.7.2).

$$5(2.7.2) \quad D_t = D_t^0(1 + k_D c + \dots)$$

Where k_D is the concentration slope constant of the diffusion coefficient. In most of the experimental cases the particles in solution are not monodisperse, so the correlation function will be given by a distribution of exponential functions that is better represented by the integral.

$$6(2.7.2) \quad F(\tau) = \int_0^\infty G(\Gamma) \cdot e^{-\Gamma\tau} d\Gamma$$

Where $G(\Gamma)$ is the decay rate function.

The solution of the integral in equation 6(2.7.2) is of fundamental importance for the study of dynamics of polydisperse particles and an enormous theoretical effort has been focused on different solution methods. One of the most generally used approaches in the case of polydisperse systems is the method of cumulants^{45,46}. In this method a moment-generating function is used and the logarithm of this function is expanded in a series to average over the scattering particles. The expansion assumes the form of equation 7(2.7.2).

$$7(2.7.2) \quad \frac{1}{2} \ln[G(\tau) - G(\infty)] = C_0 - K_1 \cdot \tau + \frac{1}{2!} K_2 \cdot \tau^2 - \frac{1}{3} K_3 \cdot \tau^3 + \dots$$

Where the coefficient K_1, K_2, K_3 etc are known as cumulants, $G(\infty)$ is the baseline and C_0 is the intercept. The relationship between the cumulants and the moment of the decay distribution rates is defined as follows.

$$8(2.7.2) \quad \begin{aligned} K_1 &= \langle \Gamma \rangle \\ K_2 &= \langle (\Gamma - \langle \Gamma \rangle)^2 \rangle \\ K_3 &= \langle (\Gamma - \langle \Gamma \rangle)^3 \rangle \end{aligned}$$

Normally only the first two cumulants are justified by the quality of the data. The first cumulant allows the calculation of translational diffusion coefficient.

2.8 Small-angle neutron scattering

In the study of polymer structure, neutron diffraction covers the same range of spatial resolution as X-ray diffraction but in the latter the probing radiation is scattered by electrons, neutrons are scattered by the nuclei. In a neutron scattering experiment, each scattering nucleus is considered to be source of a new scattering wave and the neutron scattering length defines the amplitude of the scattering wave compared with that of the incident wave.

A special factor is the large difference in scattering length of hydrogen and deuterium nuclei and this is of fundamental importance for development of neutron scattering techniques, because labelling with deuterium is less perturbative than other modifications.

If we consider the square of the scattering length amplitude, b , as the probability that a neutron will be scattered by a nucleus per incident neutron per unit solid angle, then the probability that a neutron will be scattered over all space is $4\pi b^2$ and this quantity is the coherent cross section indicated by σ . Since molecules are formed by several nuclei, the probability that an assembly of nuclei scatters a neutron is the sum of the scattering of the single nuclei. If the all nuclei in sample have the same value of b at any scattering angle, the probability of finding neutrons will depend on the sample structure; if the nuclei in the sample are randomly placed and have different scattering lengths, the scattered beam at any angle will have a mean amplitude determined by the sample structure together with random fluctuations. These fluctuations do not contribute to the scattering pattern defined by the structure and give rise to incoherent scattering. The incoherent scattering can arise from isotopes present in the sample but also from the differences in the neutron spin between the sample nuclei and the incident nuclei. In particular hydrogen has two very different scattering lengths for neutrons depending on its spin state and since the nuclear spin is generally not correlated with its position in the sample these scattering lengths give rise to spin incoherent scattering. Since hydrogen has a large incoherent scattering, in experiments dedicated to the structure determination this phenomenon forms a background that has to be subtracted from the cross section amplitude.

The quantity referred to as the scattering vector, Q , already defined in section 2.7 has dimensions of length^{-1} and normally is expressed in nm^{-1} or \AA^{-1} in neutron scattering experiments. For a steady-state source it is usual to vary Q by effectively scanning the

angle θ with a selected value of λ . On pulsed sources it is more common to use a constant θ mode and to obtain a range of Q values by time-sorting different wavelengths from a polychromatic incident beam as they arrive at the detector. Fixed-geometry instruments are ideal for studying systems where a range of length scales is involved, or where the relevant length scales are not known with certainty. On the other hand, steady-state source instruments are useful if the Q -range of interest is known.

In a small angle neutron scattering experiment a collimated radiation beam is focused on a sample illuminating a small volume, $V = A l$, where A is the area of the cross section of the beam and l is the path length of the sample. Some of the incident radiation is transmitted by the sample, some is absorbed and some is scattered. An area detector positioned at distance L , and scattering angle θ from the sample records the flux of radiation scattered into a solid angle element.

The objective of a small-angle neutron scattering experiment is to determine the differential scattering cross-section because this physical parameter contains all the information about the shape, size and possible solvent interactions of the scattering particles under investigation. The differential scattering cross-section is given by the equation 1(2.8).

$$1(2.8) \quad \frac{\partial \Sigma}{\partial \Omega}(Q) = N_p V_p^2 (\Delta \rho)^2 P(Q) S(Q) + B_{inc}$$

Where N_p is the number concentration of scattering particles, V_p is the volume of one scattering particle, $(\Delta \rho)^2$ is the contrast defined as the square of the difference in neutron scattering length between the particles and the surrounding environment, Q is the modulus of the scattering vector, B_{inc} is the background, $P(Q)$ is the form factor defined in equation 2(2.8) and $S(Q)$ is the interparticle structure factor defined in equation 3(2.8),

$$2(2.8) \quad P(Q) = \left\langle \sum_{i,j} b_i b_j \exp[iQ(r_i - r_j)] \right\rangle$$

$$3(2.8) \quad S(Q) = \frac{1}{N} \left\langle \sum_{i=1}^N \sum_{j=1}^N \exp[iQ(\bar{R}_i - \bar{R}_j)] \right\rangle$$

Where r_i and r_j are the position of vectors of the atoms in a particle; b_i and b_j are the scattering lengths of the atoms i and j ; the brackets are indicating that an average of all the orientations of the particles is taken into account. \bar{R}_i and \bar{R}_j are the vectors from the particles center and N is the total number of particles. The form factor is a function that describes how cross section is modulated through the interference effects between the radiations scattered and the different parts of the same scattering body and consequently is very dependent on the shape of the scattering body. Analytic expressions exist for most common shapes and expressions for more complex topologies can usually be deduced from these. The interparticle structure factor is modulated by interference effects between radiation scattered from different scattering bodies in the specimen and it is dependent on the degree of local order in the sample. The neutron scattering length density, ρ , is related to the bulk density of the molecule, δ , by the following formula.

$$4(2.8) \quad \rho = \frac{\delta \times N_A}{M} \sum_i b_i$$

Where N_A is the Avogadro's number and M is the molecular weight of the scattering unit. Since the small-angle neutron scattering experiment from a multi component sample is essentially a contrast-weighted summation of the scattering effects from each individual component, the technique of contrast matching can be used to simplify the scattering pattern. Therefore, the use of hydrogenated polymers in deuterated solvents or deuterated polymers in hydrogenated solvent is of great experimental interest.

For the study of polymer solutions it is important to understand the different Q domains. Since the scattering intensity as a function of Q is the Fourier transform of the pair distribution of scattering centres in the sample it is possible to say that the Q space is conjugated with the r space so when Q is small r is large⁴⁷.

In the low Q range the molecules can be interpreted as mass points and by counting the number of these points it is possible to obtain the molecular weight. So at $Q = 0$ it is possible to measure thermodynamic parameters but no structural information is obtained. If Q increases to the order of the mean square radius of gyration of the polymer in solution it is possible to have details about the shape, the structure and size of the macromolecules.

A common representation of the scattering profiles is the Kratky plot, where $Q^2(\Delta\Sigma/\Delta\Omega)$ versus Q is plotted and the shape of the curves obtained is characteristic of the form factor of the particular polymer. In figure 1(2.8) 2(2.8) and 3(2.8) the typical Kratky curve for a monodisperse coil of a linear chain, a series of star polymers with a different number of arms and branched polycondensate of the A_f -type and AB_f -type monomer are shown. The curves are calculated using the specific form factor functions⁴².

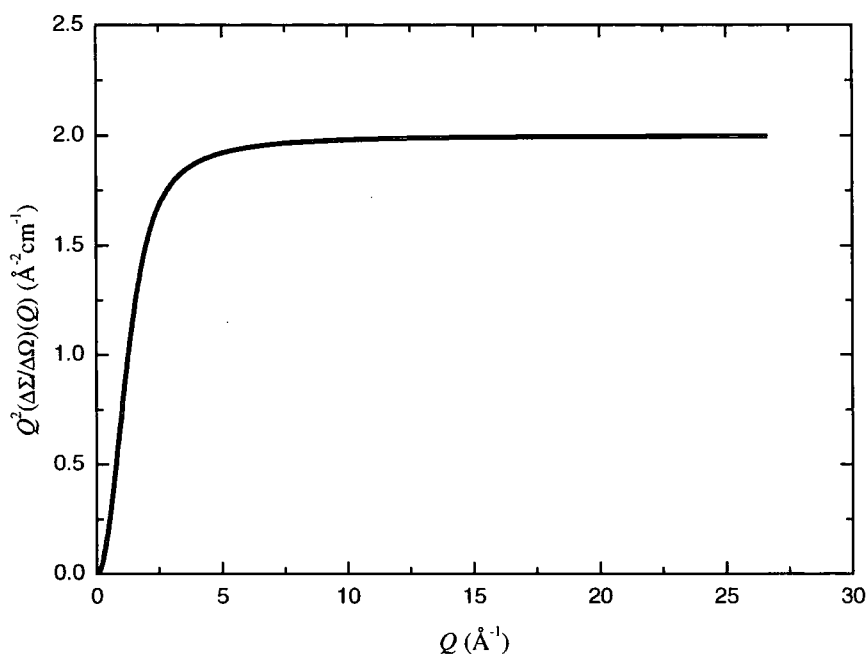


Figure 1(2.8). Typical Kratky plot for a monodisperse coil of a linear chain.

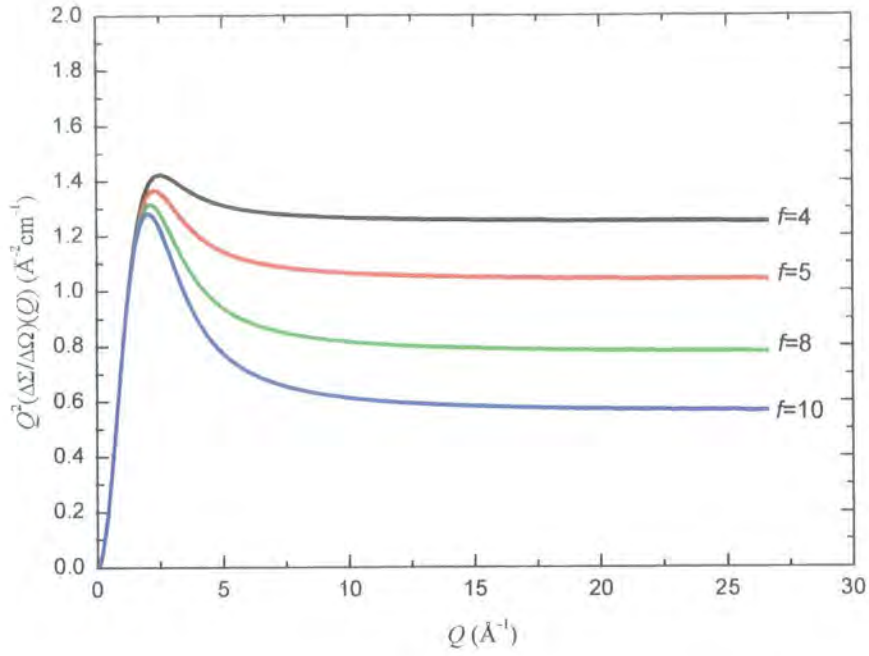


Figure 2(2.8). Typical Kratky plot for stars with different number of arms f .

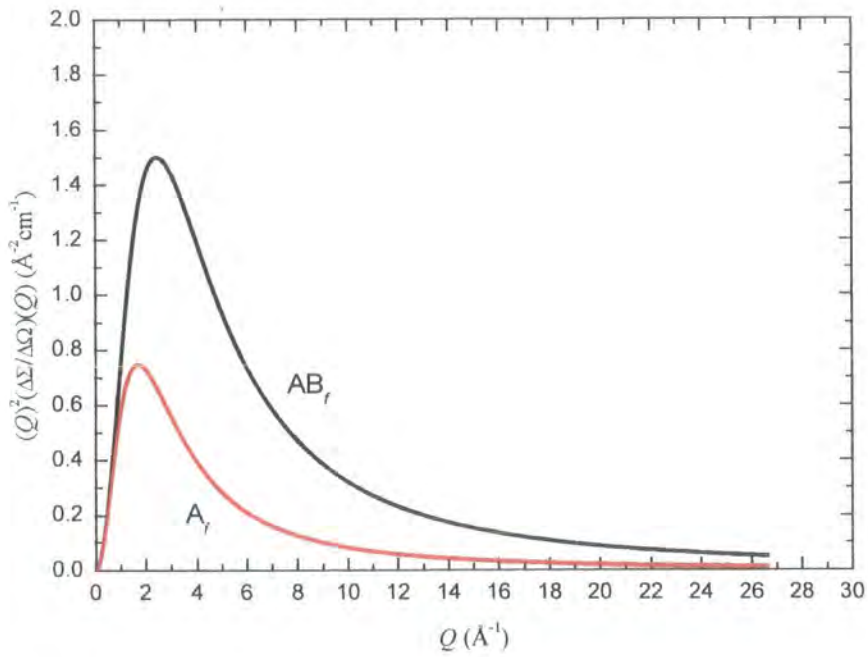


Figure 2(2.8). Typical Kratky plot for A_f and Ab_f polycondensate.

Over the past few years the number of experimental investigation of the hyperbranched and dendritic polymer by small-angle neutron scattering has increased as the interest in branched macromolecules also increased.

Ramzi et al.⁴⁸ conducted SANS experiments of poly(propyleneimine) dendrimer solutions in D₂O as a function of concentration and pH. They found that the scattering intensity decreases progressively on increasing the dendrimer concentration due to intermolecular interference. They also found that in the high Q -range, the all data set collapses on to a single curve indicating that the internal structure of the dendrimer is unaffected by interactions between neighbouring molecules. In a condition where the dendrimer molecules are charged, the electrostatic repulsion dominates and correlation peaks were observed indicating a spatial arrangement of the molecules in the polar medium. Therefore, from SANS experiments, it was possible to see how the macromolecules change from soft sphere behaviour to that of a hard particle. Zimmerman et al.⁴⁹ investigated the behaviour of tetra-acids and tetra-ester dendrimers in organic solvents and they found that hydrogen bond mediated self assembling dendrimers were formed depending on the concentration and the specific solvent polarity. Wu and Bauer⁵⁰ investigated the curing process of epoxies by SANS in bulk before the gelation threshold. Both the radius of gyration and the molecular weight of the partially cured molecular network were measured at various extents of cure.

The hyperbranched polyester investigated here will be analysed by SANS to obtain physical parameters; the details of the experimental procedure are given in section 3.9 and a discussion of the results in section 4.2.

References

1. Kienle, R. and Hovey, *J. Am. Chem. Soc.*, 1929. **51**: p. 509.
2. Carothers, *J. Am. Chem. Soc.*, 1929. **51**: p. 2566.
3. Flory, P., *Principles of polymer chemistry*. 1953: Cornell University Press, Ithaca, NY.
4. Flory, P., *J. Am. Chem. Soc.*, 1952. **74**: p. 2718.
5. Flory, P., *J. Am. Chem. Soc.*, 1941. **63**: p. 3091.
6. Stauffer, D., A. Coniglio, and M. Adam, *Adv. Polym. Sci.* 1982. **44**: p. 104.
7. Cram, D., *Science*, 1974. **183**: p. 803.
8. Lehn, J., *Science*, 1985. **227**: p. 849.
9. Suckling, C., *J. Chem. Soc. Chem. Commun.*, 1982: p. 661.
10. Hyatt, J., *J. Org. Chem.*, 1978. **43**: p. 1808.
11. Murakami, Y., *J. Chem. Soc., Perkin trans 1*, 1981: p. 2800.
12. Newcome, G., *J. Am. Chem. Soc.*, 1986. **108**: p. 849.
13. Tomalia, D., *Polym. J.*, 1985. **17**: p. 117.
14. Buhleier, E. and F. Vogtle, *Synthesis*, 1978: p. 155.
15. Tomalia, D., *Macromolecules*, 1986. **19**: p. 2466.
16. Vogtle, F., *Angew. Chem. Int. Ed. Engl.*, 1974. **13**: p. 814.
17. Frechet, J. and C. Hawker, *Synthesis and properties of dendrimers and hyperbranched polymers*. Compr. Polym. Sci. 2nd Suppl. ed. S.L. Aggarwal and S. Russo. 1996, Oxford: Pergamon Press plc.
18. Flory, P., *J. Am. Chem. Soc.*, 1947. **69**: p. 30.
19. Kienle, R. and F. Petke, *J. Am. Chem. Soc.*, 1940. **62**: p. 1053.
20. Gooden, J., *J. Am. Chem. Soc.*, 1998. **120**: p. 10180.
21. Turner, S. and B. Voit, *Macromolecules*, 1994. **27**: p. 1611.
22. Kim, Y. and O. Webster, *Macromolecules*, 1992. **25**: p. 5561.
23. Frechet, J., *Science*, 1994. **263**: p. 1710.
24. Kricheldorf, H. and O. Stober, *Macromol. Rapid. Commun.*, 1994. **15**: p. 87.
25. Feast, W.J. and N.M. Stainton, *J. Mater. Chem.* 1995. **5**(3): p. 405.
26. Hult, A. and E. Malmstrom, *J. Polym. Sci.: Part A Polym. Chem.* 1993. **31**: p. 619.
27. Massa, D.J., *et al.*, *Macromolecules*, 1995. **28**: p. 3214-3220.
28. Hult, A., M. Johansson, and E. Malmstrom, *Advances in polymer science*, 1999. **143**: p. 1-34.
29. Berbreiter, D., *Langmuir*, 1996. **12**: p. 5519.

30. Roberts, J., M. Bhalgat, and R. Zera, *J. Biomed. Mater. Res.*, 1996. **30**: p. 53.
31. Zimm, B.H. and W.H. Stockmayer, *J. Chem. Phys.*, 1949. **17**(12): p. 1301.
32. Drott, E. and R. Mendelson, *J. Polym. Sci.: Part A2*, 1970. **8**: p. 1361.
33. Bevington, J., J. Ebdon, and T. Huckerby, *NMR Spectroscopy of polymers Chapter 3*, ed. R.N. Ibbett. 1993: Blackie Academic & Professional.
34. Cheng, H., F. Schilling, and F. Bovey, *Macromolecules*, 1976. **9**: p. 363.
35. Hay, J., P. Mills, and R. Ognjanovic, *Polymer*, 1986. **27**: p. 677-680.
36. Hawker, C., R. Lee, and J. Frechet, *J. Am. Chem. Soc.*, 1991. **113**: p. 4583.
37. Holter, D. and H. Frey, *Acta Polymer.*, 1997. **48**: p. 30.
38. Barth, H. and J. Mays, *Modern methods of polymer characterisation Chapter 7*. Chemical Analysis, ed. J.D. Winefordner and I.M. Kolthoff. Vol. 113. 1991: John Wiley & Son.
39. Boyd, R. and P. Phillips, *The science of polymer molecules*. Cambridge Solid State Science. ed. E.A.D. D. Clarke, I.M. Ward. 1993. Cambridge University Press.
40. Bohdanecky, M. and J. Kovar, *Viscosity of polymers*. 1982: Elsevier.
41. Kratochvil, P., *Classical light scattering from polymer solutions*. 1987: Elsevier.
42. Burchard, W., *Applied fibre science*, ed. F. Happey. 1978: Academic Press.
43. Phillies, G., *J. Appl. Pol. Sci.: Appl. Polym. Symp.*, 1989. **43**: p. 275.
44. Flippen, R.B., *Photon correlation spectroscopy in: Modern methods of polymer characterisation*, ed. H.G. Barth and J.W. Mays. 1991: John Wiley & Sons Ltd.
45. Koppel, D., *J. Chem. Phys.*, 1972. **57**(11): p. 4814.
46. Phillies, G., *J Chem Phys*, 1988. **89**: p. 91-99.
47. Higgins, J. and H. Benoit, *Polymers and neutron scattering*. 1994: Clarendon Press-Oxford.
48. Ramzi, A. and R. Sherremberg, *Macromolecules*, 1998. **31**: p. 1621.
49. Zimmerman, S.C. and Thiyagarajian, *J. Mater. Chem.* 1997. **7**: p. 1221.
50. Wu, W. and B. Bauer, *Polymer*, 1989. **30**: p. 1384-1388.

Chapter 3

Experimental results

3.1 Materials

Dimethyl 5-(4 hydroxybutoxy) isophthalate. Synthesised in the laboratory.

Antimony (III) oxide 99.99 %. Aldrich Fine Chemicals.

Manganese (II) acetate 98 %. Aldrich Fine Chemicals.

Triphenyl phosphate 99 %. Aldrich Fine Chemicals.

4-Bromobutyl acetate 99 %. Aldrich Fine Chemicals.

Titanium butoxide 99 %. Aldrich Fine Chemicals.

Anhydrous potassium carbonate. 99+ % Aldrich Fine Chemicals.

Potassium hydroxide. Fisher Chemicals.

Magnesium sulfate 99 %. Aldrich Fine Chemicals.

Chloroform. 99.8 % Fisher Chemicals.

Dichloromethane. 99.8 % Fisher Chemicals.

Anhydrous methanol. 99.9 % Fisher Chemicals refluxed with magnesium powder.

Acetone 99.8 %. Fisher Chemicals treated with 3A molecular sieve.

Hexane 99.8 %. Fisher Chemicals.

1M Hydrochloric acid by dilution of 32% hydrochloric acid Fisher Chemicals.

Tetrahydrofuran anhydrous 99.9%. Aldrich Fine Chemicals.

Tetrahydrofuran-D8 99.5% atom D. Apollo Scientific limited.

Chloroform-D 99.8 atom D. Apollo Scientific limited.

3.2 Syntheses

3.2.1 Synthesis of the hyperbranched polyester

The monomer is dimethyl 5-(4-hydroxybutoxy) isophthalate and its chemical structure is shown in figure 1(3.2.1). It is a typical AB₂ unit that leads, by polycondensation, to the related hyperbranched polyester. Feast et al.¹ have already described the polymerisation of this monomer.

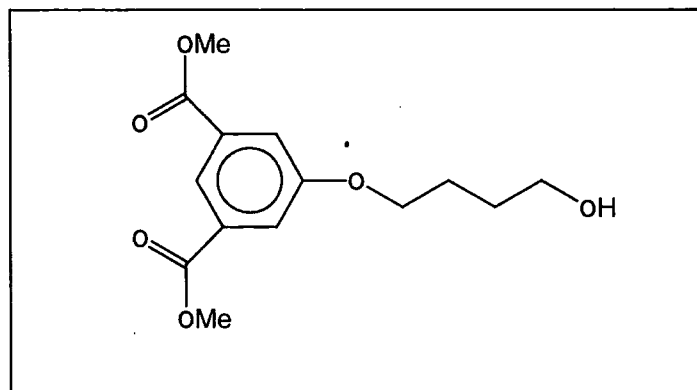


Figure 1(3.2.1). *Dimethyl 5-(4-hydroxybutoxy) isophthalate*

In the bulk polymerisation of the monomer, large changes in viscosity are encountered during the reaction. For effective mixing throughout the reaction, efficient stirring is important in this kind of polymerisation. The polycondensation reaction was carried out using the apparatus schematically shown in figure 2(3.2.1). In this reaction vessel, the space between the stirrer blades and the vessel walls is small (~2mm) to facilitate intimate mixing. An IKA Eurostar mechanical stirrer with a stirrer rod held in place by a rubber seal inserted into the glass gland rotates the stainless stirrer at 125 r.p.m.

The stirrer and reaction vessel were securely clamped onto a stable stand to ensure that there is no twisting or misalignment during the reaction. The reaction time and temperature was controlled by using a Eurotherm temperature controller with thermocouples and a 1kW heating band surrounding the oil bath.

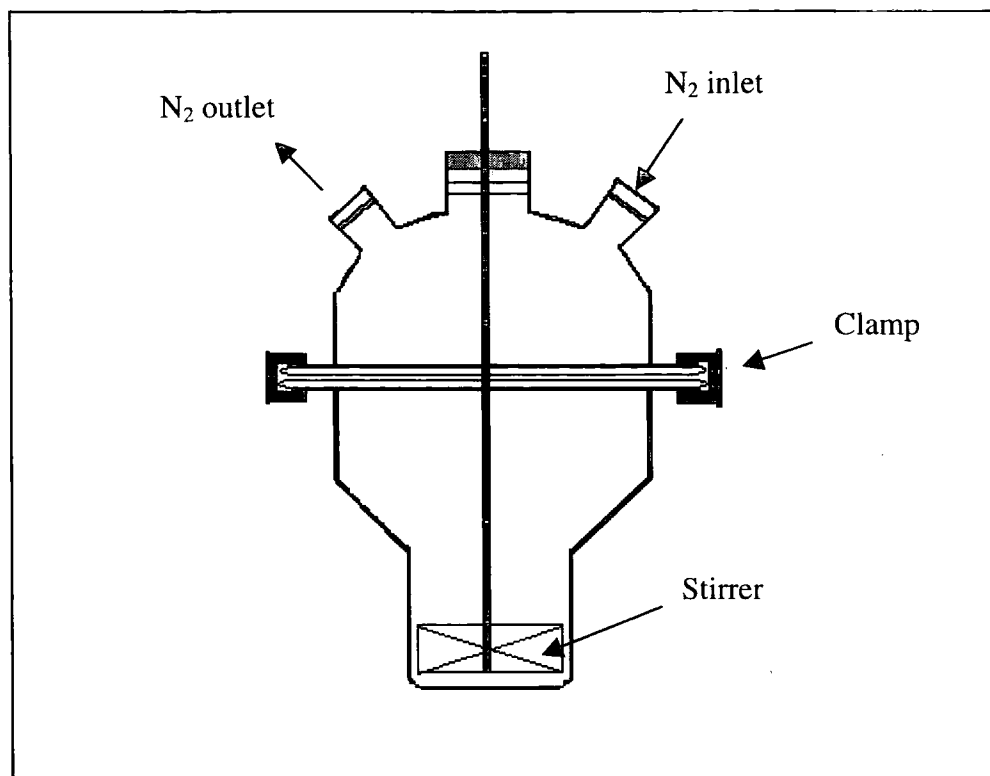


Figure 2 (3.2.1). Schematic picture of reaction vessel.

Dimethyl 5-(4-hydroxybutoxy) isophthalate (20g, 0.709 mol) was introduced into the reaction vessel with the catalysts, antimony (III) oxide (15.5 mg , 0.075 % mol), manganese (II) acetate (13.3 mg , 0.107 % mol) and the thermal degradation inhibitor triphenyl phosphate (11.1 mg, 0.048 % mol). Whilst stirring the solid monomer under a flow of nitrogen, the reaction flask was placed in an oil bath. The oil bath was heated from room temperature to 583 K at 10 degrees per minute and the reaction was carried out for 15 hours. After this time, the nitrogen flow was switched off and the reaction mixture cooled to room temperature. The mixture solidified to a brown glass that was dissolved in chloroform (200 ml), and this solution added drop wise from a separating funnel to a large excess of methanol (600 ml). The precipitated polymer was collected by filtration and dried under vacuum at room temperature to give a white powder with a mass of about 45 grams.

Thermo gravimetric analysis shows that the polymer is reasonably stable, having a weight loss of 2% at 454 K, differential scanning calorimetry shows a typical glass transition at 307.8 K as shown in Figure 3(3.2.1).

Size exclusion chromatography in chloroform by triple detector gave $\overline{M}_w = 137 \times 10^3 \text{ g mol}^{-1}$. $\overline{M}_n = 20 \times 10^3 \text{ g mol}^{-1}$. The data obtained by SEC will be discussed in detail in section 3.4.

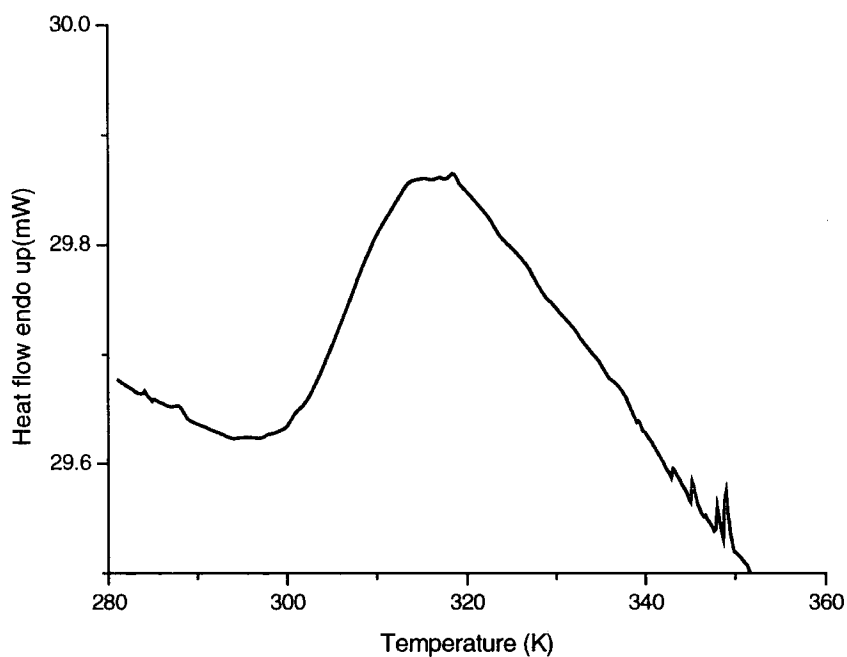


Figure 3(3.2.1). Typical DSC for the hyperbranched polyester.

3.2.2 Synthesis of the analogous linear monomer

The synthesis of the AB linear monomer was performed in two steps. The first was the synthesis of the methyl 3-(4-acetoxybutoxy) benzoate and the second was the hydrolysis of the acetate to give the desired product as shown in Figure 1(3.2.2).

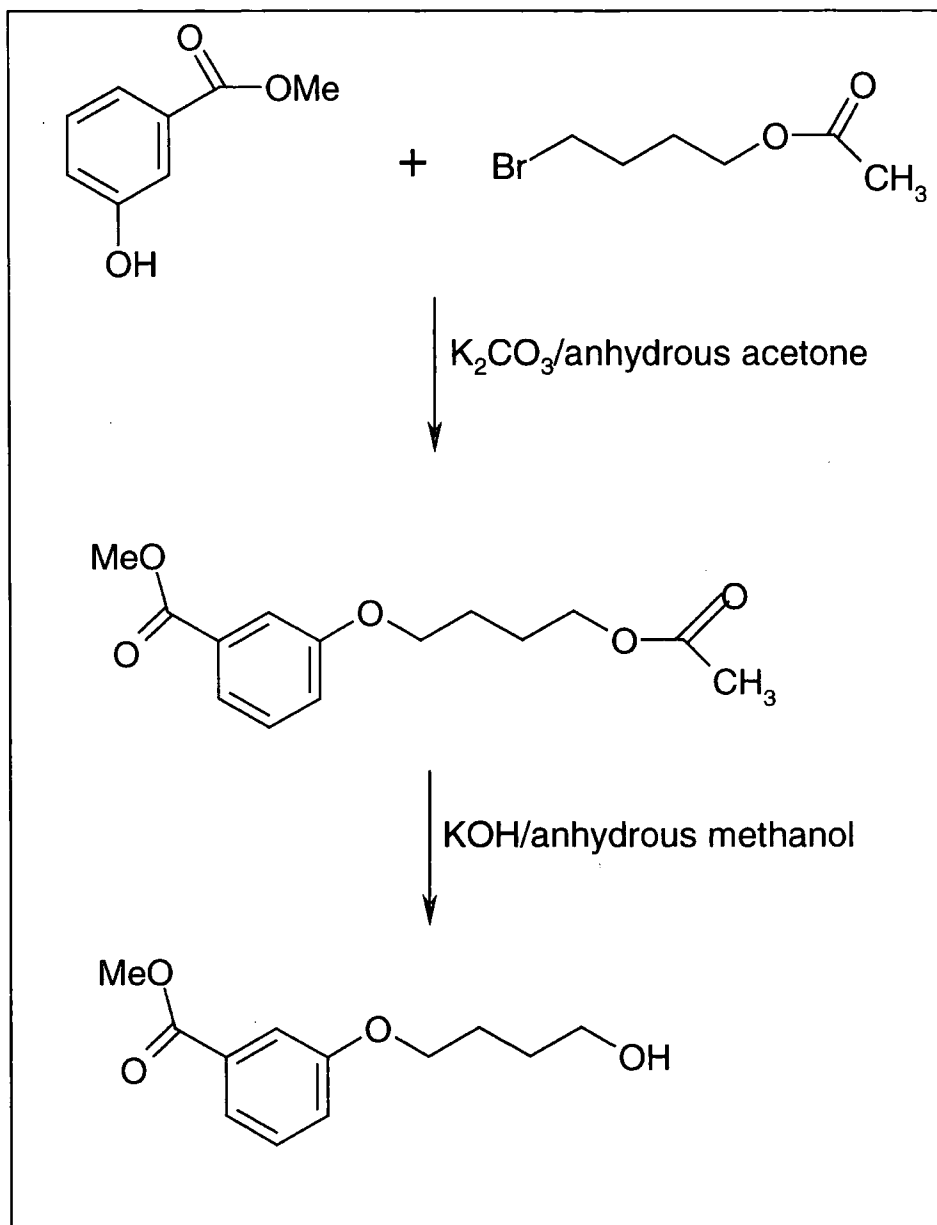


Figure 1(3.2.2). Reaction steps for the synthesis of the linear analogous monomer.

3.2.2.1 Synthesis of methyl 3-(4-acetoxybutoxy) benzoate

Methyl 3-hydroxy benzoate (47 g, 0.31 mol), 4-bromobutyl acetate (72 g, 0.37 mol) and a suspension of anhydrous potassium carbonate (42.8 g, 0.31 mol) in anhydrous acetone (1l) were charged into 2 liters, 3 necked round-bottomed flask with a magnetic stirrer and thermometer and reflux condenser with a calcium chloride drying tube on the top. The reaction mixture was stirred under reflux for 120 hours.

After the reaction mixture was cooled to room temperature, it was filtered and the residue washed with acetone. The acetone solution was collected and the acetone evaporated under reduced pressure to yield pale brown oil. The mixture was distilled under vacuum (1mm Hg) to give the product (methyl 3-(4-acetoxybutoxy) benzoate as colorless oil,

B.p. = 423 ± 2 K (1mm Hg).

Elemental analysis: experimental C 63.06 %; H 6.67%. Calculated for $C_{14}H_{18}O_5$, C 63.15%; H 6.76%.

$^1\text{H-NMR}$ (CDCl_3 400 MHz); δ 1.78 (4H, $\text{CH}_2\text{CH}_2\text{CH}_2\text{CH}_2$), δ 1.98 (3H, $\text{CH}_3\text{-C=O}$), δ 3.83 (3H, OCH_3), δ 3.95 (2H, ArOCH_2), δ 4.07 ($\text{CH}_2\text{O-C=O}$), δ 7.0, 7.26, 7.47, 7.53 (4H, Ar-H).

$^{13}\text{C-NMR}$ (CDCl_3 , 100 MHz); δ 20.71 ($\text{CH}_3\text{-C=O}$), δ 25.13, 25.58 (CH_2), δ 51.91 (ester OCH_3), δ 63.82 ($\text{CH}_2\text{O-C=O}$), δ 67.22 (ArOCH_2), δ 114.35, 119.64, 121.72, 129.17 (aromatic C-H), δ 131.17 (aromatic C-COOCH₃), δ 158.65 (aromatic C-O), δ 166.66 (ester C=O), δ 170.86 (acetate C=O).

IR (liquid); 3109 cm^{-1} (aryl-H C-H stretch), 2952 cm^{-1} (saturated C-H stretch), 1741 cm^{-1} (aliphatic C=O stretch), 1723 cm^{-1} (aromatic C=O stretch), 1586 cm^{-1} (aryl-H C-H bend), 1445 cm^{-1} (saturated C-H bend), 1245 cm^{-1} (aryl C-O stretch).

MS (EI+); 266(M), 152 (M-(CH_2)₄OC(O)CH₃+H), 121 (M-(CH_2)₄OC(O)CH₃-OCH₃+H), 115 (M-(CH₃OC=O)C₆H₃O).

See Appendix A for full details of ^1H and ^{13}C NMR, IR, MS spectra of methyl 3-(4-acetoxybutoxy) benzoate.

3.2.2.2 Synthesis of methyl 3-(4-hydroxybutoxy) benzoate

Methyl 3-(4-acetoxybutoxy) benzoate (46.1 g, 0.17 mol), potassium hydroxide (0.38 g, 0.007 mol) and anhydrous methanol (0.5 l.) were charged into a 1 litre, 2 necked round bottomed flask equipped with a thermometer, magnetic stirrer and reflux condenser with calcium chloride drying tube. The reaction mixture was stirred and heated at 303 K for 18 hours, then acidified to pH 1 with aqueous hydrochloric acid solution (1M) and the methanol removed under reduced pressure. The resulting oil was dissolved in dichloromethane (200 ml) and the mixture washed with distilled water (4×500 ml).

The combined organic extract was dried with magnesium sulphate, filtered and the solvent removed under reduced pressure to yield methyl 3-(4-hydroxybutoxy) benzoate (71.58 %, 33 g).

Elemental analysis: experimental C 63.90 %; H 7.03%. Calculated C 64.28%; H 7.14%.

$^1\text{H-NMR}$ (CDCl_3 , 400 MHz); δ 1.75 (2H, HOCH_2CH_2 and 1H OH), δ 1.89 (2H, $\text{ArOCH}_2\text{CH}_2$), δ 3.72 (2H, CH_2OH), δ 3.89 (3H, OCH_3), δ 4.03 (2H, ArOCH_2), δ 7.00-7.60 (4H, Ar-H).

$^{13}\text{C-NMR}$ (CDCl_3 , 100 MHz). δ 25.65 (HOCH_2CH_2), 29.32 ($\text{ArOCH}_2\text{CH}_2$), δ 52.15 (ester OCH_3), δ 62.43 (CH_2OH), δ 67.88 (ArOCH_2), δ 114.57, 119.87, 121.92, 129.35 (aromatic C-H), δ 131.31 (aromatic C-COOH₃), δ 158.79 (aromatic C-O), δ 166.98 (ester C=O).

IR (liquid); 3397 cm^{-1} (broad O-H stretch), 3189 cm^{-1} (aryl-H C-H stretch), 2950 cm^{-1} (saturated C-H stretch), 1722 cm^{-1} (aliphatic C=O stretch), 1585 cm^{-1} (aryl-H C-H bend), 1445 cm^{-1} (saturated C-H bend), 1245 cm^{-1} (aryl C-O stretch).

MS (EI+); 224(M), 193 (M-OCH₃), 152 (M-(CH₂)₄OH+H), 121 (M-(CH₂)₄OH-OCH₃+H).

See Appendix B for full details of ^1H and ^{13}C NMR, IR, MS spectra of methyl 3-(4-hydroxybutoxy) benzoate.

3.2.3 Polymerisation of Methyl 3-(4-hydroxybutoxy) benzoate

Methyl 3-(4-hydroxybutoxy) benzoate (20 g, 0.089 mol), the catalysts antimony (III) oxide (19.5 mg, 0.075 % mol), manganese (II) acetate (16.4 mg, 0.107 % mol) and the thermal degradation inhibitor triphenyl phosphate (13.9 mg, 0.048 % mol) were introduced into the reaction vessel shown in Figure 2(3.2.1)

Whilst stirring (~120 rpm) the monomer under a flow of nitrogen, the reaction flask was placed in an oil bath. The oil bath was heated from room temperature to 583 K at 10 degrees per minute and the polymerisation carried out for 15 hours. The reaction mixture was cooled at room temperature to give a white solid that was dissolved in chloroform. The chloroform solution was poured into a large amount of hexane to precipitate the polymer (Linear 4) that was collected by filtration and dried under vacuum.

Thermo gravimetric analysis gave a 2% weight loss at 613 K, differential scanning calorimetry analysis showed the following glass transition, T_g , crystallization, T_c and melt transition, T_m .

T_g at 279.1 K, T_c at 323.3 K, T_m at 397.9 K as it is shown in Figure 1(3.2.3)

Size exclusion chromatography in chloroform by triple detector gave $M_w = 6.3 \times 10^3$ g mol^{-1} . $M_n = 4.4 \times 10^3$ g mol^{-1} .

$^1\text{H-NMR}$ (CDCl_3 , 400 MHz); broad peak δ 1.09 (2H, HOCH_2CH_2 and 1H OH ; 2H, $\text{ArOCH}_2\text{CH}_2$), δ 3.82 (2H, CH_2OH), δ 3.98 (3H, OCH_3), δ 4.31 (2H, ArOCH_2), δ 6.99-7.55 (4H, Ar-H).

$^{13}\text{C-NMR}$ (CDCl_3 , 100 MHz); δ 25.47 (HOCH_2CH_2) 25.88 ($\text{ArOCH}_2\text{CH}_2$), δ 64.63 (CH_2OH), δ 67.44 (ArOCH_2), δ 114.70, 119.69, 121.89, 129.37 (aromatic C-H), δ 131.53 (aromatic C-COOH), δ 158.79 (aromatic C-O), δ 166.98 (ester C=O).

IR (KBr disc); 2950 cm^{-1} (saturated C-H stretch), 1708 cm^{-1} (aliphatic C=O stretch), 1585 cm^{-1} (aryl-H C-H bend), 1445 cm^{-1} (saturated C-H bend), 1286 cm^{-1} (aryl C-O stretch).

3.2.4 Linear polyester transesterification

With the aim of obtaining different higher molecular weights for the linear polyester, the transesterification reaction was applied to a sample of the linear polymer. The first experiment was heating the linear polyester at 538 K under vacuum of 1 mm Hg for 4 hours (Linear 3). Two similar experiments were carried out using 5 mg of titanium butoxide as catalyst at 473 K under vacuum of 1 mmHg and a reaction time of 30 min and 60 min respectively (Linear 2, Linear1).

Differential scanning calorimetry (Figure 1(3.2.4) shows small differences in the crystallisation and melting temperature onset as shown in table 1(3.2.4). The data regarding the molecular weight determination will be discussed in section 3.4 and 3.5.

Table 1(3.2.4). DSC results for the linear polyester samples.

Linear	T_g (K)	T_c (K)	T_m (K)
3	283.2	319.6	400.5
2	284.5	326.4	395.9
1	285.7	328.0	398.6

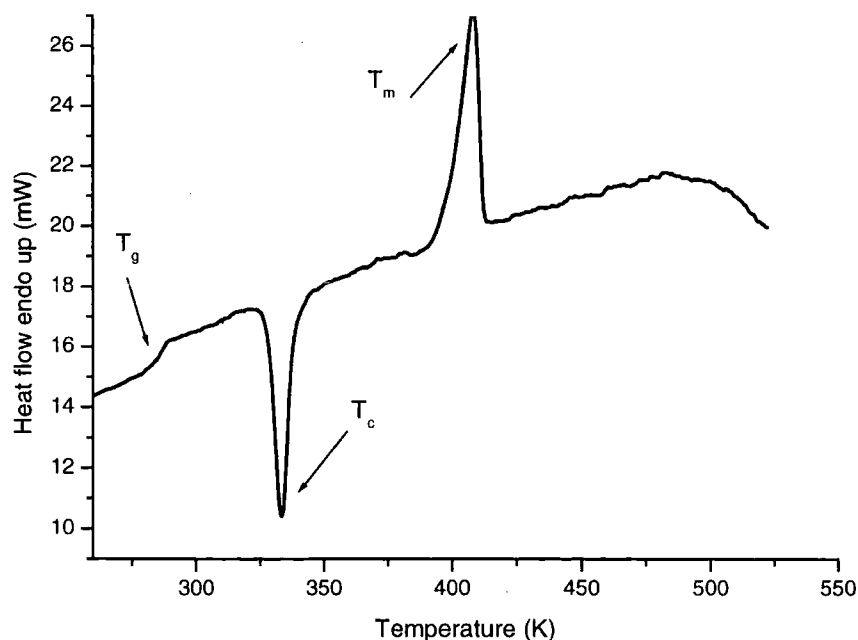


Figure 1(3.2.4). DSC trace for the linear 4.

3.3 Fractionation

The fractionation of poly dimethyl 5-(4-hydroxybutoxy) isophthalate was carried out by the addition of a non-solvent to a solution of the polymer. The polymer was dissolved in toluene and the non-solvent used was methanol.

A 5% w/v solution was placed in a two necked separating funnel inserted into a thermostatic bath with mechanical stirrer and heating control. A dropping funnel was placed in one neck, whilst the stirrer entered through the second neck (figure 1(3.3)).

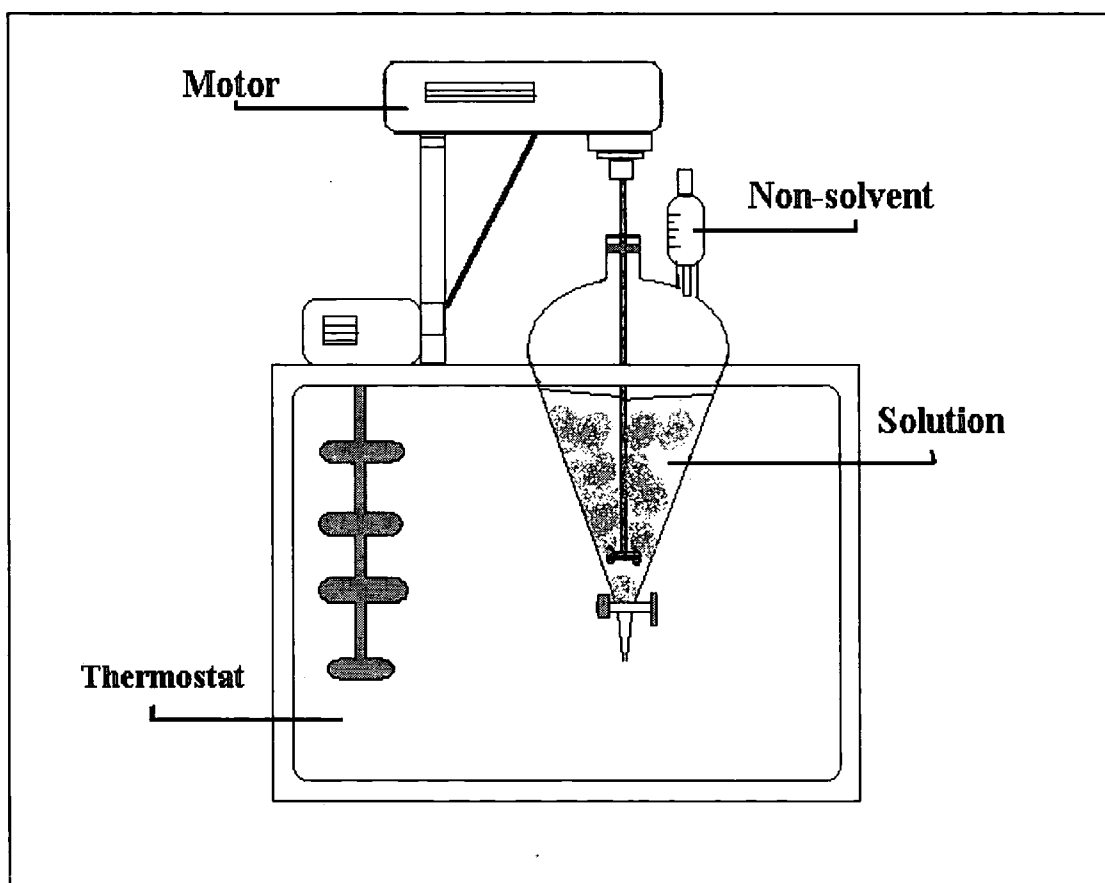


Figure 1(3.3). *Schematic apparatus for the fractionation.*

The non-solvent was added to the stirred solution with the bath temperature at 303 K. As soon as turbidity appeared, addition of non-solvent was ceased. The temperature was then increased to 308 K until the solution became clear again and then allowed to cool slowly to 303 K with the stirrer switched off to allow the phase separation.

After this time two separated phases were evident and the lower phase was withdrawn using a syringe with a long needle. This procedure was used to prevent possible precipitation of more material on removing the separating funnel from the bath.

The collected fractions were then dissolved in toluene, precipitated in a large amount of methanol and dried in vacuum. The same procedure was used for all fractions except the last one, which was collected by evaporation of the solvent mixture. The numbers given to the fractions correspond to the order they were precipitated from the starting material as shown in table 1(3.3).

Table 1(3.3). *Non-solvent additions and the amount of polymer obtained in the fractionation.*

Sample	Methanol (ml)	Amount (g)
1	148	3.7
2	2	1.8
3	6	1.4
4	2	0.9
5	8	1.5
6	10	2.1
7	10	1.4
8	10	0.8
9	14	0.8
10	26	1.2
11	70	0.8
12	Solvent evap.	0.6
Total		17.0

In figure 2(3.3) are shown the SEC traces of the first six fractions.

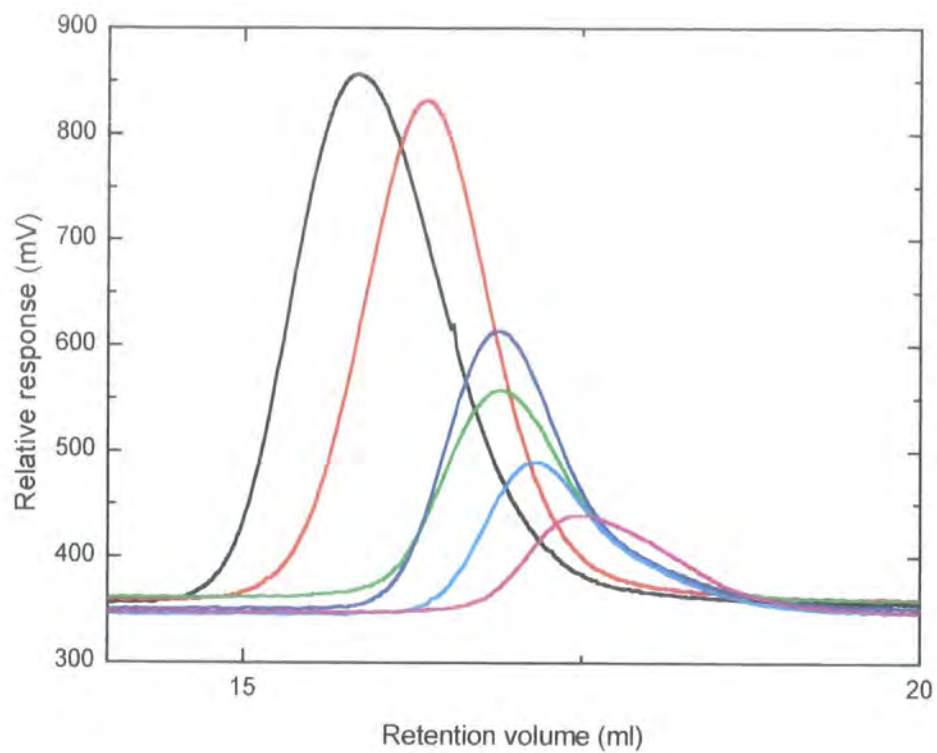


Figure 2(3.3). *Chromatograms of the first six hyperbranched fractions.*

3.4 SEC data

Size exclusion chromatography, SEC, was performed in THF and chloroform. Both the instruments had a triple detector (differential refractometer, differential viscometer and a right angle laser light scattering detector working at 670 nm connected in series). For each instrument the working temperature was 303 K with a mobile phase nominal flow rate of 1 ml min^{-1} . The separation was achieved across a bank of 3 gel columns with a porosity range of 10^2 to 10^5 \AA .

Chloroform SEC

The response of the refractive index detector for the unfractionated hyperbranched polyester shows a large polydispersity and a bimodal distribution, figure 1(3.4).

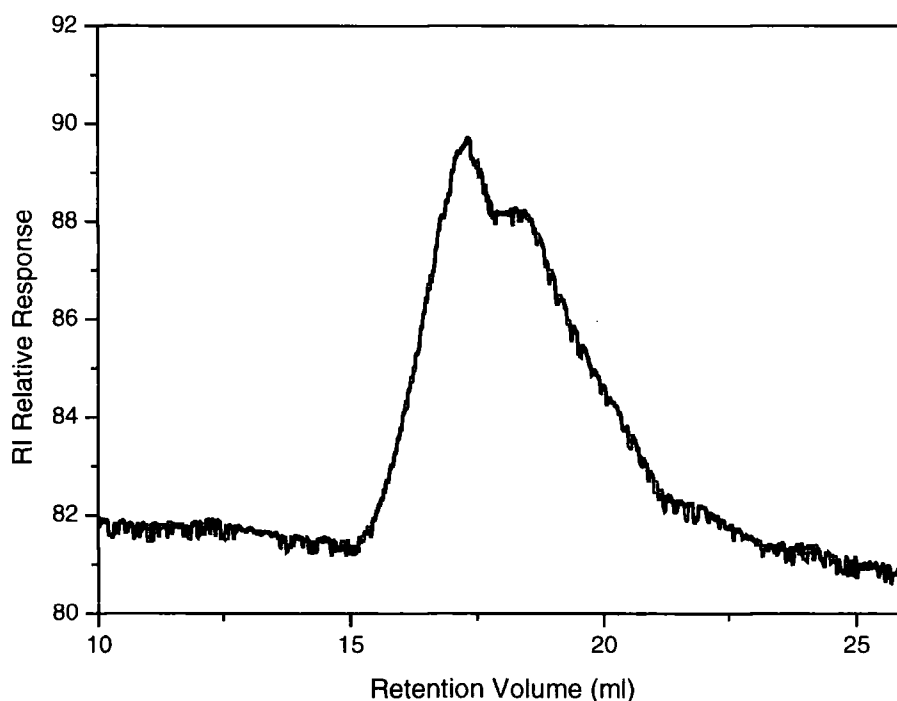


Figure 1(3.4). *RI detector response; unfractionated hyperbranched polyester.*

For a correct analysis by the light scattering detector, the experimental specific refractive index of the hyperbranched polymer in chloroform was experimentally determined for different wavelengths (633 nm, 546 nm, 488 nm and 436 nm), the dn/dc for 670 nm was obtained by extrapolation of a Cauchy dispersion plot (Figure 2 (3.4)), a value of $0.104 \pm 0.002 \text{ cm}^3 \text{ g}^{-1}$ being obtained.

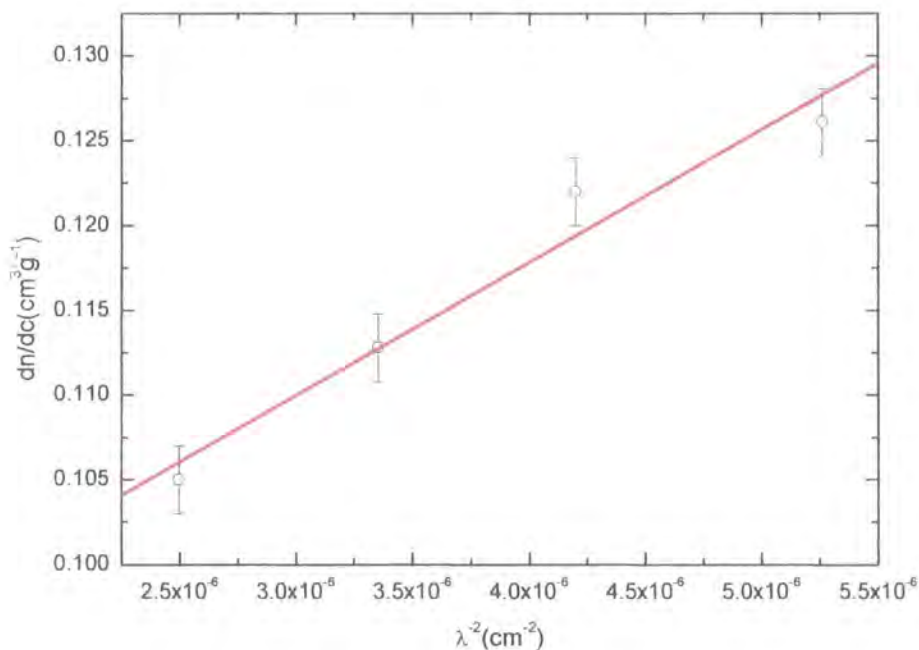


Figure 2(3.4). Dispersion plot; hyperbranched polyester in chloroform.

A typical chromatogram obtained by the right angle light angle detector for the unfractionated polymer is shown in Figure 3a(3.4) and for fraction 2 in Figure 3b (3.4).

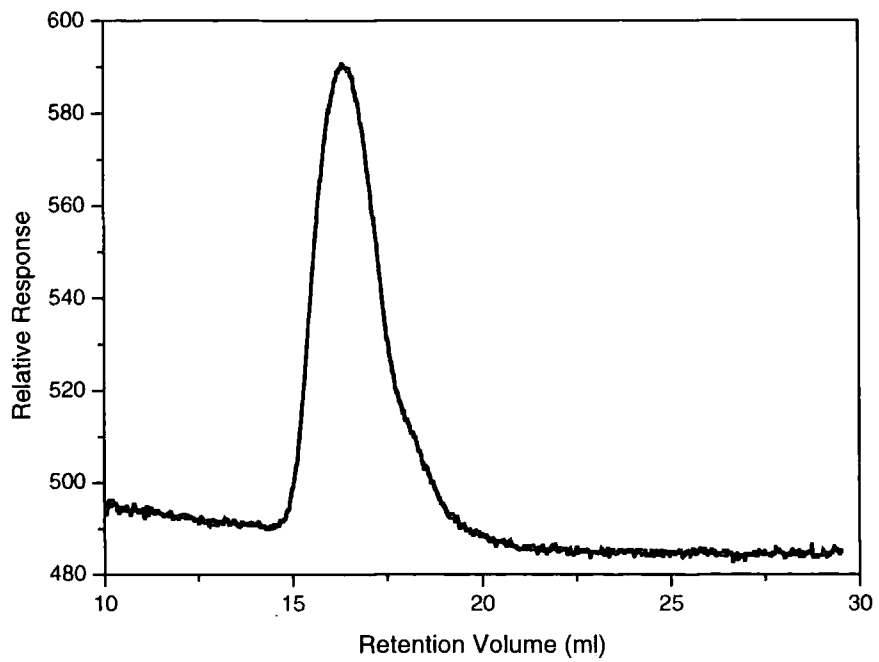


Figure 3a(3.4). *Light scattering detector; unfractionated hyperbranched material.*

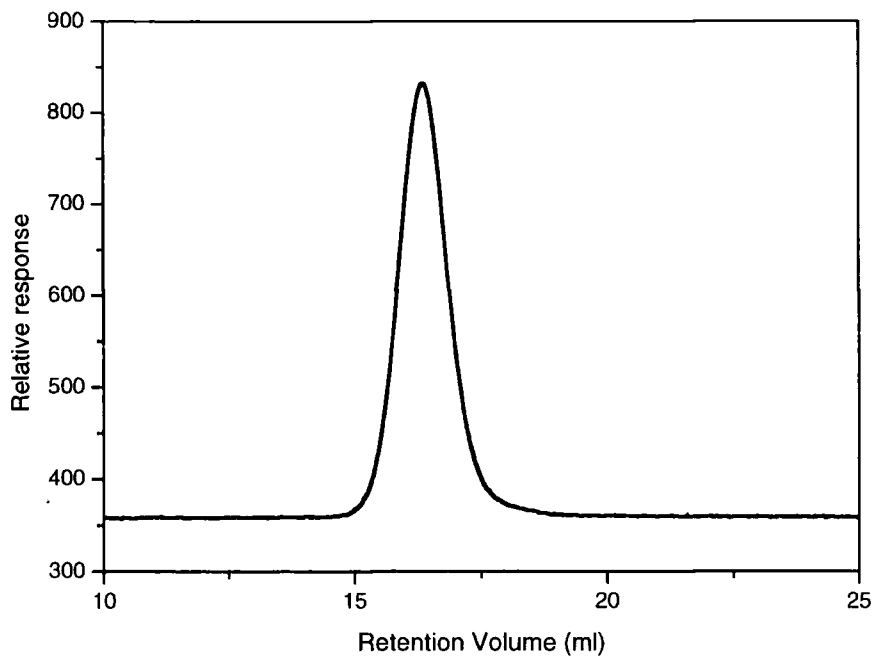


Figure 3b(3.4). *Light scattering detector; hyperbranched fraction 2.*

All data obtained in chloroform are presented in table 1(3.4) the unfractionated material is fraction 0. The intrinsic viscosity refers to the values obtained by the viscosity detector. The polydispersity is indicated with Pd.

Table 1(3.4). SEC data; hyperbranched fractions in chloroform.

Sample	\overline{M}_n (g mol ⁻¹)	\overline{M}_w (g mol ⁻¹)	\overline{M}_z (g mol ⁻¹)	Pd	$[\eta]$ (ml g ⁻¹)
0	20 200	137 200	319 800	6.8	29.3
1	102 300	452 800	818 600	4.4	54.5
2	130 500	316 300	538 300	2.4	48.5
3	92 700	149 100	208 100	1.6	36.5
4	71 700	134 200	183 300	1.8	34.2
5	45 900	100 300	137 200	2.1	31.9
6	50 700	75 900	99 700	1.5	28.8
7	44 400	62 900	84 900	1.4	25.6
8	30 400	45 800	58 500	1.5	23.5
9	27 900	35 200	42 900	1.2	20.6
10	16 800	21 500	26 100	1.2	16.9
11	9 610	13 400	18 300	1.3	13.8
12	3 810	5 590	7 700	1.4	9.2

The chloroform SEC was used to analyse the linear polyester, also in this case the experimental differential refractive index was measured for different wavelength and the value for 670 nm extrapolated. In this case the dn/dc at 303 K is $0.114 \pm 0.002 \text{ cm}^3 \text{ g}^{-1}$. The results are given in table 2(3.4) and an example of the chromatogram obtained for the linear polyester is given in figure 3c(3.4).

Table 2(3.4). SEC data; linear polyester in chloroform.

Linear	\overline{M}_n (g mol ⁻¹)	\overline{M}_w (g mol ⁻¹)	\overline{M}_z (g mol ⁻¹)	Pd	$[\eta]$ (ml g ⁻¹)
1	22 100	51 000	94 100	2.3	42.7
2	14 600	27 200	53 500	1.8	24.4
3	9 200	12 100	16 300	1.3	27.6
4	5 400	7 400	10 300	1.3	14.8

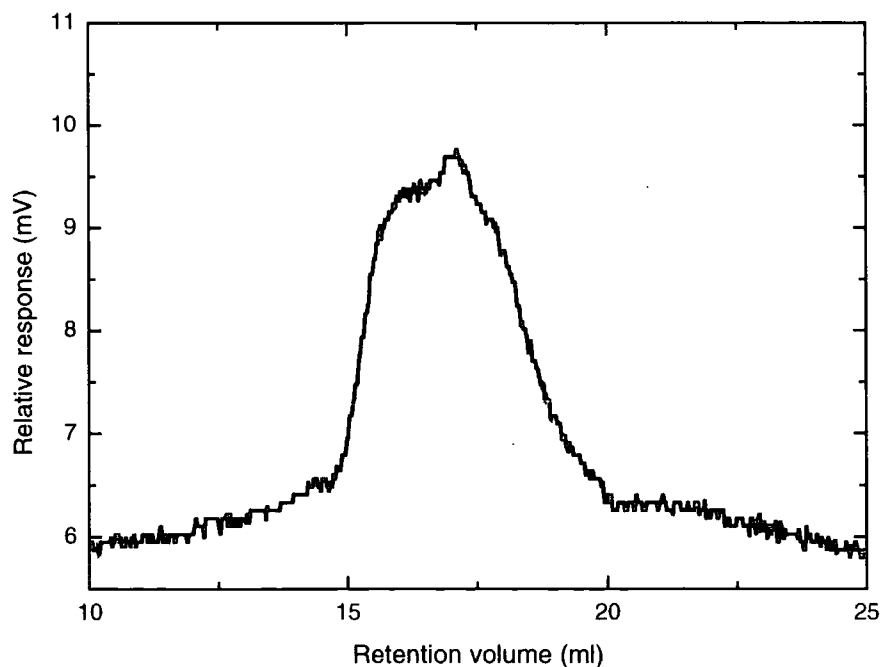


Figure 3c(3.4). Light scattering detector trace for the linear1.

Tetrahydrofuran SEC

The SEC analysis in THF of the highest molecular weight fractions of the hyperbranched polymer showed an additional peak in the higher molecular weight area of the chromatogram (Figure 4(3.4)). The dn/dc value for the hyperbranched polymer in THF at 670 nm was $0.143 \pm 0.002 \text{ cm}^3 \text{ g}^{-1}$.

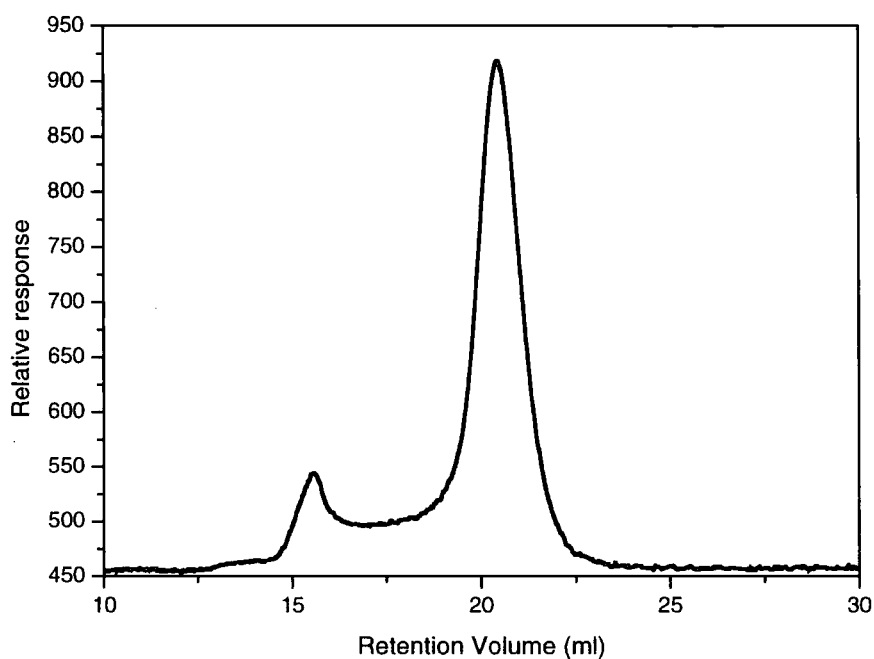


Figure 4(3.4). *Light scattering detector; hyperbranched fraction 2.*

The second peak in the higher molecular weight region could be due to some aggregate formed in the elution process. Since the aggregation process should be concentration dependent, some chromatograms at different dilutions were collected and compared as shown in figure 4a(3.4).

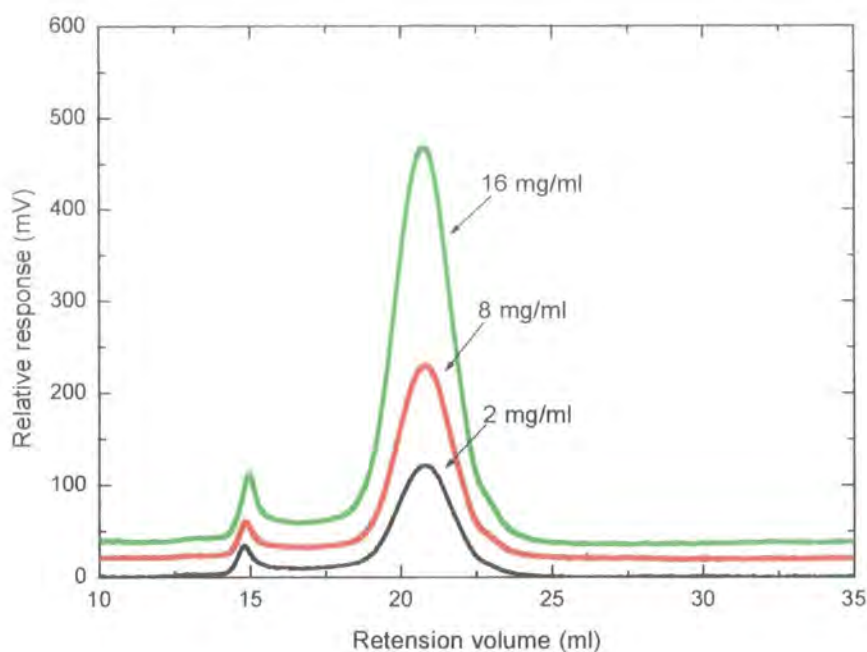


Figure 4a(3.4). *Light scattering detector trace for different concentrations.*

The expected situation would be a decrease of the second peak with the dilution, but from the comparison of the chromatograms the relative intensity of the two peaks does not change with dilution. Since the hypothesis of aggregation cannot be proved, it may be possible that some other process caused the second peak like interaction with the packing material of the column.

The data from THF SEC are given in table 3(3.4). Where a double peak was present, only the main peak has been analysed. Even with this restriction the polydispersities obtained are larger than those obtained from chloroform SEC.

Table 3(3.4). SEC data; hyperbranched fractions in THF.

Sample	\overline{M}_n (g mol ⁻¹)	\overline{M}_w (g mol ⁻¹)	\overline{M}_z (g mol ⁻¹)	Pd	$[\eta]$ (ml g ⁻¹)
0	16 000	132 000	502 600	8.2	21.2
1	76 200	412 100	1 211 000	5.4	30.9
2	61 100	261 400	676 500	4.2	27.5
3	38 200	175 000	312 000	4.5	24.7
4	51 700	154 400	233 100	2.9	23.9
5	49 900	127 300	181 900	2.5	22.6
6	36 100	93 700	131 800	2.6	20.6
7	36 200	65 400	84 800	1.8	16.2
8	28 300	51 800	68 000	1.8	17.5
9	28 100	41 300	50 400	1.5	16.7
10	22 300	30 500	37 000	1.4	15.1
11	13 800	18 200	22 400	1.3	11.5
12	8 900	11 600	14 900	1.3	10.2

Because of the poor polymer-solvent interaction in THF, the data obtained by SEC in THF are not considered reliable; in fact the first requisition to have size exclusion chromatography is the perfect solubility and in this case this is not verified.

3.5 Degree of branching

One of the methods to calculate the degree of branching of a hyperbranched polymer is based on NMR spectroscopy and relies on the possibility of distinguishing discrete resonance for the three sub-unit: terminal (*T*), linear (*L*) and branched (*B*).

The integration of these peaks allows the determination of the relative percentage of each sub-unit and these percentages can be used in the degree of branching formula 1(2.5) and 6(2.5). Quantitative ^{13}C -NMR has been used to calculate the degree of branching of the hyperbranched polyester and the aromatic carbon atoms taken into consideration are indicated in Figure 1(3.5).

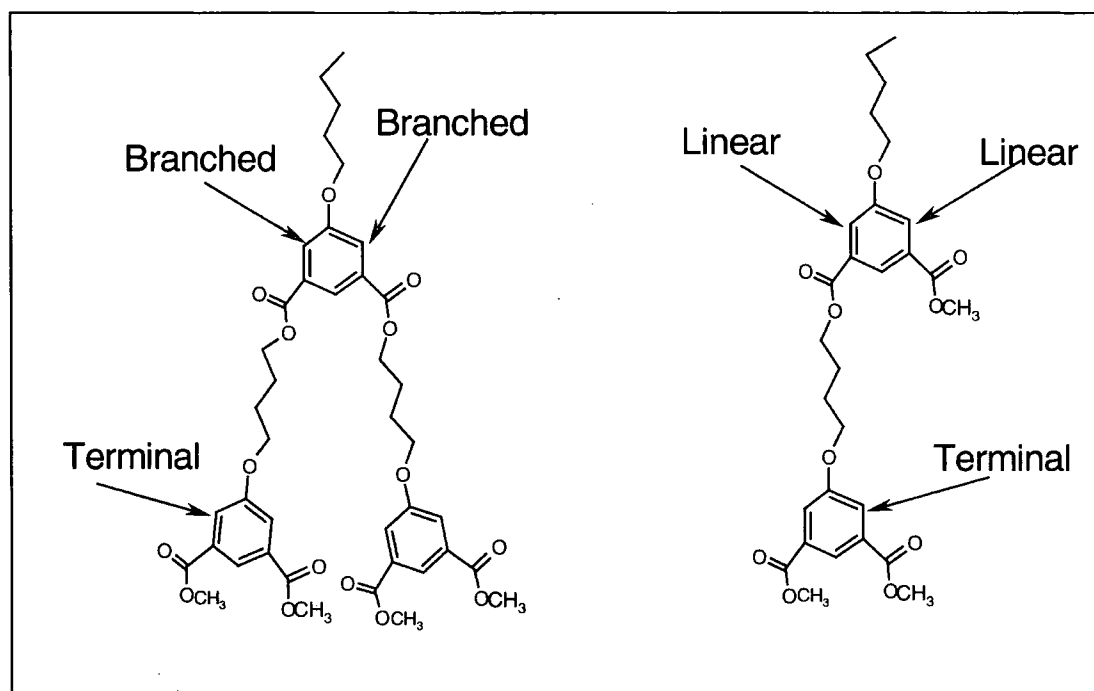


Figure 1(3.5). Aromatic carbons considered for the quantitative ^{13}C -NMR.

About 60 mg of polymer was dissolved in 1 ml deuterated chloroform, in a suitable NMR tube and analysed using a Varian VRX-400S spectrometer. The aromatic carbons in the 3 sub-units, linear, branched and terminal have different chemical environments and also different degrees of freedom; they produce multiple resonances in the region 119.3 – 119.9 ppm.

Since 4 peaks are expected (one for branched, one for terminal and two for linear), the signal was curve-fitted, deconvoluted and the integrals of the 4 peaks obtained as shown in figure 2(3.5).

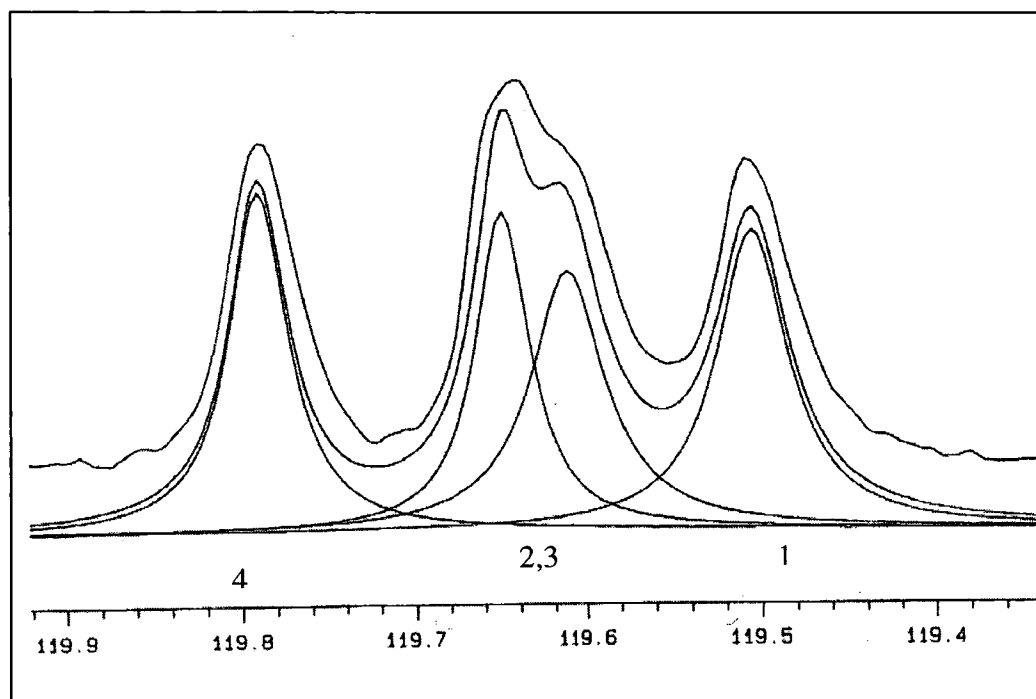


Figure 2(3.5). Aromatic carbon peaks considered for the degree of branching; the signal (upper line), curve fit (intermediate line) and deconvolution curves (lower line).

This analysis was applied to the unfractionated hyperbranched polymer and fraction 2 and 10 and the results are given in table 1(3.5).

Table 1(3.5). Results of the quantitative ^{13}C -NMR experiments.

Sample	Parameters	Peak1	Peak2	Peak3	Peak4
Unfr. material	Width (Hz)	4.9	5.3	3.7	4.0
	Integral	507	473	412	475
Fraction 2	Width (Hz)	5.3	5.1	4.0	4.1
	Integral	322	258	292	299
Fraction 10	Width (Hz)	7.2	5.6	3.7	4.0
	Integral	649	477	291	374

A reasonable assumption for the peak assignment is that the linear unit should give two signals very close to each other, so peaks 2 and 3 are attributed to the linear sub-unit. Secondly, the peak width is proportional to the mobility of the molecules in solution and we assume that the branched sub-unit has less mobility than the terminal one due to structural constraints. As a general rule the wider the peak the slower is the movement of the molecule and since peak 1 in all three samples has larger width compared to the peak 4, it is assigned to the branched sub-unit. By the same argument peak 4 is assigned to the terminal sub-unit.

Substituting the integrals in the degree of branching formula 1(2.5) the values obtained are given in table 2(3.5)) and using the formula 6(2.5) in table 3(3.5).

With a 10% error on the peak integration this propagates to a 20% error in the degree of branching.

Table 2(3.5). *Degree of branching by Frechet formula 1(2.5).*

Sample	Degree of branching
Unfr. material	0.52 ± 0.1
Fraction 2	0.53 ± 0.1
Fraction 10	0.57 ± 0.1

Table 3(3.5). *Degree of branching by the Frey formula 6(2.5).*

Sample	Degree of branching
Unfr. material	0.53 ± 0.1
Fraction 2	0.53 ± 0.1
Fraction 10	0.62 ± 0.1

From these results it is not possible to say if there is any change in the degree of branching among the different fractions because of the large error. The average value of 0.5 ± 0.1 for the degree of branching is in agreement with calculation of Frey².

3.6 Viscometry data

Viscosity measurements were performed by an automatic viscometer Schott AVS 350 connected with Schott Visco Doser AVS 20 automatic burette. The capillary diameter was 0.46 mm.

Chloroform and THF (dried with molecular sieve 3A and filtered) were used as solvents and each polymer solution was equilibrated for about one day before being filtered through a membrane filter (0.22 μm pore diameter) and 15 ml placed in the viscometer. A temperature of 298 K was used and the concentration range was 1- 0.2 % w/v. After each in situ dilution a delay of 20 min was included to ensure complete mixing. The instrument automatically calculated the intrinsic viscosity by extrapolation to infinite dilution. An example of this extrapolation is shown in Figure 1(3.6).

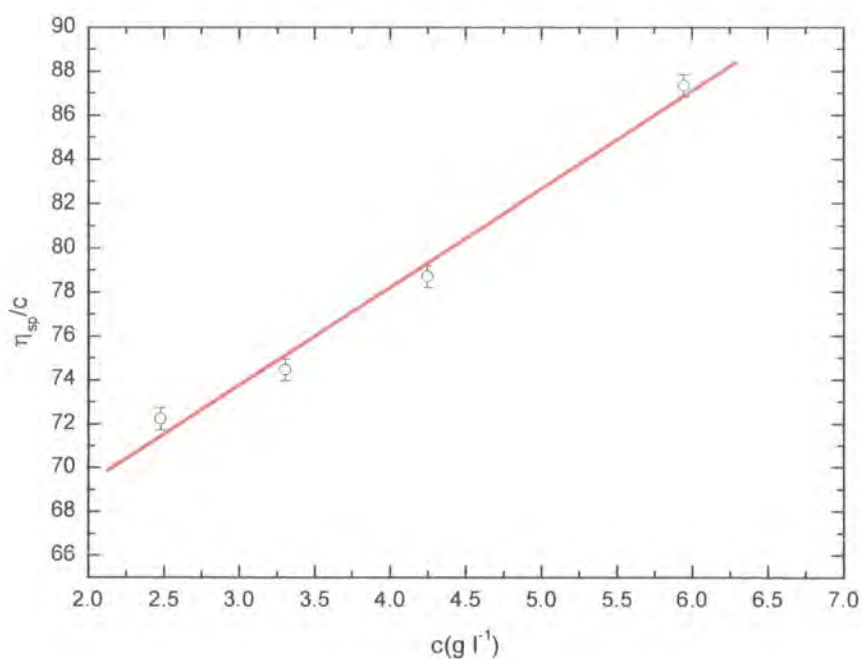


Figure 1(3.6). Zero concentration extrapolation of the reduced viscosity.

Intrinsic viscosities and Huggins constants, k_H , of the hyperbranched polymer fractions in chloroform are given in table 1(3.6).

Table 1(3.6). *Intrinsic viscosities; hyperbranched fractions in chloroform.*

Sample	$[\eta]$ (ml g ⁻¹)	k_H
1	60.4	0.012
2	57.2	0.30
3	37.9	0.50
4	37.6	0.35
5	33.6	0.28
6	28.9	0.39
7	27.1	0.34
8	24.8	0.44
9	21.6	0.34
10	18.3	0.59
11	15.5	0.35
12	10.1	0.29

The errors of the slope and the intercept obtained by the least square linear regression were propagated in the calculation of the physical parameters, the intrinsic viscosity has an average uncertainty of $\pm 2\%$, that for the Huggins constant is $\pm 10\%$.

Viscosity data were also obtained for the analogous linear polyester in chloroform and the results are shown in table 2(3.6).

Table 2(3.6). *Intrinsic viscosities; linear fractions in chloroform.*

Linear	$[\eta]$ (ml g ⁻¹)	k_H
1	47.7	0.36
2	26.3	0.39
3	24.7	0.36
4	20.2	0.33

The viscosity of the hyperbranched polymer fraction was measured in THF under the same conditions as the chloroform solutions (Table 3(3.6)). Some of the fractions were unavailable in usable quantities because material was lost during recovery after each set of experiments.

Table 3(3.6). *Intrinsic viscosities; hyperbranched fractions in THF.*

Sample	$[\eta]$ (ml g ⁻¹)	k_H
1	29.3	0.95
2	25.7	0.46
3	28.5	1.25
4	17.7	1.18
5	18.8	0.63
6	13.5	1.27
8	11.7	2.88
9	12.6	0.94
10	9.4	1.90

3.7 Static light scattering data

As already explained in section 2.7.1 the specific refractive index increment, dn/dc is an experimental parameter used in static light scattering experiments. The specific refractive index increment was measured using a Brice-Phoenix differential refractometer consisting of a thermostat vat, a white light lamp with a series of filters able to produce four wavelengths (633 nm, 546 nm, 488 nm, 436 nm) the light being collimated by a series of lenses. The cell is divided diagonally into two spaces, one for the solvent and the other for the solution. The instrument was used as set out in the manufacturer's handbook.

The differential refractive index, Δn , was measured in 4 different concentrations in the range 0.4 – 4 % w/v for the hyperbranched polymer in chloroform and in THF at 298 K. The plot of Δn versus concentration was linear as expected and the slope of the linear regression is the dn/dc . Of particular interest in this section is measurement of the dn/dc at 488 nm, the laser light wavelength of the light scattering instrument (Figure 1a (3.7), Figure 1b(3.7)).

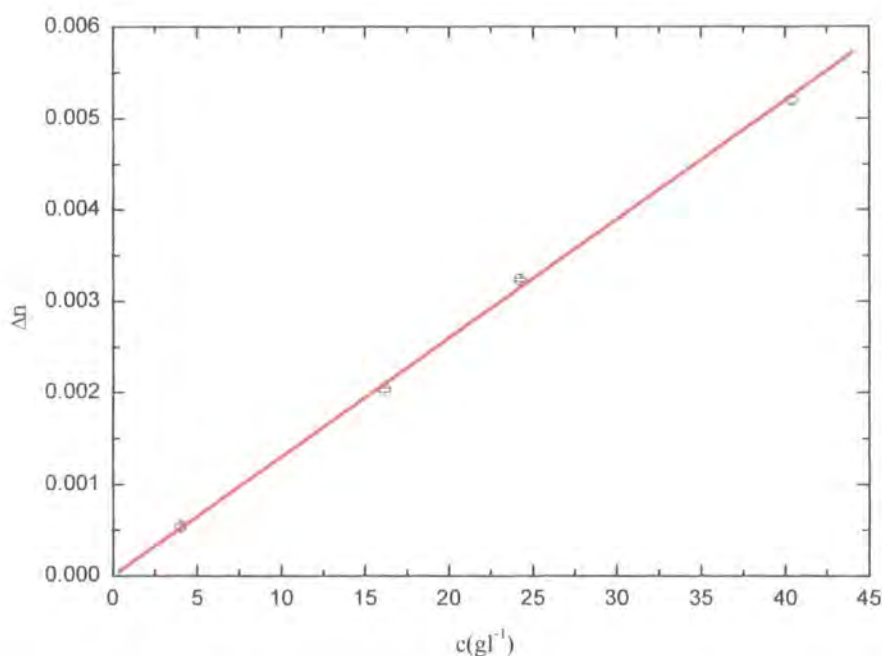


Figure 1a (3.7). Concentration dependence of Δn at 298 K 488 nm in chloroform.

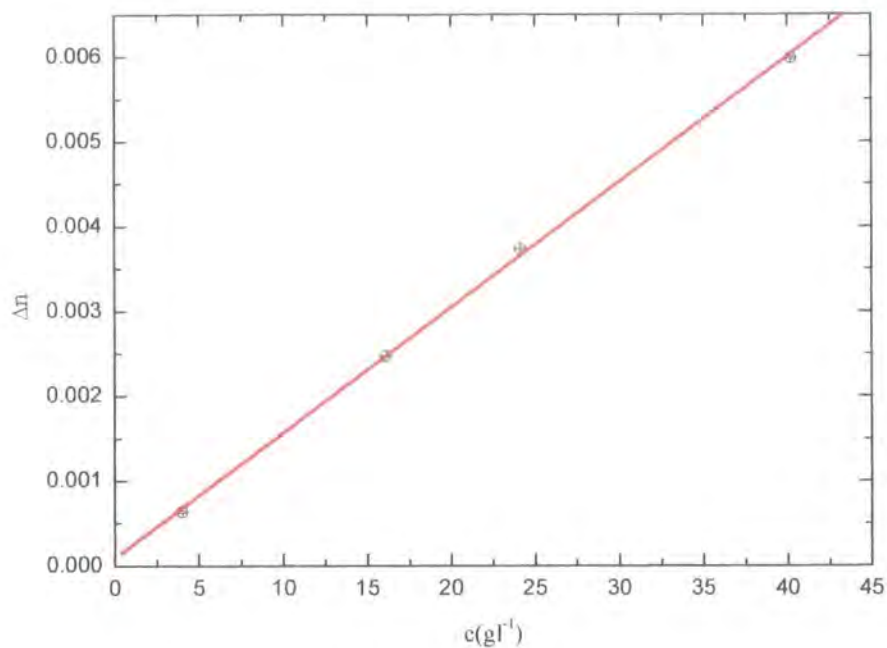


Figure 1b(3.7). Concentration dependence of Δn at 298 K 488nm in THF.

The value for the dn/dc obtained is $0.129 \pm 0.004 \text{ cm}^3 \text{ g}^{-1}$ in chloroform and $0.148 \pm 0.003 \text{ cm}^3 \text{ g}^{-1}$ in THF (Figure 2(3.7)).

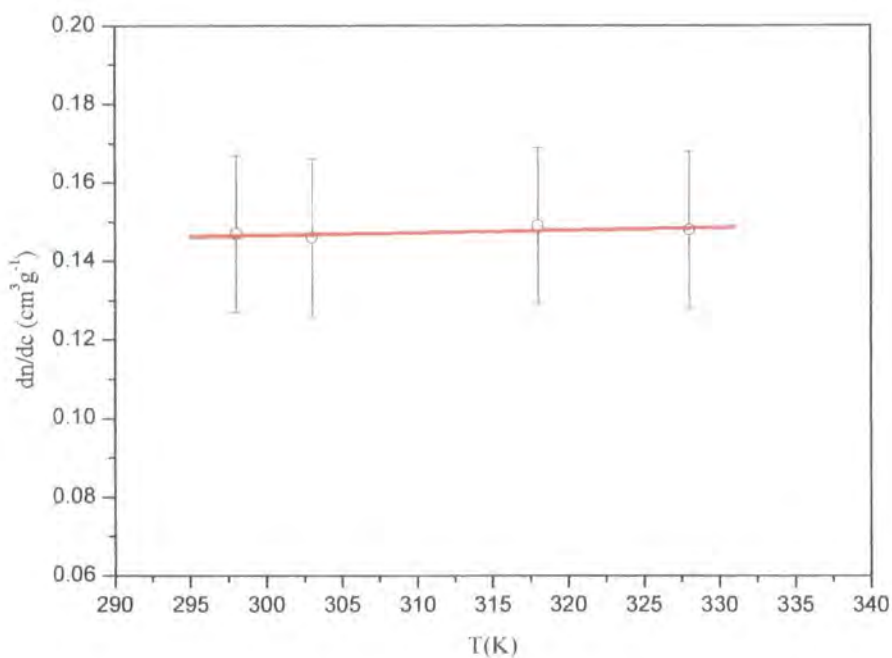


Figure 2(3.7). Temperature dependence of dn/dc for 488 nm light in THF.

Since THF appeared to be a poor solvent for the hyperbranched polymer (see the second virial coefficient data), static light scattering experiments at temperature higher than 298 K were used and dn/dc was measured also at 303 K, 318 K and 328 K. The temperature dependence of the refractive index increment is shown in figure 2(3.7)). The differences of dn/dc with temperature were within the experimental error.

Static light scattering

Static light scattering experiments were performed at 298 K with a fully computerised Malvern 4700 photogoniometer equipped with a monochromatic Ar-ion laser ($\lambda_0 = 488$ nm) focused onto the sample cell, which is held in a glass vat filled with xylene. Xylene was chosen because it has a refractive index close to optical glass and reduces the scattering from the interfaces with the vat and the cell. The photomultiplier tube is mounted on a goniometric arm controlled by a stepper motor. Measurements were carried out in an angular region from 30° to 150° with 11 intermediate angles.

The two solvents used were chloroform and THF. Solutions were prepared in a suitable concentration range with the maximum concentration always less than 1% w/v. All solutions were filtered several times through membrane filters (0.22 μm pore size diameter) to remove dust or particles and then placed in glass cells.

Toluene was used to calibrate the instrument and a complete scan of the background radiation and the solvent scattering intensity was performed before every sample analysis. The scattered intensities collected for the eleven angles were then subtracted from the scattered intensities from each solution and typical Zimm plots (Figure 3a(3.7) and Figure 3b(3.7)) were obtained from the software of the instrument. Since the instrumental software does not give the relative error for the data obtained, some of the Zimm plots have been re-calculated by the use of Excel and Origin. Zero angle and zero concentration extrapolation lines have been obtained by least squares and the errors obtained for the slope and intercept coefficient have been propagated in the calculation of physical parameters. From these calculations, an error of 5% on the weight average molecular weight, 15% on the radius of gyration and 10% on the second virial coefficient were typical.

The data obtained for the hyperbranched polyester in chloroform are presented in table 1(3.7). It was not possible to analyse the fractions 11 and 12 with confidence because of the very low scattering intensity of the samples (approaching that of the pure solvent).

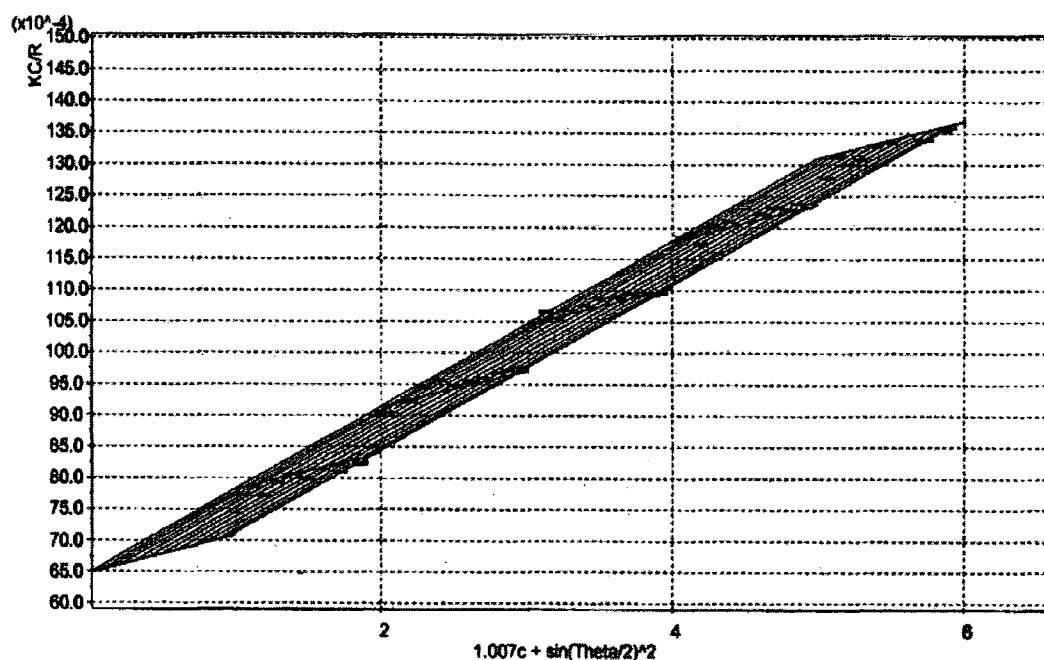


Figure 3a(3.7). Typical Zimm plot for the hyperbranched polyester in chloroform.

Table 1(3.7). Static light scattering data; hyperbranched fractions in chloroform.

Sample	\bar{M}_w (g mol ⁻¹)	R_g (nm)	A_2 (cm ³ mol g ⁻²)
1	519 800	30.3	0.11×10^{-3}
2	328 200	20.3	0.34×10^{-3}
3	154 000	14.0	0.67×10^{-3}
4	142 900	13.6	0.67×10^{-3}
5	118 500	15.6	0.87×10^{-3}
6	83 700	11.9	1.03×10^{-3}
7	63 500	13.9	0.77×10^{-3}
8	47 600	8.5	1.19×10^{-3}
9	36 000	14.0	1.12×10^{-3}
10	20 200	7.1	1.41×10^{-3}

The hyperbranched polyester fractions were investigated by the same technique also in THF and the data relative to the characterisation in THF are shown in Table 2(3.7).

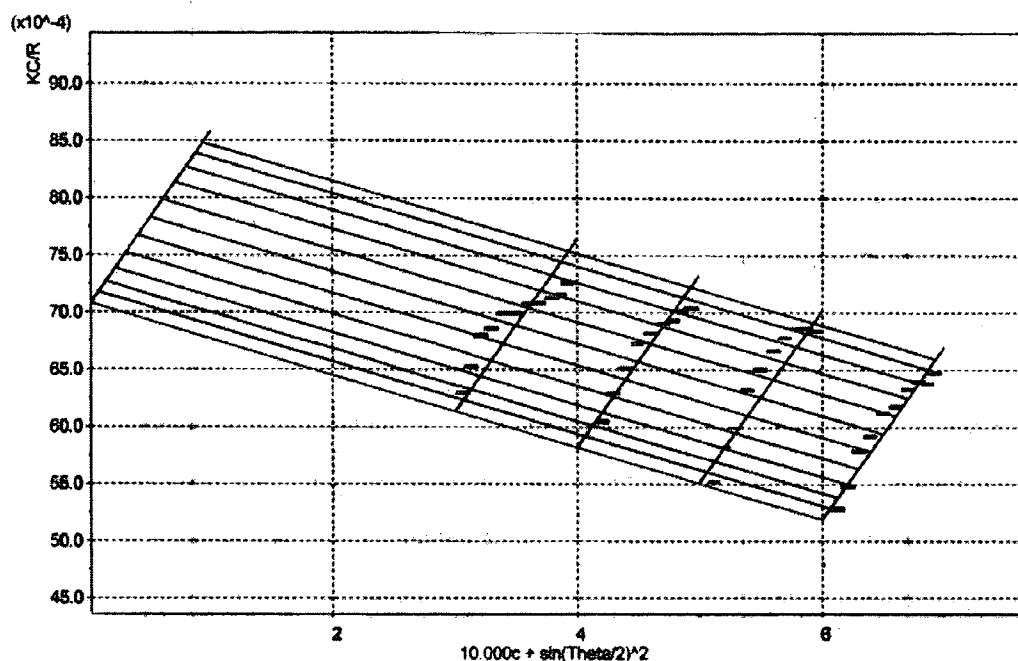


Figure 3b(3.7) Typical Zimm plot for the hyperbranched polyester in THF.

Table 2 (3.7). Static light scattering data; hyperbranched fractions in THF.

Sample	\overline{M}_w (g mol ⁻¹)	R_g (nm)	A_2 (cm ³ mol g ⁻²)
1	414500	20.2	-0.20×10^{-3}
2	215700	14.1	-0.70×10^{-3}
3	131400	11.8	-0.20×10^{-3}
4	141200	11.4	-0.40×10^{-3}
5	118800	12.0	-0.06×10^{-3}
6	63200	11.4	-1.12×10^{-3}
8	50000	7.9	-1.19×10^{-3}
9	27500	7.7	-0.81×10^{-3}
10	13100	3.8	-0.68×10^{-3}

The analogous linear polyester was analysed in chloroform under the same experimental conditions as the hyperbranched polymer. The experimental refractive index increment for this polymer was 0.126 ± 0.002 cm³ g⁻¹.

Additional scattering was noted in the static light scattering for the linear polyester and this problem was attributed to aggregation of the polymer in solution. This conclusion was reached on the basis of the much higher molecular weight obtained from the classical light scattering compared to those from SEC. The same concentration range has been analysed at a fixed angle (90°) using a He-Ne laser light beam (633 nm), but no better results were obtained.

Table 3 (3.7). *Static light scattering data; linear fractions in chloroform.*

Linear	\bar{M}_w (g mol ⁻¹)	R_g (nm)	A_2 (cm ³ mol g ⁻²)
1	148 600	36.2	2.22×10^{-3}
2	50 800	19.7	1.05×10^{-3}
3	46 450	51.4	0.90×10^{-3}
4	23 300	31.8	4.46×10^{-3}

Another series of experiments were carried out using a very dilute concentration range to avoid the aggregation of the polymer, but even in this situation the result are not attributable to molecular species because of the higher molecular weights (Table 4 (3.7)). In this very dilute regime the second virial coefficient is negative and this reinforces the assumption that the polymer-solvent interactions are poor.

Table 4(3.7). *Static light scattering data; linear fractions in chloroform in very dilute regime.*

Linear	\bar{M}_w (g mol ⁻¹)	R_g (nm)	A_2 (cm ³ mol g ⁻²)
1	71 400	27.4	-0.0035
2	46 700	23.9	-0.0044
3	44 100	38.1	-0.0025
4	25 800	42.3	-0.0055

For the reason outlined above, the molecular weight used for the linear polyester are those obtained by SEC.

3.8 Dynamic light scattering data

Dynamic light scattering experiments were performed using a Brookhaven photogoniometer equipped with a vertically polarised He-Ne laser (633 nm.), a BI-9000AT correlator and electronic temperature controller. In this instrument the laser beam is collimated by optical lenses to the sample cell in a vat filled with xylene. Light was collected for a scattering angle of 90° and solutions were maintained at 298 K. Cumulant analysis of the correlation function is one of the most common methods to obtain diffusion coefficients and was applied to the data of the different samples. The typical equation 7(2.7.2) of the cumulant analysis has been written in a different form in 1(3.8).

$$1(3.8) \quad G(t) = \exp \left[2 \cdot \left(C_0 - K_1 t + \frac{1}{2} K_2 t^2 \right) \right] + B$$

Where $G(t)$ is the correlation function at the time increment, B is the background. The coefficients K_1 , K_2 are related to the translational diffusion coefficient as already mentioned in section 2.7.2.

Equation 1(3.8) was fitted to the data using the non-linear least squares procedure available in Origin and the translational diffusion coefficient was calculated from the formula defined in 4(2.7.2). In the theoretical expressions the concentration dependence of D_c is normally expressed by the relationship given in 5(2.7.2).

Typical curves collected for the hyperbranched polymer fractions in chloroform and THF are shown in figure 1a(3.8) and 1b(3.8).

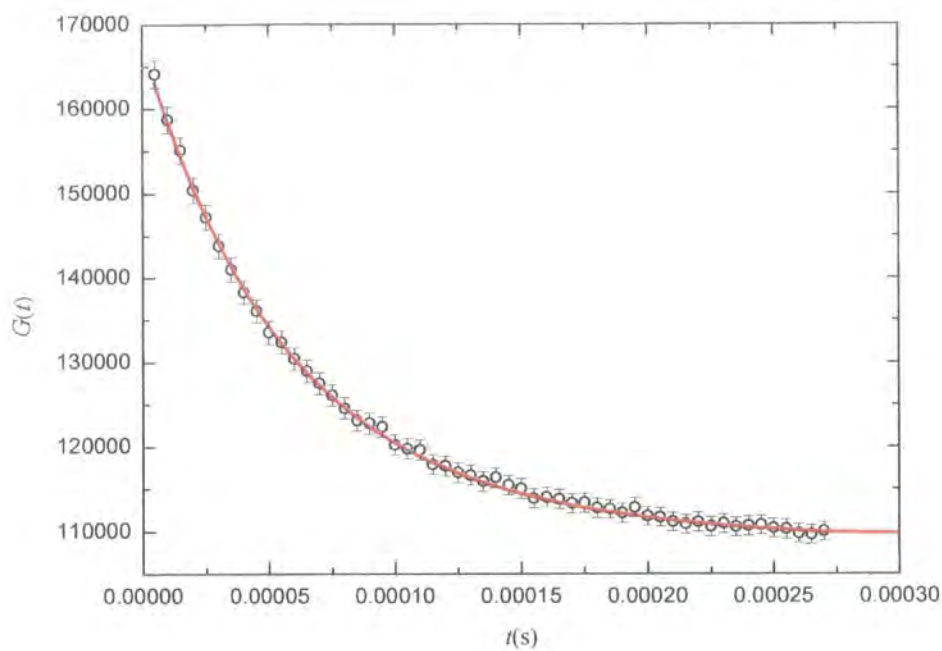


Figure 1a (3.8). Example of cumulant analysis fit; hyperbranched fraction in chloroform.

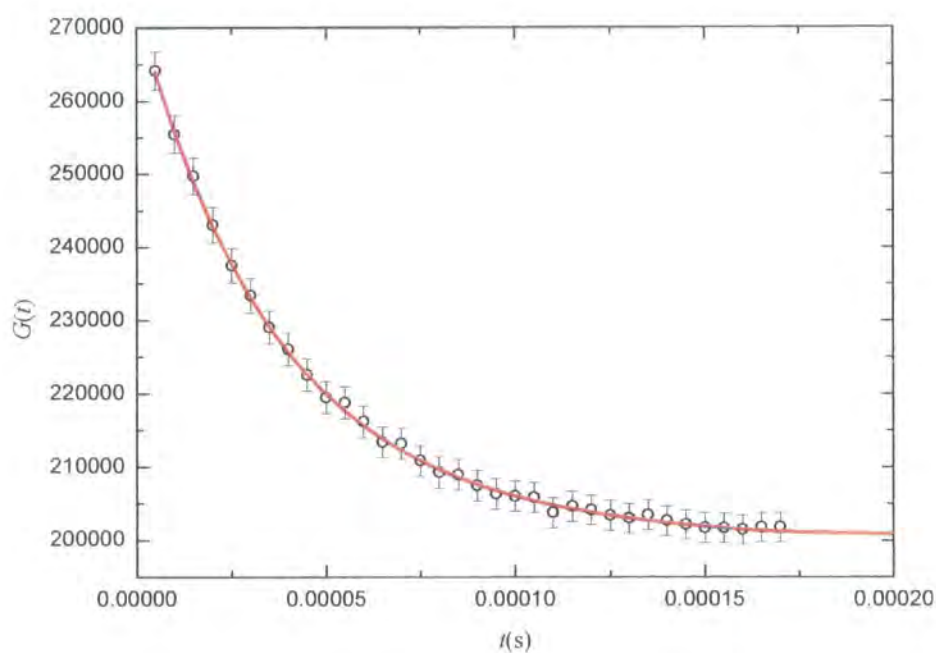


Figure 1b (3.8). Example of cumulant analysis fit; hyperbranched fraction in THF.

The data relative to the dynamic light scattering for the different concentrations are collected in Appendix C.

Extrapolation to zero concentration (Figure 2(3.8)) gave D_l and the k_d by linear least squares fitting.

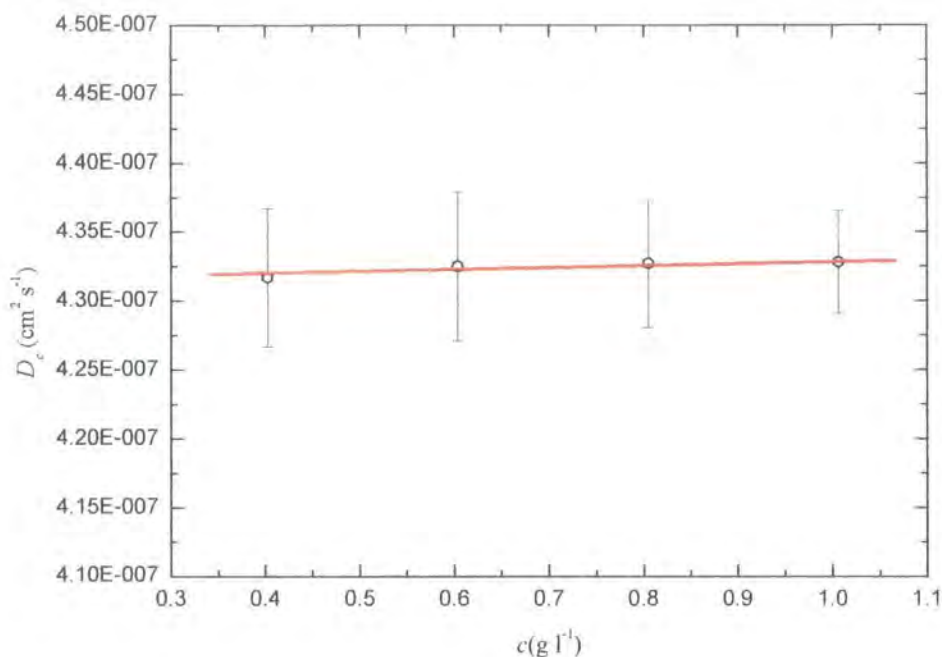


Figure 2(3.8) Example of zero concentration extrapolation of D_c .

The error on the slope and the intercept calculations were propagated in the calculation of D_0 and k_d leading to an error of 5% and 10% respectively.

The hydrodynamic radius, R_h , from the Stokes-Einstein equation 3(3.8) and the results are given in table 2a(3.8) and 2b(3.8).

$$3(3.8) \quad D_0 = \frac{k \cdot T}{6 \cdot \pi \cdot \eta \cdot R_h}$$

Where k is the Boltzmann's constant, T the temperature, η the solvent viscosity.

Table 2a(3.8). *Dynamic light scattering results; hyperbranched fractions in chloroform.*

Sample	D_0 (cm ² s ⁻¹)	k_D (ml g ⁻¹)	R_h (nm)
1	2.09E-07	13.2	19.5
2	3.30E-07	24.3	12.4
3	3.70E-07	34.4	10.4
4	4.12E-07	41.6	9.5
5	4.68E-07	40.4	8.7
6	4.13E-07	43.6	9.9
7	4.57E-07	44.1	8.9
8	5.47E-07	43.7	7.5
9	8.13E-07	50.6	6.5
10	8.83E-07	45.6	4.9

Table 2b(3.8). *Dynamic light scattering results; hyperbranched fractions in THF.*

Sample	D_0 (cm ² s ⁻¹)	k_D (ml g ⁻¹)	R_h (nm)
1	3.57E-07	-43.5	13.3
2	4.51E-07	-63.6	10.5
3	6.00E-07	-44.4	7.9
4	4.74E-07	-58.6	10.0
5	6.83E-07	-46.1	6.9
6	6.95E-07	-12.1	6.8
8	7.35E-07	-32.1	6.5
9	9.19E-07	-3.3	5.2
10	1.21E-06	-5.7	3.9

Linear polyester

Dynamic light scattering data were obtained for the linear polyester in chloroform. Table 3a(3.8) summarises the value of the extrapolation to infinite dilution. The diffusion coefficients for the different concentrations are collected in Appendix C.

The results will be discussed in section 4.2.

Table 3a(3.8). *Dynamic light scattering results; linear analogue in chloroform.*

Sample	D_0 (cm ² s ⁻¹)	k_D (ml g ⁻¹)	R_h (nm)
Linear 1	2.92E-07	-78.7	13.9
Linear 2	5.06E-07	-49.4	8.0
Linear 3	4.30E-07	-12.1	9.5
Linear 4	9.63E-07	-51.9	4.2

3.9 SANS data

LOQ experiments

The first small angle neutron scattering data were collected using the LOQ diffractometer at ISIS, Rutherford Appleton Laboratory. LOQ is a fixed geometry instrument. In LOQ the different wavelengths are selected by a disc chopper that operates at 25 Hz choosing alternate pulses of neutrons from the target. This provides a useful wavelength range of 2.0 - 9.8 Å. The neutrons are collimated to an 8 mm diameter beam on the sample. The available Q range on LOQ is 0.006 Å⁻¹ to 0.22 Å⁻¹, limited by the size of the beam stop at low Q and the size of the detector at high Q . The neutron path from the source to the sample position and from the sample position to the detector is in high vacuum to minimise air scattering, but the sample position is at ambient conditions. Samples were placed in a twenty-position temperature controlled cell rack, the position, temperature and sample exposure time were controlled by the use of a command file on the instrument computer.

LOQ was calibrated by measuring the scattering from a D-PS/H-PS blend of known molecular weight and radius of gyration with a D-PS volume fraction of 0.5. This calibration enables absolute values of the scattering cross section to be obtained. For each sample, two measurements were required; first is the transmission of the sample as a function of the wavelength measured by applying a small collimation window to the incident beam and placing a scintillation detector after the sample.

The same measurement was made for the direct beam and by difference the transmission factor of the sample was obtained. Secondly the total scattering was collected on the area detector. The raw scattering data were corrected for detector efficiency, background, converted to a radial distribution and hence to scattering cross sections dependent on Q .

The first SANS experiment were made using deuterated chloroform solutions with concentration range from 1% to 5% w/v. For small angle neutron scattering technique the magnitude of the scattering length density is of fundamental importance as mentioned in section 2.8.

From the scattering length densities of the solvent and the polymer repeat unit, the contrast factor, $(\Delta\rho)^2$ can be calculated. The contrast factor was calculated using the branched sub-unit molecular weight ($M = 251 \text{ g mol}^{-1}$, $\rho = 1.335 \text{ g cm}^{-3}$) of the

hyperbranched polymer and the coherent scattering lengths for the different nuclei are taken from literature³. The results are shown in the table 1(3.9).

Table 1 (3.9). Contrast calculations for the hyperbranched polymer in D-THF and CDCl₃.

Solvent	δ (g cm ⁻³)	$\Delta\rho$ (cm ⁻²)	$(\Delta\rho)^2$ (cm ⁻⁴)
D-THF	0.895	$3.41 \times 10^{+10}$	$1.16 \times 10^{+21}$
CDCl ₃	1.50	$8.01 \times 10^{+09}$	$6.42 \times 10^{+19}$

An example of the scattering for solutions in deuterated chloroform can be seen in figure 1(3.9).

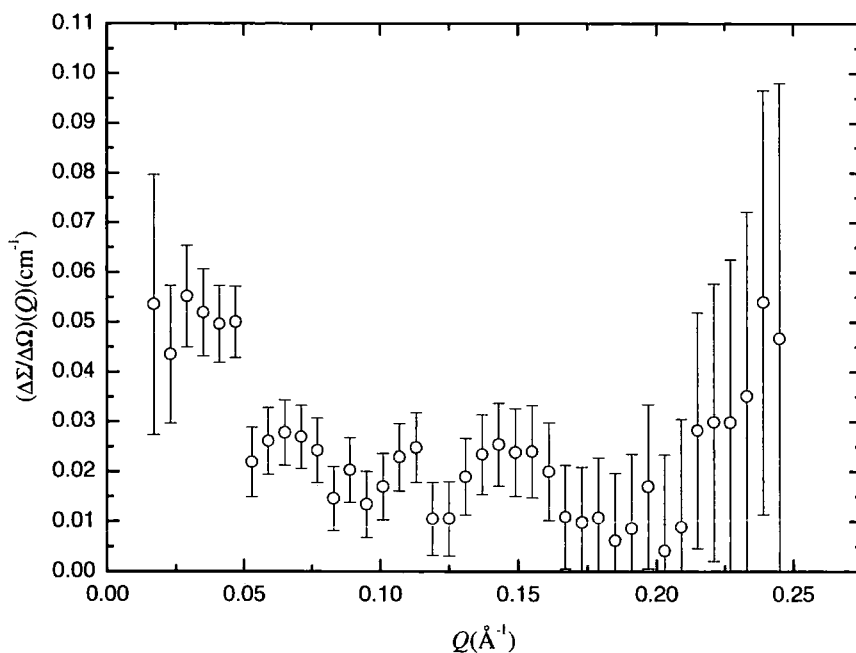


Figure 1(3.9). SANS plot for the fraction 2 (5%); deuterated chloroform.

The scattering cross section in all data was very weak, large errors are evident even for very long acquisition times. These problems are due to the poor contrast between deuterated chloroform and the polymer and also because chlorine absorbs neutrons decreasing the scattering intensity. These problems are not evident in deuterated THF

solutions and a new series of experiments were carried out with solutions of the hyperbranched polymer in deuterated THF. Typical scattering plots are shown in figure 2a(3.9) to 2c(3.9).

Since the linear polymer was only partially soluble in chloroform, it was not possible to have SANS data for this polymer.

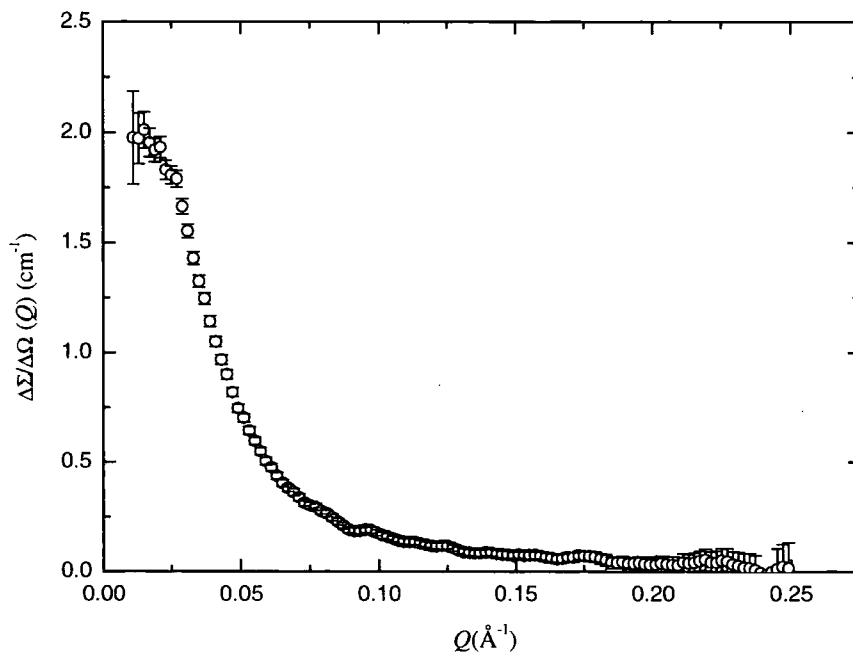


Figure 2a(3.9). SANS cross section; hyperbranched fraction 2 (5%); D-THF by LOQ.

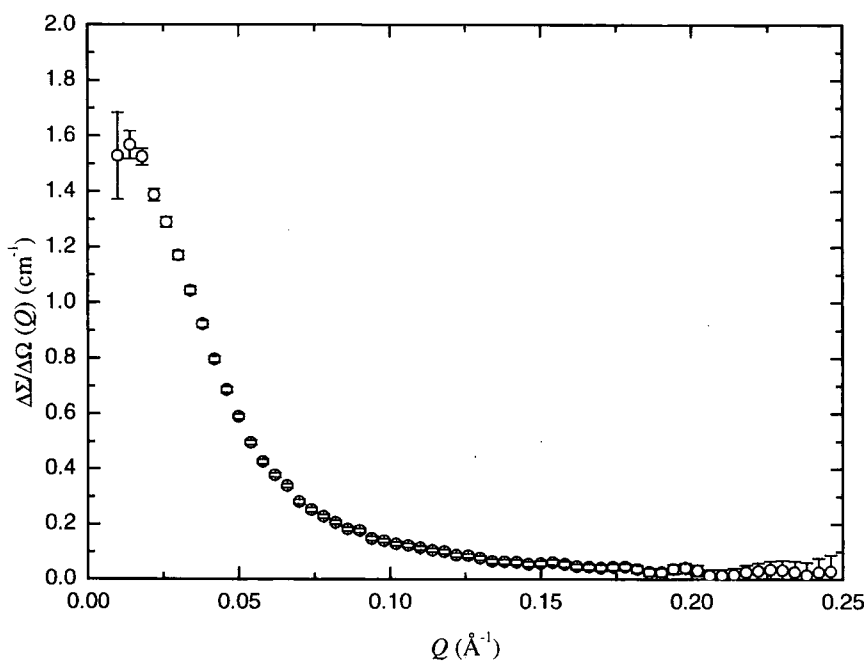


Figure 2b(3.9). SANS cross section; hyperbranched fraction 5 (5%); D-THF by LOQ.

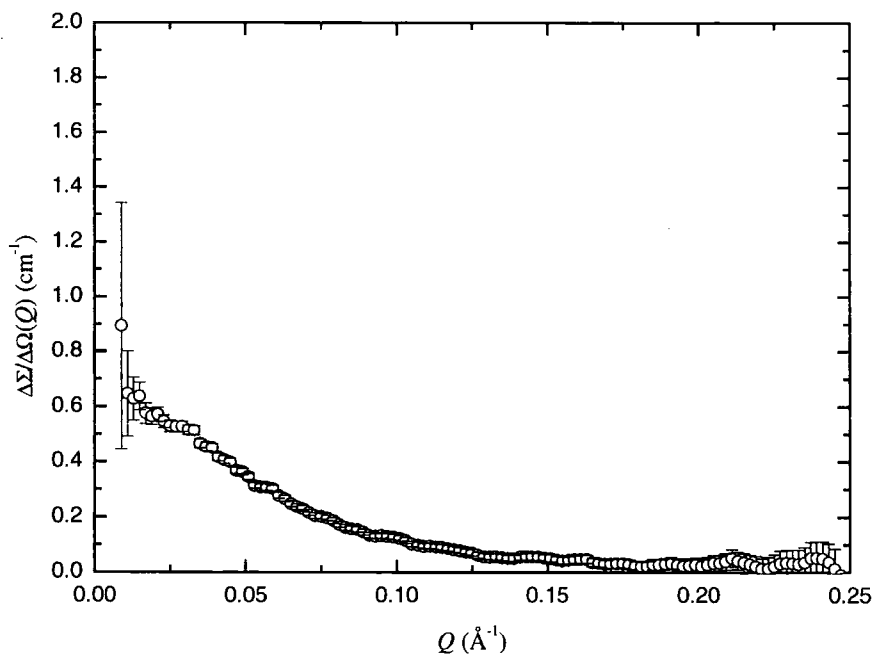


Figure 2c(3.9). SANS cross section; hyperbranched fraction 10 (5%); D-THF by LOQ.

D22 experiments

The second series of SANS experiments was performed using the D22 diffractometer at the Istitute Laue Langevin in Grenoble (France). D22 is a fixed wavelength instrument. For the detector calibration, water was used because its high scattering cross-section and proven reproducibility. For each sample, a set of spectra were obtained, transmission runs for empty holder, empty cell, cell + solvent, sample, and scattering for empty cell, cell + solvent and the sample. All spectra were stored in individual files and by the use of specific programs a radial distribution function was obtained. The spectra were afterwards normalised to the same monitor count and the background and pure solvent scattering was subtracted. Typical scattering curves obtained by this instrument are shown in figure 3a(3.9) to 3c(3.9).

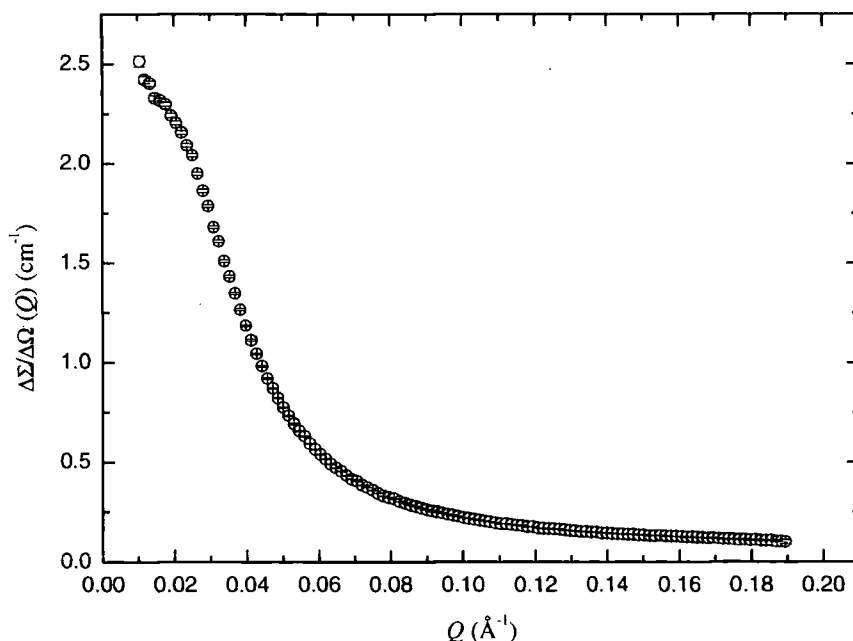


Figure 3a(3.9). SANS cross section; hyperbranched fraction 2 (5%) in D-THF by D22.

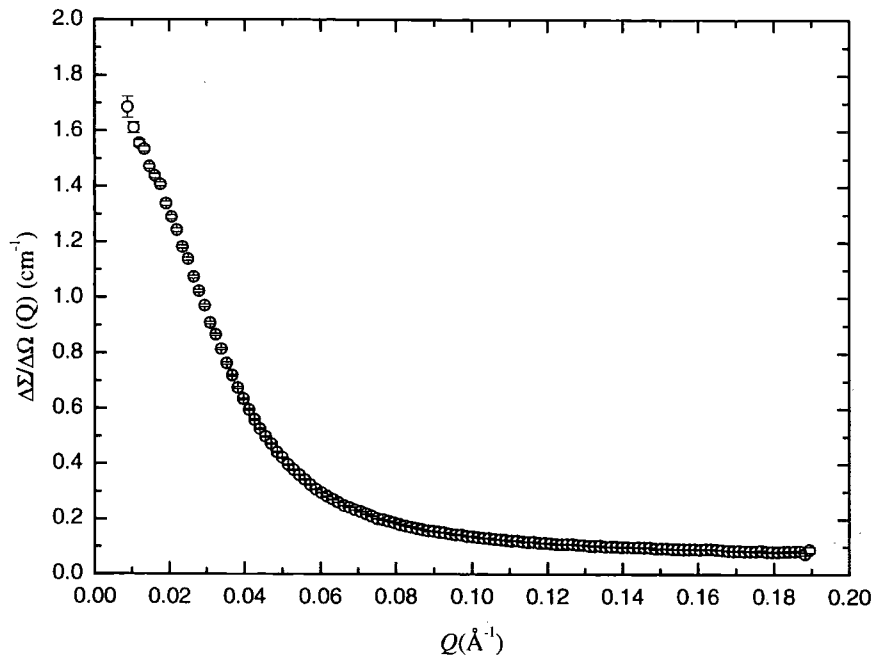


Figure 3b(3.9). SANS cross section; hyperbranched fraction 5 (5%); D-THF by D22.

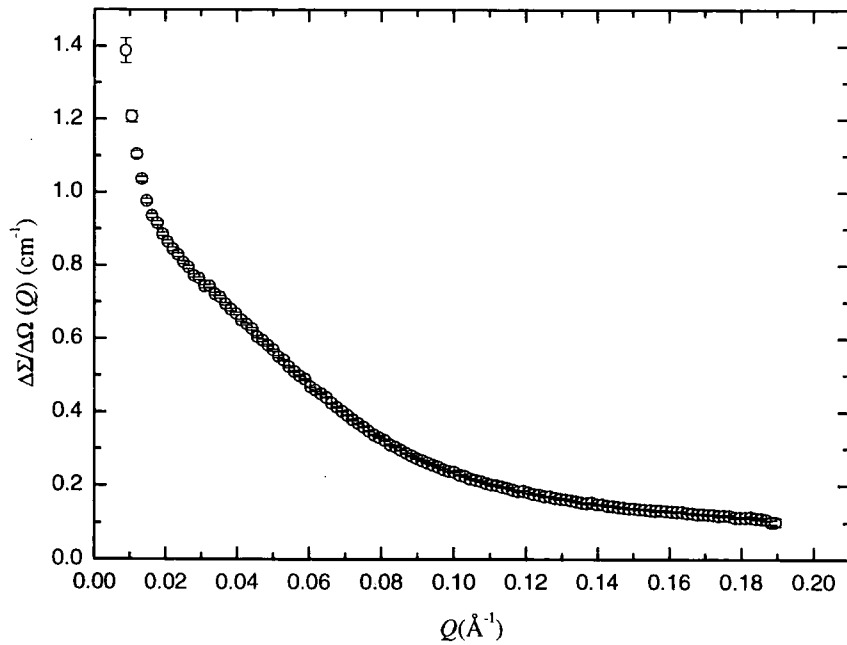


Figure 3c(3.9). SANS cross section; hyperbranched fraction 10 (5%); D-THF by D22.

The results and analysis of the small neutron scattering data will be discussed in detail in section 4.2.

References

1. Feast, W.J. and A.J. Keeney, *Chem. Commun* 1997: p. 1749.
2. Holter, D. and H. Frey, *Acta Polymer*. 1997. **48**: p. 30.
3. King, S.M., *Modern techniques for polymer characterisation*, ed. R.A.Pethrick and J.V. Dawkins. 1999: John Wiley & Sons Ltd.

Chapter 4

Analysis and Discussion

Note: references for section 4.1 are on page 140.

4.1 Dilute solutions

The dilute regime corresponds to the situation where the possibility of contact between molecules is negligible; the polymer-solvent interactions affect the thermodynamic behaviour of the solution and influence the spatial dimensions of the macromolecules via the excluded volume phenomenon. In this section, the behaviour of the hyperbranched and linear polyesters in the dilute regime in chloroform and THF solutions will be investigated, discussed and compared with other polymeric systems.

The first issues to be studied are the Mark-Houwink-Sakurada plots that were produced by the double log plot of intrinsic viscosity versus weight average molecular weight. Figure 1(4.1) uses molecular weights obtained by light scattering detection in SEC analysis and figure 2(4.1) uses classical intensity light scattering molecular weight values (both in chloroform).

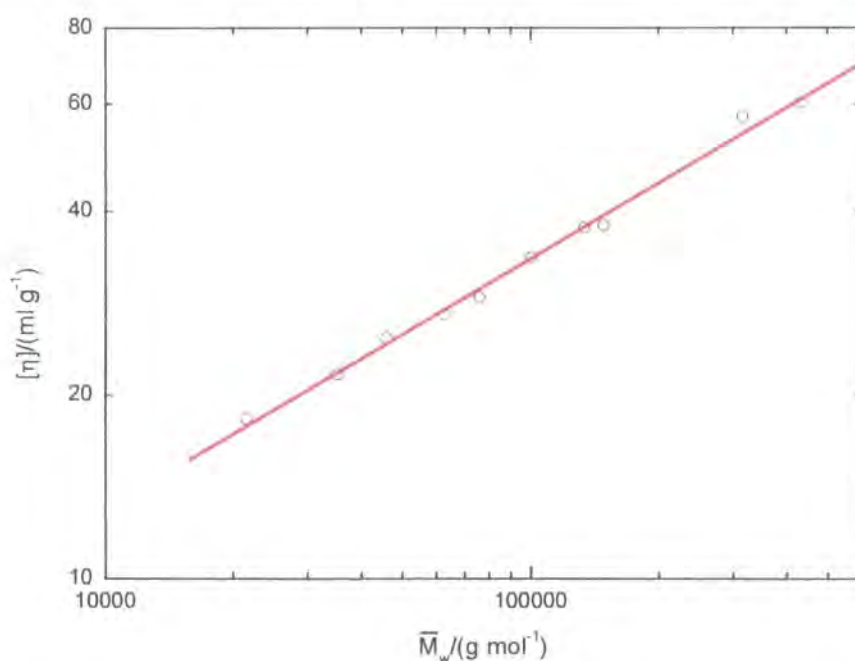


Figure 1(4.1). Mark-Houwink-Sakurada plot: hyperbranched fractions in chloroform (\bar{M}_w by SEC).

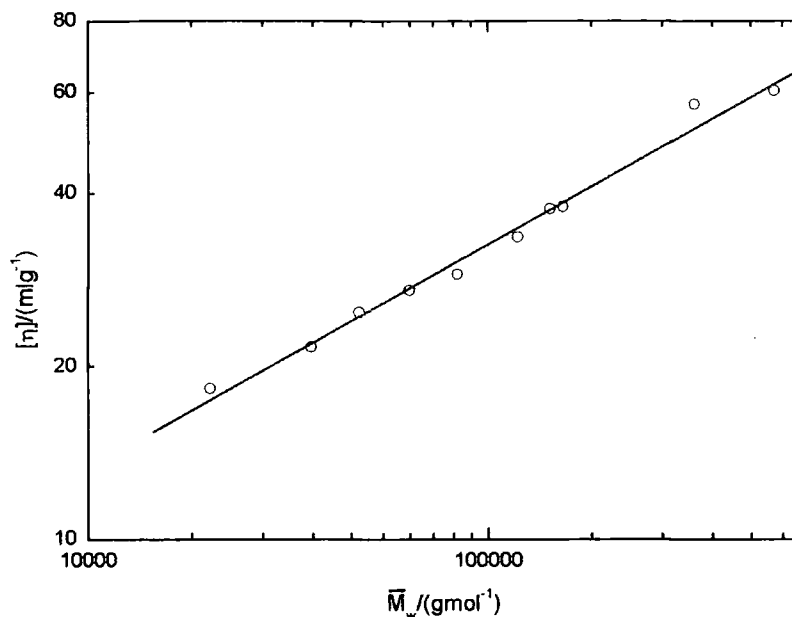


Figure 2(4.1). *Mark-Houwink-Sakurada plot: hyperbranched polymer in chloroform and \bar{M}_w by classical light scattering.*

The results of linear least squares regression are given in the relationship 1(4.1) in the case of \bar{M}_w obtained by SEC and 2(4.1) for \bar{M}_w by classical light scattering experiments:

$$1(4.1) \quad [\eta] = (0.29 \pm 0.02) \bar{M}_w^{(0.41 \pm 0.02)} (\text{ml g}^{-1})$$

$$2(4.1) \quad [\eta] = (0.36 \pm 0.05) \bar{M}_w^{(0.39 \pm 0.02)} (\text{ml g}^{-1})$$

The coefficients $K_{[\eta]}$ obtained are slightly different but comparable within the experimental error, while the exponents $a_{[\eta]}$ are in very good agreement proving that light scattering analysis by SEC gives the same results as classical light scattering for hyperbranched polymers. The same plot was produced for THF solutions (Figure 3(4.1)) with the \bar{M}_w obtained by the classical light scattering. For reasons explained in section 3.4 the molecular weight obtained by SEC in THF have been not taken into account for any further comparison.

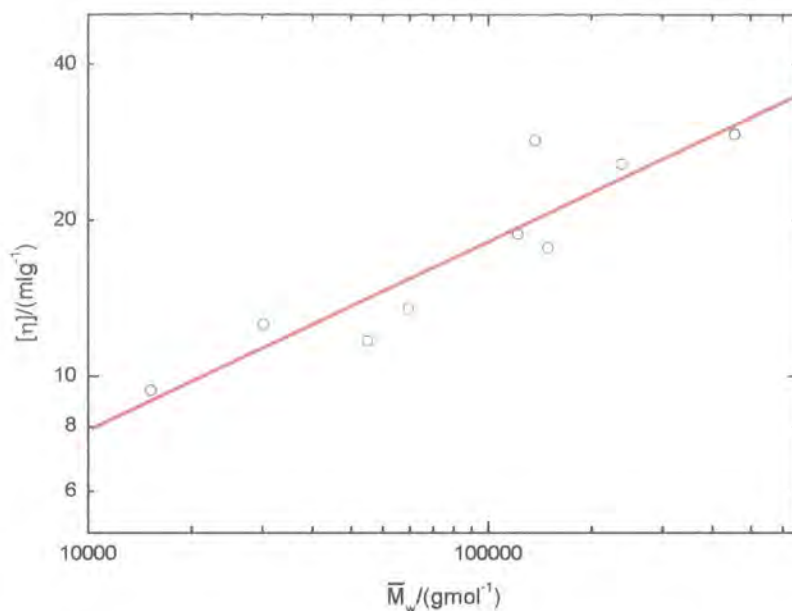


Figure 3(4.1). Mark-Houwink-Sakurada plot: hyperbranched fractions in THF (\bar{M}_w by classical light scattering).

The result in this case is given in equation 3(4.1).

$$3(4.1) \quad [\eta] = (0.3 \pm 0.1) \bar{M}_w^{(0.36 \pm 0.05)} \text{ (ml g}^{-1}\text{)}$$

The exponent $a_{[\eta]}$ in this case is slightly lower but, within the experimental error, is the same as that obtained in chloroform.

In the case of linear polymers the expected values for $a_{[\eta]}$ are in the range 0.5- 0.8, but for hyperbranched polymers values in the range of 0.2 to 0.4 are typical as shown by Turner et al¹.

The intrinsic viscosity is a measure of the effective volume of the polymer particles including the solvent, which in effect flows with the particle. An increase in branching at a fixed molecular weight would be expected to reduce the intrinsic viscosity, in accordance with the observation.



The value of the exponent for the hyperbranched polyester is in agreement with $a_{[\eta]} = 0.40$ found for glycogen² fractions. Some similarities in the behaviour of the hyperbranched polyester with glycogen fractions are evident but the latter were obtained by degradation of the starting material and the polydispersity of the fractions varies between 29 and 6.

For the linear polyester analogue the same plot was possible using data obtained by SEC (Figure 4(4.1)). As pointed out in section 3.7 it has been not possible to measure reliable physical parameters by static light scattering.

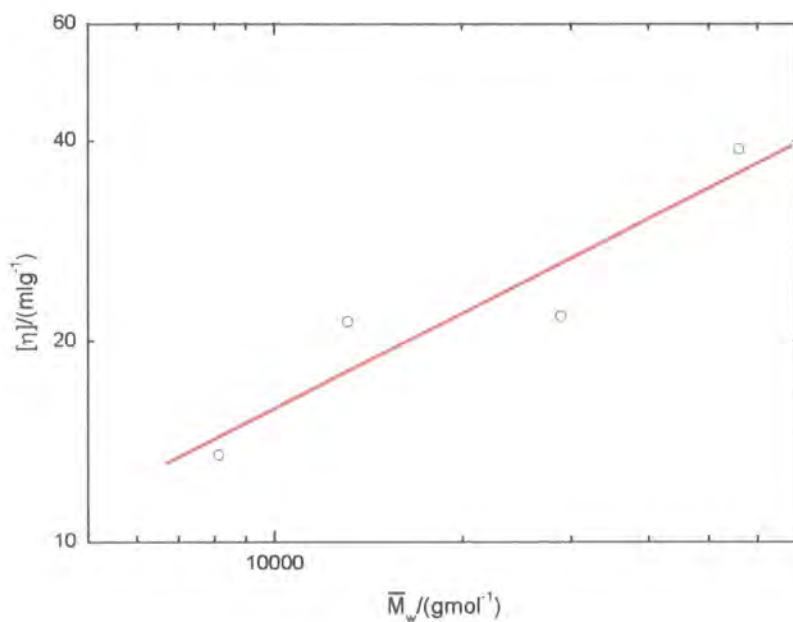


Figure 4(4.1). *Mark-Houwink-Sakurada plot: linear fractions in chloroform (\bar{M}_w by SEC).*

The linear least squares fit to these data is:

$$4(4.1) \quad [\eta] = (0.2 \pm 0.1) \bar{M}_w^{(0.5 \pm 0.1)} \text{ (ml g}^{-1}\text{)}$$

The exponent value of 0.5 indicates that chloroform is a θ solvent and this explains the poor solubility of the polymer and the problems encountered in the static light scattering experiments.

The Huggins constant, k_H , for the hyperbranched polyester shows no a molar mass dependence neither in chloroform (Figure 5a(4.1)) nor in THF (Figure 5b(4.1)) except that fraction 1 gave a higher value of k_H in chloroform.

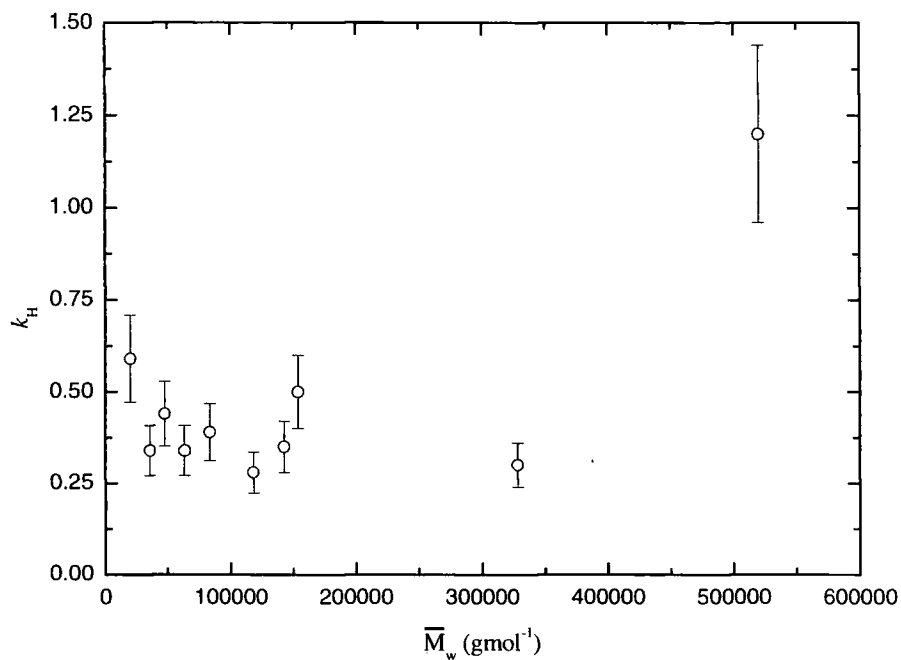


Figure 5a(4.1). Molar mass dependence of k_H in chloroform.

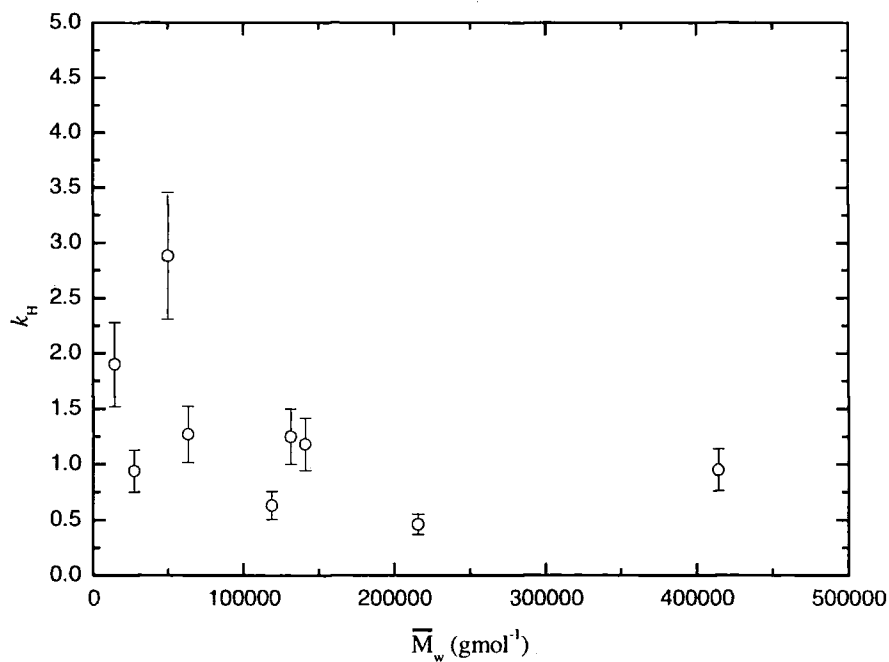


Figure 5b(4.1). Molar mass dependence of k_H in THF.

An average value of $k_H = 0.35 \pm 0.1$ in chloroform and $k_H = 1.2 \pm 0.5$ in THF was obtained. In general k_H is independent of molecular weight.

For linear polymers in good solvent k_H equals 0.33 and values between 0.5 and 1 have been determined for polymers in poor solvents. A general rule is that k_H increases as the solvent becomes poorer, reaching values of 0.55 or more on approaching the theta condition³.

Assuming that the same arguments for k_H of linear polymers applies to hyperbranched polymers, chloroform represents a good solvent and THF a poor solvent.

The branching factors

The comparison of the physical parameters of branched polymers with their linear polymer analogues is a common method for the characterisation of branched systems. From a geometrical point of view, polymers may generally be divided into segments that, while in the case of the linear polymers will be attached to only one or two of the others, in some cases are attached to three or more others and they are called branched units with a functionality f .

Branched polymers are often characterised in terms of the branching factors introduced by Zimm and Stockmayer⁴. A factor g_0 was defined as the ratio of the radius of gyration of the branched polymer to that of the linear analogue with the same molecular weight.

$$5(4.1) \quad g_0 = \frac{\langle s^2 \rangle_{0,b}}{\langle s^2 \rangle_{0,l}}$$

Where the subscript 0 is for the ideal solution condition, b is for branched and l for linear. Measuring the radius of gyration and the molecular weight of branched polymer fractions and knowing a relationship between the radius of gyration and the molecular weight for the analogous linear polymer the analogous experimental branching factor g can be calculated. Another branching factor is g' , already introduced in section 2.6 is the ratio of the intrinsic viscosities of the branched polymer and the linear analogue of the same molecular weight.

Different scaling laws relating the g' and g_0 have been proposed and these calculations enable the derivation of other physical parameters like the expansion factor of the intrinsic viscosity radius, α_η .

$$6(4.1) \quad g' = g_0^\omega \cdot \left(\frac{\alpha_{\eta,b}}{\alpha_{\eta,l}} \right)^3$$

Zimm and Kilb proposed scaling law $g' = g_0^{0.5}$ for star shaped molecules, but the value of the exponent ω changes for other branched systems. Some experimental evidence in favour of this scaling law with $\omega=0.5$ comes from the work of Schaeffgen and Flory⁵ on the viscosity and molecular weights of a series of linear and star polyamides with 4-arms and 8-arms. In the specific case of AB₂ polycondensate, Zimm and Stockmayer⁴ proposed an equation for the branching factor, g_0 , of polydisperse samples defined in equation 7a(4.1) and one for fractionated materials defined in 7b(4.1).

$$7a(4.1) \quad \langle g_3 \rangle = \frac{6}{n_w} \left[\frac{1}{2} \left(\frac{2+n_w}{n_w} \right)^{\frac{1}{2}} \ln \left(\frac{(2+n_w)^{\frac{1}{2}} + (n_w)^{\frac{1}{2}}}{(2+n_w)^{\frac{1}{2}} - (n_w)^{\frac{1}{2}}} \right) - 1 \right]$$

$$7b(4.1) \quad \langle g_3(m) \rangle = \left[\left(1 + \frac{m}{7} \right)^{\frac{1}{2}} + \frac{4m}{9\pi} \right]^{-\frac{1}{2}}$$

Where n_w and m are the average number of branched units and the subscript 3 is for trifunctional monomer units.

By the use of the Mark-Houwink-Sakurada coefficients of the linear and hyperbranched polyester, the intrinsic viscosity for the analogous linear fractions of the same molecular weight can be calculated and the branching factor g' obtained and compared with the theoretical one.

It is reasonable to apply the formula 7b(4.1) to hyperbranched polyester because the samples are obtained by solution fractionation and so they have a narrower molecular weight distribution compared to the starting material.

The average number of branched units can be calculated in first approximation from the degree of branching by the relationship 8(4.1).

$$8(4.1) \quad m = \frac{\overline{M}_w}{M_0} \cdot Db$$

Where M_0 is the molecular weight of the branched unit (266 g mol^{-1}). The data obtained by this calculation are shown in table 1(4.1).

Table 1(4.1). $\langle g_3(m) \rangle$ and g' ; hyperbranched fractions.

Sample	m	$\langle g_3(m) \rangle$	g'
1	977	0.081	0.42
2	617	0.101	0.50
3	289	0.145	0.48
4	269	0.150	0.50
5	223	0.163	0.49
6	157	0.192	0.50
7	119	0.217	0.54
8	89	0.247	0.57
9	68	0.279	0.57
10	38	0.355	0.64

The double log plot of $\langle g_3(m) \rangle$ versus $\log g'$ allows the evaluation of the exponent ω as shown in figure 6(4.1).

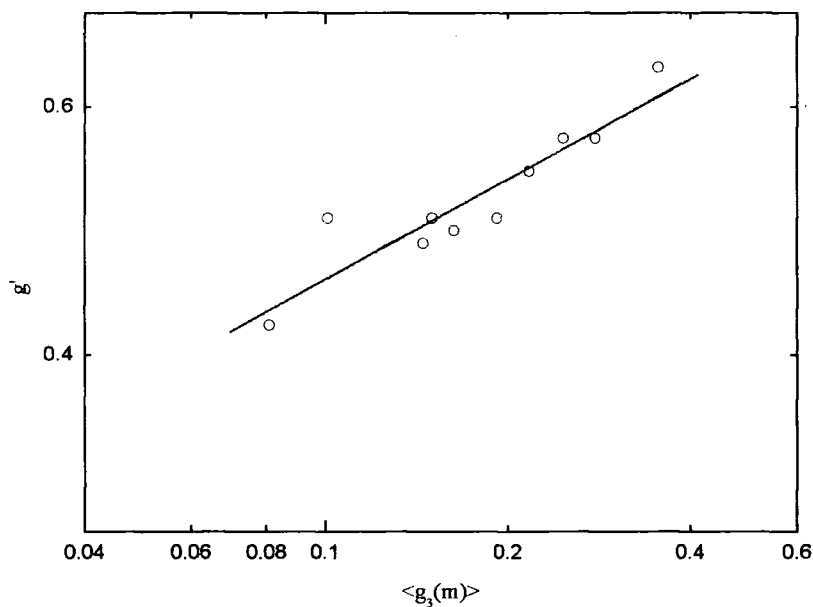


Figure 6(4.1). $\langle g_3(m) \rangle$ versus g' ; hyperbranched fractions.

From linear regression we have

$$9(4.1) \quad g' = (0.8 \pm 0.1) \langle g_3(m) \rangle^{(0.24 \pm 0.03)}$$

The exponent suggests a scaling law of the type $g' = \langle g_3(m) \rangle^{1/4}$ between the two branching factors and $\left(\frac{\alpha_{n,b}}{\alpha_{n,l}} \right)^3$ equals 0.8 ± 0.1 from 6(4.1).

The exponent is much lower than 0.5 proposed by Zimm and Stockmayer and deviates from 0.6 found for fractions of randomly branched polystyrene. This unexpected result may have an explanation in the branching heterogeneity of the hyperbranched polyester and also in the narrow molar mass distribution of the fractions.

Ioan and Burchard² proposed a slightly different treatment of the same problem assuming a constant branching density for the various samples and considering the proportionality between the molar mass and the number of branching points as follows.

$$10(4.1) \quad M = M_0 n_b \equiv \frac{1}{\lambda} n_b$$

M_0 is the molecular weight of the branching unit, n_b is number of branched units and λ is introduced to write the branching factor g in terms of molecular weight M as shown in 11(4.1).

$$11(4.1) \quad g = \left[\left(1 + \frac{\lambda M}{7} \right)^{1/2} + \frac{4\lambda M}{9\pi} \right]^{1/2}$$

For hyperbranched macromolecules they defined a new g_{Hb} factor (12(4.1)).

$$12(4.1) \quad g_{Hb} = \frac{6(1 + 2qM)^{1/2}}{\left[1 + (1 + 2qM)^{1/2} \right]^2}$$

Where $q = \alpha \times (1-\alpha) \times M_0$ and α is the branching probability. Equation 12(4.1) applies to non-fractionated samples in which the branching process has been restricted by the constraint that B can only react with A and it is only slightly different from equation 7b(4.1) that refers to monodisperse fractions with random branching.

In general, current theories on polymer branching are based on idealised models that cannot take into account the heterogeneities in branching and the effect of the excluded volume at the same time.

Unperturbed dimensions

It is of considerable interest to derive information about the dimensions of a macromolecule when the intra- and inter-molecular interactions are balanced, this condition being obtained when a polymer is in the theta solvent. However, as an ideal solvent is not always readily available, techniques have been sought to obtain unperturbed dimensions from measurements in non-ideal solvents. Several graphical procedures have been proposed that use the intrinsic viscosities of polymer fractions of known molecular weight. Stockmayer and Fixman⁶ suggested the simplest approach to the calculation of the unperturbed dimensions for linear polymers proposing equation 13(4.1).

$$13(4.1) \quad [\eta] \times \overline{M}_w^{-1/2} = K_\theta + 0.51\Phi_0 B \overline{M}_w^{1/2}$$

Where $\Phi_0 = 2.8 \times 10^{23}$ is the universal viscosity constant, K_θ is related to the unperturbed mean squared end-to-end distance, $\langle r^2 \rangle_0$, by equation 14(4.1) and B to the interaction parameter as shown in equation 15(4.1).

$$14(4.1) \quad K_\theta = \Phi_0 \left(\frac{\langle r^2 \rangle_0}{\overline{M}_w} \right)^{3/2}$$

$$15(4.1) \quad B = 2 \frac{v^2(1+2\chi)}{V_1 N_A}$$

Where v is the specific volume of polymer, V_1 is the molar volume of solvent; N_A is Avogadro's number. Equation 13(4.1) is valid for the intrinsic viscosity of flexible chain polymers in all solvents and its notable feature is the clean separation of the effects of short- and long-range interactions into two independent terms.

The Stockmayer-Fixman plot for the linear polyester is given in figure 7(4.1).

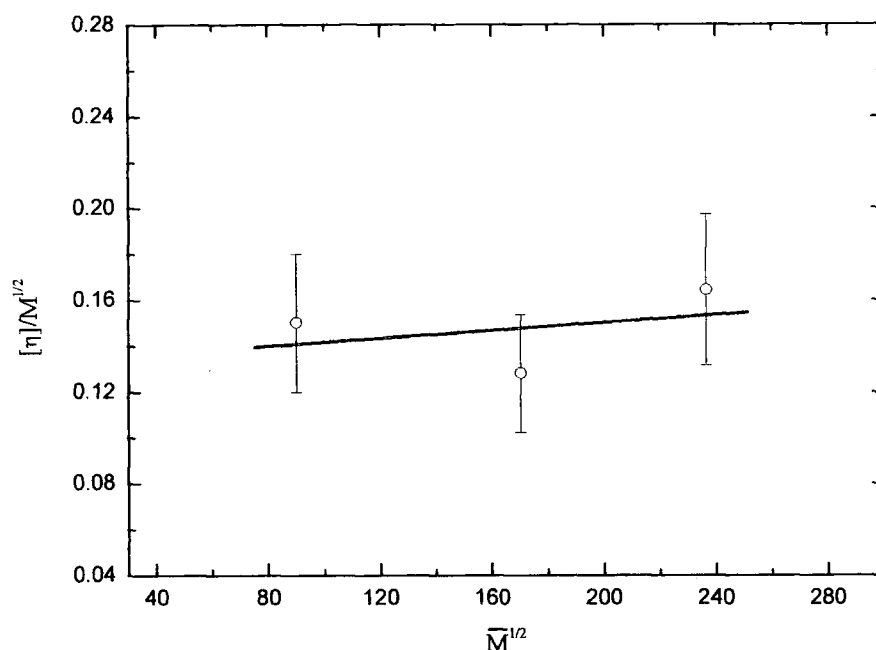


Figure 7(4.1). Stockmayer-Fixman plot: linear polyester.

The results of the linear regression are shown in the following equations and the normalised end-to-end distance is given in equation 16(4.1). The weight average molecular weight was used for molar mass of the polymer fractions.

$$B = (8 \times 10^{-5} \pm 2 \times 10^{-4}) \text{ ml g}^{-2} \text{ mol}$$

$$K_{\theta} = (0.13 \pm 0.04) \text{ ml g}^{-1}$$

$$16(4.1) \quad \left(\frac{\langle r^2 \rangle_0}{M_w} \right)^{1/2} (\times 10^4) = (800 \pm 200) \text{ nm}$$

Because of the small number of data and the large errors in the calculation, a quantitative definition of the interaction parameter has not been attempted, but the normalised end-to-end distance is comparable with other linear polyesters⁷. Since the linear polyester dissolved in chloroform is in the θ condition, the $K_{[\eta]}$ of the Mark-Houwink-Sakurada can be considered equivalent to K_{θ} and the normalised end-to-end distance obtained by this means is given in equation 17(4.1).

$$17(4.1) \quad \left(\frac{\langle r^2 \rangle}{M_w} \right)^{1/2} (\times 10^4) = (900 \pm 200) \text{ nm}$$

The values of the normalised end-to end distance obtained by the two methods are comparable within the experimental error.

Possible unperturbed dimension for the hyperbranched polymer

Ganazzoli and La Ferla⁸ have made some hypothesis about the unperturbed state of dendrimers. In their work, the unperturbed state is achieved when the intermolecular free energy vanishes and they predicted the θ temperature to be almost independent of the number of segments between adjacent branch points. The possibility of obtaining unperturbed dimensions for a hyperbranched system is a challenging problem that could open new investigations and better understanding of their solution behaviour. The application of the Stockmayer-Fixman equation to hyperbranched polymers may give information about the unperturbed radius of gyration of the polymer, however the particularly low value of the exponent $a_{[\eta]}$ results in negative values of the B factor that is physically meaningless. In the formulation of a possible modified Stockmayer-Fixman for highly branched systems this low value of $a_{[\eta]}$ must be considered.

In the present work the graphical approach of the Stockmayer-Fixman is adopted using the Zimm and Kilb⁹ relationship 18(4.1) for highly branched polymers.

$$18(4.1) \quad [\eta] = K_{[\eta]} M^{a_{[\eta]} - 1/4}$$

Which in a more complete form can be written as:

$$19(4.1) \quad [\eta] = K_{[\eta]} M^{\left(\frac{1+3\varepsilon}{2}\right) \frac{1}{4}}$$

In the case of θ condition $\varepsilon = 0$ and $a_{[\eta]} = 1/2$ and equation 19(4.1) becomes;

$$20(4.1) \quad [\eta]_{\theta} = K_{\theta} M^{1/4}$$

Equation 20(4.1) establishes a new θ condition for highly branched molecules that will be used to reformulate the Stockmayer-Fixman equation.

It is useful to introduce the Einstein equation for suspensions of solid spheres defined in terms of the equivalent hydrodynamic molecular dimension.

$$21(4.1) \quad [\eta] = \Phi \frac{\langle r^2 \rangle_0^{3/2}}{M} \alpha_h^3 = [\eta]_\theta \alpha_h^3$$

Substituting equation 21(4.1) in 20(4.1) and introducing equation 22(4.1) for the expansion factor¹⁰.

$$22(4.1) \quad \alpha_h^3 = 1 + \frac{BM^2}{K_\theta}$$

A modified version of the Stockmayer-Fixman is obtained in equation 23(4.1).

$$23(4.1) \quad [\eta] = K_\theta M^{1/4} + BM^{3/4}$$

Therefore, the plot of $\frac{[\eta]}{M_w^{1/4}}$ versus $\bar{M}_w^{1/2}$ gives the parameters K_θ and B as defined in

14(4.1) and 15(4.1). The modified Stockmayer-Fixman was applied to the data obtained in chloroform, considered a good solvent, and the plot is shown in figure 8(4.1). A linear regression was possible for 9 of the fractions, only the highest molecular weight deviating from the least squares fit.

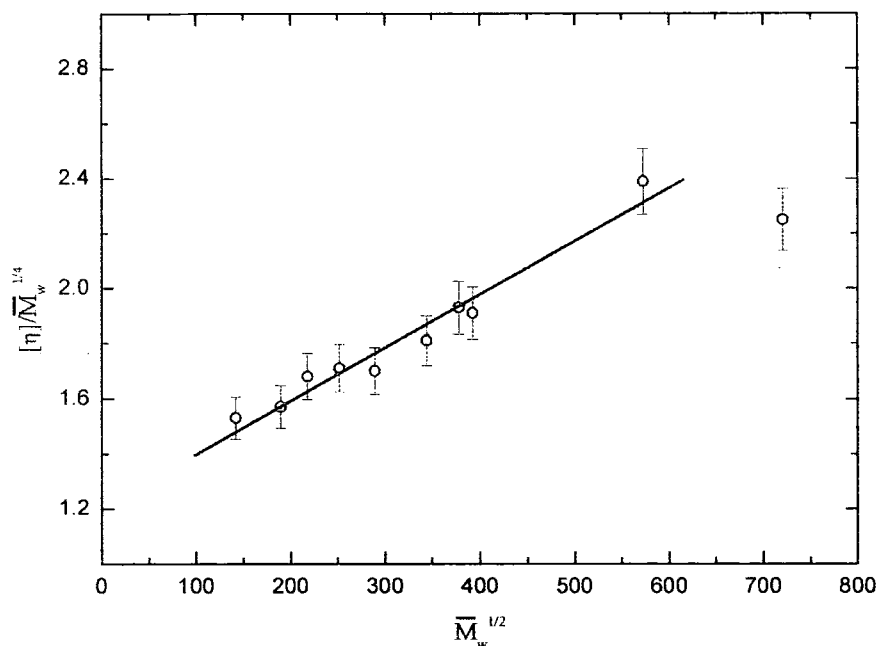


Figure 8(4.1). *Modified Stockmayer-Fixman: hyperbranched fractions in chloroform.*

The results of the linear regression are shown in the following equations.

$$B = (2 \times 10^{-3} \pm 1 \times 10^{-4}) \text{ ml g}^{-2} \text{ mol}$$

$$K_{\theta} = (1.23 \pm 0.04) \text{ ml g}^{-1}$$

And the relative normalised equivalent end-to end distance is given in 24(4.1).

$$24(4.1) \quad \left(\frac{\langle r^2 \rangle}{M_w} \right)^{1/2} (\times 10^4) = (1650 \pm 70) \text{ nm}$$

The value is much bigger than the one for the linear polymer, but this was expected because of the lower intrinsic viscosities measured for the hyperbranched system.

In the case of branched structure, it is convenient to use the mean square radius of gyration as a measure of the average size of the molecule rather than the end-to-end distance, because the multiplicity of the ends leads to ambiguity of the definition of the latter. The mean squared radius of gyration for linear chains is related to the end-to-end distance by the following equation;

$$25(4.1) \quad \langle s^2 \rangle = \frac{\langle r^2 \rangle}{6}$$

By the comparison of equations 5(4.1) and 25(4.1) it is possible to have a relationship between the equivalent end-to-end distance, $\langle r^2 \rangle_{eq}$, and the radius of gyration in the case of branched polymers as in 26(4.1).

$$26(4.1) \quad \langle s^2 \rangle_b = g_0 \langle s^2 \rangle_l = \frac{1}{6} g_0 \langle r^2 \rangle_{eq}$$

Introducing the equivalent end-to-end distance and the g_0 value into equation 26(4.1), the unperturbed radius of gyration for the hyperbranched polyester was obtained. The results of the calculation are shown in the table 2(4.1).

Table 2(4.1). *Unperturbed radii of gyration; hyperbranched fractions.*

Sample	\bar{M}_w (g mol ⁻¹)	R_g (nm)
1	519800	13.8
2	328200	12.2
3	154000	10.0
4	142900	9.8
5	118500	9.3
6	83700	8.5
7	63500	7.9
8	47600	7.3
9	36000	6.7
10	20200	5.7

These values of the radii of gyration are comparable with the experimental results obtained in THF by static light scattering given in section 3.7, so the configuration of the polymers in this solvent can be considered very close to the unperturbed situation.

The relations above provide a method for the calculation of the unperturbed radius of gyration of branched polymers from intrinsic viscosity and molecular weight data obtained in good solvent conditions.

Molar mass dependence of the radius of gyration and hydrodynamic radius

The molar mass dependence of the radius of gyration was studied by the relationship 27(4.1).

$$27(4.1) \quad R = K_{R_g} \bar{M}_w^{u_{R_g}}$$

The molar mass dependence of the radius of gyration was obtained by the common double log plot as shown in figure 9a(4.1) and 9b(4.1) for chloroform and THF solutions respectively.

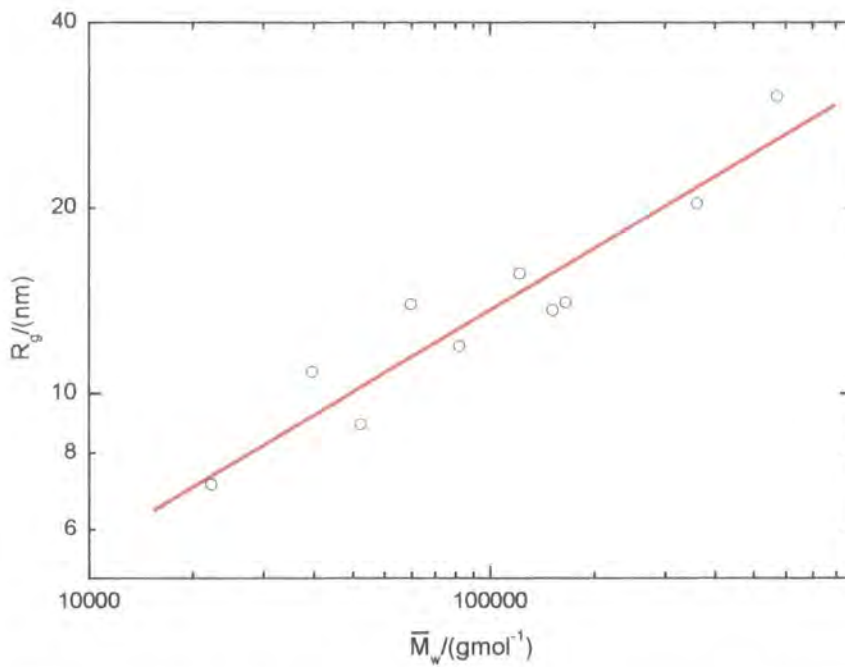


Figure 9a(4.1). R_g versus \bar{M}_w : hyperbranched fractions in chloroform.

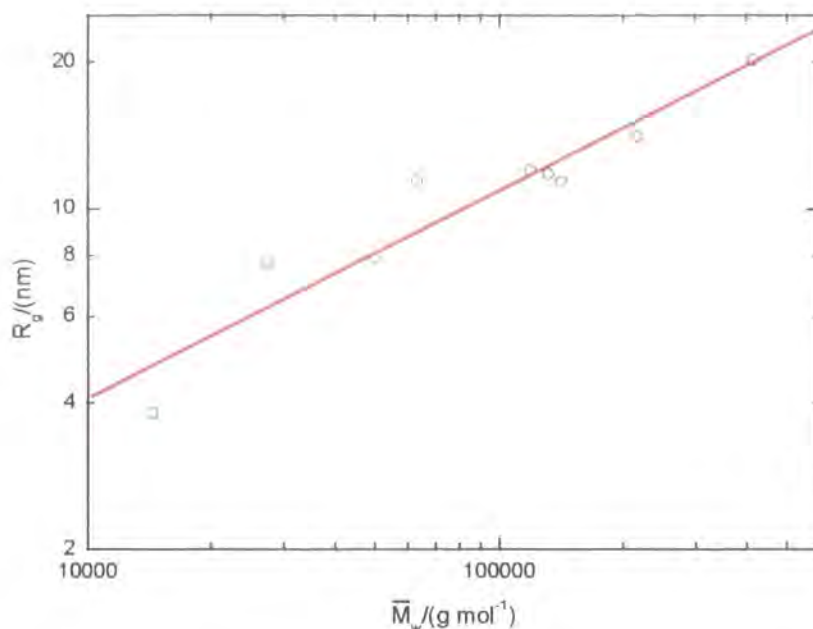


Figure 9b(4.1). R_g versus \bar{M}_w : hyperbranched fractions in THF.

The results of the least square linear fits are given in the expression 28a(4.1) for chloroform and in 28b(4.1) for THF solutions.

$$\mathbf{28a(4.1)} \quad R_g = (0.16 \pm 0.04) \bar{M}_w^{(0.39 \pm 0.05)} \text{ (nm)}$$

$$\mathbf{28b(4.1)} \quad R_g = (0.08 \pm 0.01) \bar{M}_w^{(0.42 \pm 0.05)} \text{ (nm)}$$

As already explained in section 3.7, it was not possible to obtain reliable radii of gyration for the analogous linear polyester.

The a_{R_g} exponents in the two solvents are comparable within experimental error although the radii of gyration obtained in THF are slightly smaller than the ones measured in chloroform. This fact is also evident from the smaller K_{R_g} value obtained in THF and can be explained by a screening effect due to the poorer polymer-solvent interaction, while in a good solvent like chloroform it is reasonable to consider the polymer swollen with R_g values slightly larger than in THF.

In branched systems the exponents a_{R_g} are commonly found with values close to 0.5 and sometimes even lower, while for linear polymer, typical values are in the range 0.6-0.8,

the a_{R_g} exponent, normally, varies between 0.33 for hard sphere to 1.0 for rigid rod. These low exponents in the case of branched systems seem to suggest poor solvent behaviour, however, the second virial coefficients are clearly positive and indicate good solvent behaviour¹¹.

Since equation 27(4.1) represents a power law between a length (the radius of gyration) and the molar mass of the object under investigation, it is possible to consider an exponent $d_f = 1/a_{R_g}$ characteristic of particle's morphology, which can be three-dimensional, two-dimensional or one-dimensional. In all the cases where d_f is an integer, the objects correspond to Euclidean solids. For $d_f = 3$ the object is a sphere, $d_f = 2$ is a flat disc and $d_f = 1$ a thin rod.

This consideration introduces fractal dimension analysis relating the exponent with particular geometrical structures. A fractal object can be explained as a structure that displays the same behaviour independently of the length scale. In other words if two pieces of different size are cut from a fractal object and the smaller is optically magnified to the same size of the larger, then the structure appear indistinguishable. The fractal dimension can be explained by rewriting equation 27(4.1) as follows:

$$29(4.1) \quad M = KR_g^{d_f}$$

For the hyperbranched polyester the exponents obtained gave a fractal dimension $d_f = 2.5 \pm 0.3$ in chloroform and $d_f = 2.4 \pm 0.3$ in THF. Since the values obtained are not integer, they define fractal objects in which the polymer segment density is not constant but changes in a well-defined manner with increasing R_g .

In general for linear polymer coils, $d_f = 5/3$ and 2 for a good solvent and θ solvent respectively¹². Branching usually increases d_f with respect to that of its linear counterpart and from theoretical calculation, randomly branched polymers are characterised by $d_f = 2$ in a good solvent and $d_f = 2.28$ in a θ solvent. Occasionally a fractal dimension of 3 was found for dendrimers, indicating homogeneous polymer segment distribution¹³. An alternative method to derive d_f uses the Mark-Houwink-Sakurada exponent according to the equation 30(4.1).

$$30(4.1) \quad d_f = \frac{3}{(1 + a_{[\eta]})}$$

The fractal dimension is not normally affected by polydispersity provided it is not excessively high. However Daoud¹⁴ considered randomly branched polymers with an extremely broad molecular weight distribution and showed that in this particular case the experimentally observed value for d_{eff} is affected by a very high polydispersity. The measured fractal dimension of the highly polydisperse samples is related to the effective fractal dimension according to the equation 31(4.1).

$$31(4.1) \quad d = \frac{d_{eff}}{3 - \tau}$$

Where τ is a critical polydispersity exponent that was predicted by Flory and Stockmayer to be equal to 2.5 and by percolation theory to be 2.2. Alternatively τ can be obtained experimentally by SEC moments using the relationship 32(4.1).

$$32(4.1) \quad M_w \approx M_z^{(3-\tau)}$$

The double log plots of z-average molecular weight \overline{M}_w versus \overline{M}_z (obtained by SEC) plots are shown in figure 10a(4.1) and 10b(4.1) for the chloroform and THF solution respectively.

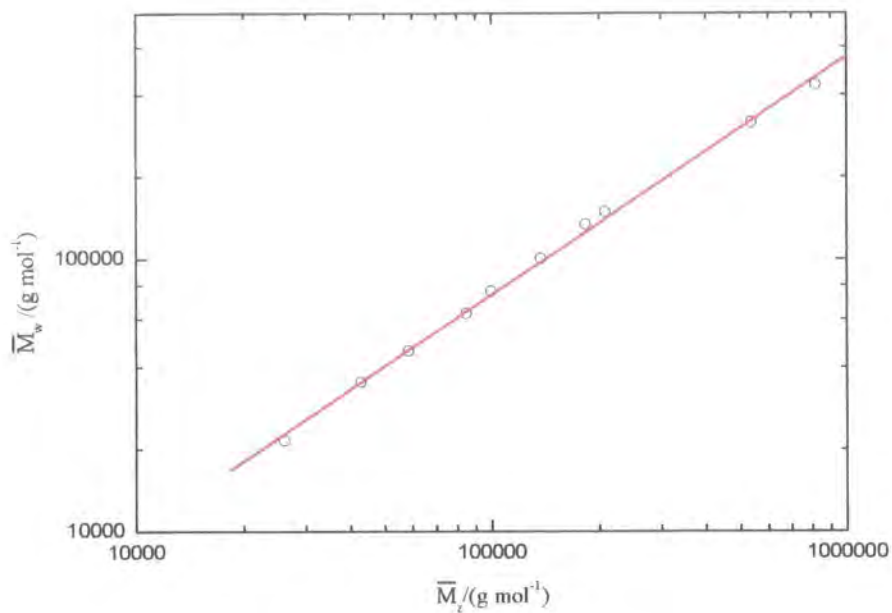


Figure 10a(4.1). \bar{M}_w versus \bar{M}_z ; hyperbranched fractions in chloroform.

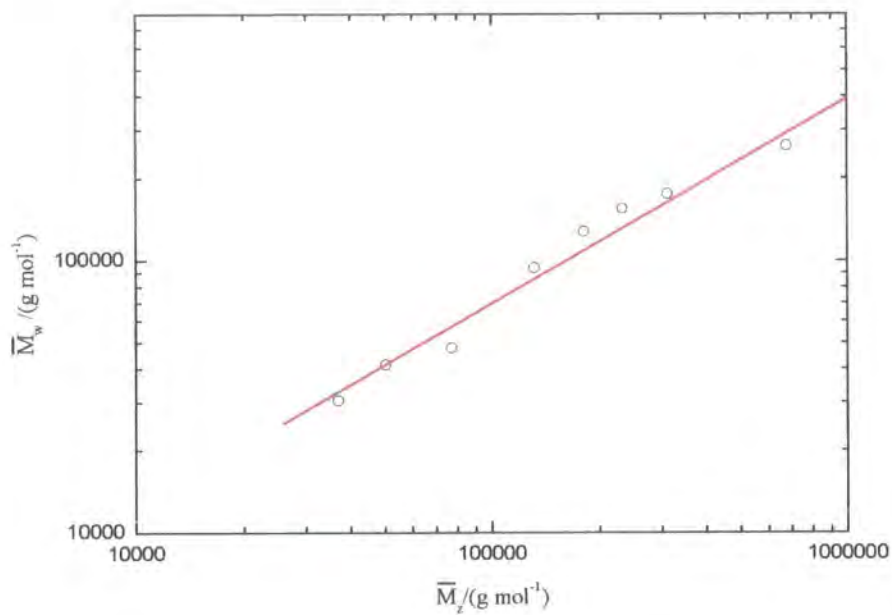


Figure 10b(4.1). \bar{M}_w versus \bar{M}_z ; hyperbranched fractions in THF.

The calculation of τ by the least squares fit gave a value of 2.13 ± 0.02 in chloroform and 2.2 ± 0.1 in THF. The value obtained in chloroform being more reliable because in THF the SEC analysis was perturbed by the presence of bimodal peaks as already explained in section 3.4. With the τ coefficient the calculation of the effective fractal dimension by equation 29(4.1) gave $d_{eff} = 2.17 \pm 0.05$ in chloroform and 2.08 ± 0.05 in THF. The value of $d_f = 2.1 \pm 0.2$ obtained in chloroform and 2.2 ± 0.3 in THF calculated by equation 30(4.1) are in agreement with these within experimental error.

The fractal dimension is a characteristic of the particular system under investigation and different values has been found for different structures. A fractal dimension of 2.44 is characteristic of a particle that has an internal structure between a hard sphere ($d_f=3$) and a fully swollen randomly branched macromolecule in a thermodynamically good solvent ($d_f=2$). On the other hand, a fractal dimension of 2.5 is predicted by theory for branched clusters that are not swollen, either for thermodynamic reasons or because of steric hindrance. The results obtained for the hyperbranched polyester in the two solvents are comparable within experimental error and it is not possible to distinguish quantitatively between the two different values. The study of the solution behaviour by fractal dimension analysis has been applied to other highly branched systems that show many similarities to the hyperbranched polymers. Glycogen and amylopectin appear to be the biological analogues of hyperbranched systems² because also in these polymers the functional group A only reacts with B (α -D-glucose monomer) and a higher branching density can be achieved in comparison to the A_3 -type polymers. These biological analogues have been understood as fractal object and a fractal dimension of 2.86 has been derived in the case of glycogen.

Hanselmann and Burchard¹⁵ have studied starch fractions for the same reason. The relationship R_g versus \overline{M}_w followed a straight line in the double log plot with an exponent 0.41 ± 0.01 that gave a fractal dimension of 2.43 ± 0.05 and a very similar behaviour has been found for waxy corn and potato starches with $d_f = 2.36 \pm 0.03$.

Bauer¹⁶ in the study of randomly branched polycyanurates, found a fractal dimension of 2.44 close to that of non-swollen cluster, although all measurements have been made in a good solvent, which gave high positive second virial coefficients. The explanation could be due to the fact that swelling of this macromolecule is scarcely possible and evidently the fractal structure of the non-swollen cluster, fixed during the reaction in melts, remains essentially preserved even in the good solvent.

The impossibility of distinguishing between good and poor solvent situation in our case is probably due to the experimental error or because the structure is stabilised and fixed by intra-molecular interactions.

The same correlation with the molar mass is possible for the hydrodynamic radius as shown in figure 11a(4.1) and 11b(4.1) for the chloroform and the THF data respectively.

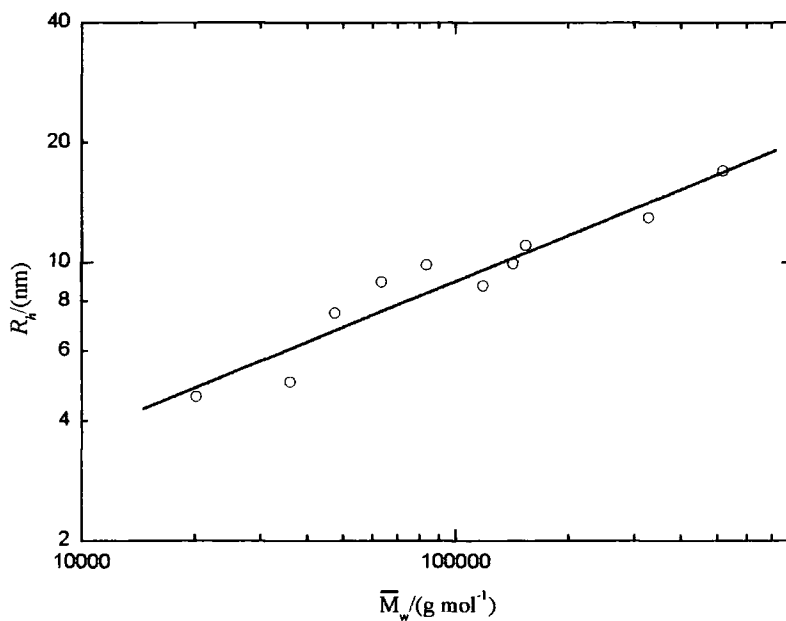


Figure 11a(4.1). R_h versus \bar{M}_w : hyperbranched fractions in chloroform.

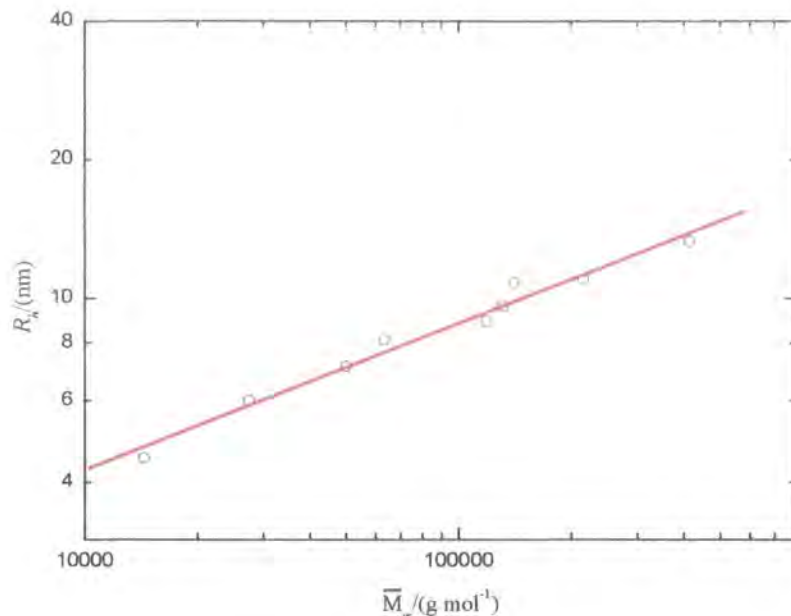


Figure 11b(4.1). R_h versus \overline{M}_w : hyperbranched fractions in THF.

The results obtained by the linear least squares fit are given in equations 33a(4.1) and 33b(4.1) for chloroform and THF solution respectively.

$$\mathbf{33a(4.1)} \quad R_h = (0.15 \pm 0.01) \overline{M}_w^{(0.35 \pm 0.04)} \text{ (nm)}$$

$$\mathbf{33b(4.1)} \quad R_h = (0.15 \pm 0.02) \overline{M}_w^{(0.35 \pm 0.04)} \text{ (nm)}$$

Exponents a_{Rh} obtained in chloroform and THF are identical, thus the hyperbranched polyester has the same hydrodynamic behaviour in the two solvents.

It is not clear why the hydrodynamic radius gives different molar mass dependence of the radius of gyration, but this is a situation already found by Galinsky and Burchard¹⁷ when studied starch fractions as an example of non-random branched molecules and they proposed two principal explanations to this problem. The first is the effect of the polydispersity and the second is the possibility that this type of macromolecules is able to change the shape.

In the limit of good solvent behaviour, for linear chains the exponent for the molar mass dependence of the radius of gyration, intrinsic viscosity and second virial coefficient obey the scaling relationships 34(4.1).

$$34(4.1) \quad a_{[\eta]} = 3a_{R_g} - 1$$

Introducing $a_{[\eta]} = 0.4$ in the 34(4.1) a value of $a_{R_g} = 0.46$ is obtained, higher than the value found experimentally in chloroform.

Bauer and Burchard¹⁶ investigated the scaling properties of a hyperbranched polycyanurates by the introduction of the polydispersity factor τ with the relationship 35(4.1) between the exponents.

$$35(4.1) \quad a_{R_g}^B = a_{R_g} (3 - \tau)$$

Where $a_{R_g}^B$ applies to molecularly uniform branched clusters. The application of the 35(4.1) to the hyperbranched polyester fractions gave $a_{R_g}^B = 0.34 \pm 0.05$ in chloroform and 0.36 ± 0.05 in THF which are close to the values of a_{R_h} obtained in both solvents.

Second virial coefficient, thermodynamic radius and viscosity radius

The molar mass dependence of the second virial coefficient can be represented by the following relationship.

$$36(4.1) \quad A_2 = K_{A_2} \bar{M}_w^{-a_{A_2}}$$

Figure 12a(4.1) represents the molar mass dependence of the second virial coefficient for the hyperbranched polymer fractions in chloroform and THF and in figure 12b(4.1) is shown the double log plot in the case of chloroform.

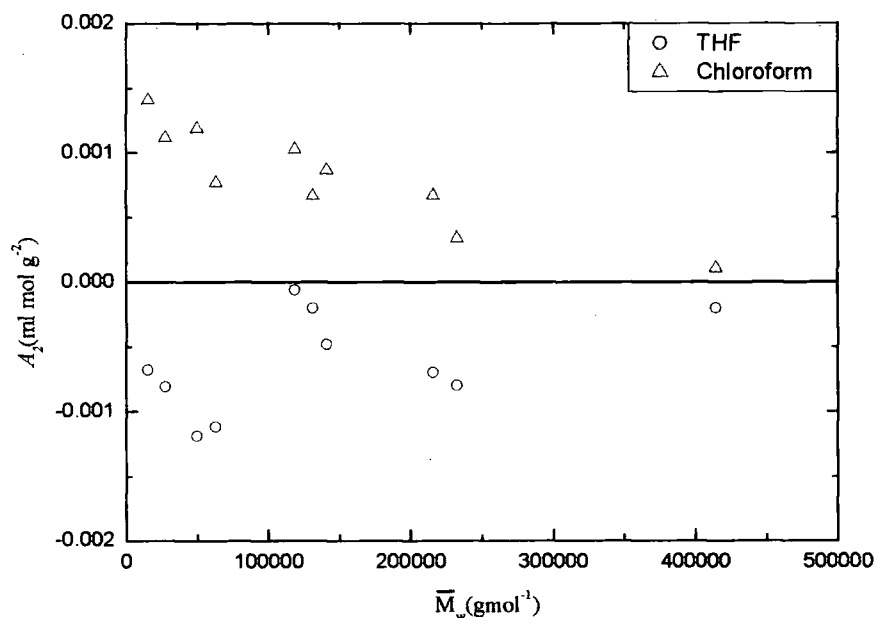


Figure 12a(4.1). Molar mass dependence of A_2 in chloroform and THF

In chloroform the values of the second virial coefficient increase with decreasing molecular weight as expected because the higher molecular weight polymers have a more positive free energy of mixing. In THF the data show no dependence on the molar mass and they are negative indicating a poor solvent condition.

Flory and Krigbaum¹⁸ concluded that A_2 should decrease with increasing molecular weight, but the predicted molar mass dependence was weaker than observed in experiments. The experimental data reported for linear polymers in good and poor

solvents indicate that A_2 is a decreasing function of molecular weight for a relatively narrow range (less than two decades) and a power law describes this function with the exponents found in the range 0.2-0.3. These considerations are limited to linear polymers in solvents in which A_2 is not negative. Available data on A_2 for polymer solutions below the θ condition are scarce. Tong et al¹⁹ undertook a systematic work on polystyrene in cyclohexane and Tanako et al.²⁰ did similar work on polyisoprene in dioxane. Interestingly these data indicated that A_2 in this regime is virtually independent of molecular weight and varies only with temperature.

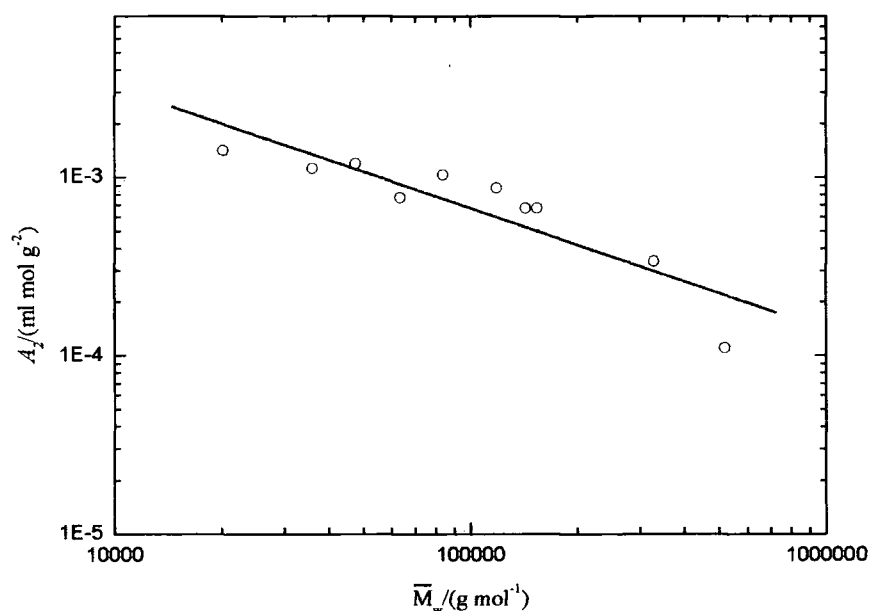


Figure 12b(4.1). A_2 versus \bar{M}_w : hyperbranched fractions in chloroform.

For the hyperbranched polyester in chloroform $a_{A_2} = 0.6 \pm 0.1$ was obtained, in good agreement with the predicted value of 0.67 for randomly branched chains¹¹.

In general, the exponent a_{A_2} changes from a value of about 0.2 for linear chains to 0.65 for a branched system, but there are no theories that give a complete explanation of this behaviour.

Bauer²¹ used polycyanurates fractions as examples of a randomly branched polymer and, after the characterisation by static light scattering and size exclusion

chromatography, The molar mass dependence of the second virial coefficient gave $A_2 = (0.31 \pm 0.1) \bar{M}_w^{(0.66 \pm 0.05)}$ and the relationship below was proposed.

$$37(4.1) \quad a_{[\eta]} + a_{A2} = 1.$$

Equation 37(4.1) also applies for the hyperbranched polyester discussed here.

Thermodynamic and viscosity radii

The analysis of the branching using branching factors is a valuable method to determine the type of branching and the branching density but this technique has the disadvantage that data of the linear analogue are needed and this is not always possible. Two other radii can be calculated, the thermodynamically effective equivalent radius, R_T defined in equation 38(4.1) and the viscosity radius, R_η defined in equation 39(4.1).

$$38(4.1) \quad R_T = \left(\frac{3}{16\pi} \frac{A_2 M^2}{N_A} \right)^{1/3}$$

$$39(4.1) \quad R_\eta = \left(\frac{[\eta] M}{(10\pi/3) N_A} \right)^{1/3}$$

The molar mass dependences of the two radii are shown in figure 13(4.1).

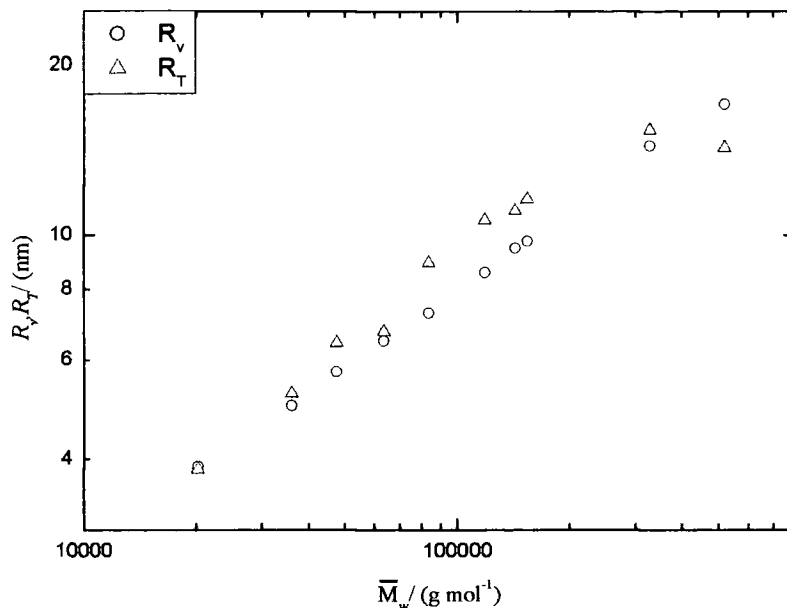


Figure 13(4.1). Molar mass dependence of R_T and R_v

The ratio between the different radii has been proposed as a sensitive measure of branching and it has been experimentally demonstrated that the ratio is close to unity when the thermodynamic and hydrodynamic interactions act over a similar distance.

Roovers and Martin²² studied the relationship between the radii in the case of star polymer. In the approximation of uniform-density hard spheres they proposed the relationship 40(4.1).

$$40(4.1) \quad R_g = \left(\frac{3}{5}\right)^{0.5} R_T$$

In regular star polymers the ratio of the principal axes approaches unity but as the number of arms increases the ratio of the principal axes varies. On the introduction of more arms, the segment density increases in the coil and the distribution becomes narrower and this effect makes star polymers much more close to the hard sphere model than linear polymers.

The hyperbranched fractions described here gave an average value of $R_T/R_g = 1.6 \pm 0.3$ that can be considered in agreement within the experimental error with the theoretical value of 1.77 obtained by the 40(4.1). Bauer et al¹⁶ studied star polyisoprenes with up to

56 arms and from the ratio R_T/R_g they concluded that the hard sphere limit is reached when the number of arms is approximately 30.

Diffusion coefficient

The power law defined in equation 41(4.1) was used to study molar mass dependence of the diffusion coefficient.

$$41(4.1) \quad D_0 = K_D \overline{M}_w^{-a_D}$$

The double log plots for the chloroform and THF solutions are shown in figures 14a(4.1) and 14b(4.1) respectively. An increase in the diffusion coefficient with the decreasing molecular weight was found in both solvents as expected.

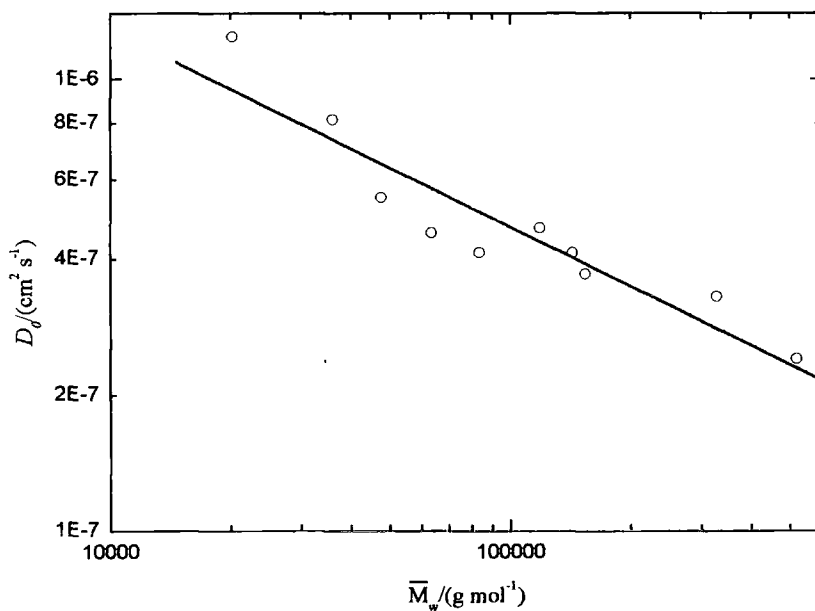


Figure14a(4.1). D_0 versus \overline{M}_w : hyperbranched fractions in chloroform.

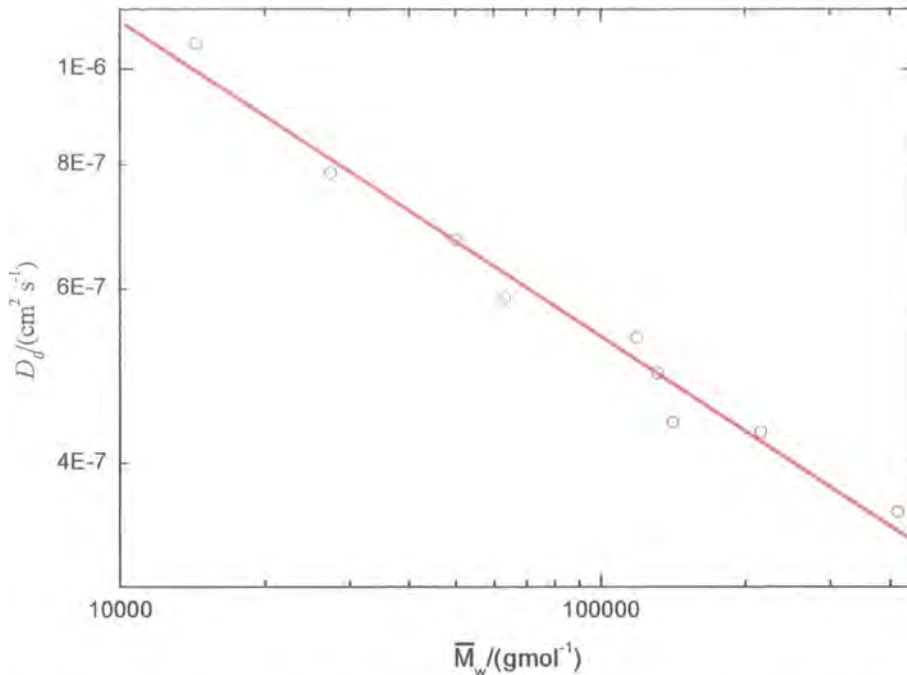


Figure 14b(4.1). D_0 versus \bar{M}_w : hyperbranched fractions in THF.

The scaling relationships obtained in chloroform and THF are shown in the equation 42a(4.1) and 42b(4.1) respectively.

$$\mathbf{42a(4.1)} \quad D_0 = (2.6 \times 10^{-5} \pm 5 \times 10^{-6}) \bar{M}_w^{(-0.35 \pm 0.03)} \quad (\text{cm}^2 \text{ s}^{-1})$$

$$\mathbf{42b(4.1)} \quad D_0 = (2.1 \times 10^{-5} \pm 5 \times 10^{-7}) \bar{M}_w^{(-0.33 \pm 0.05)} \quad (\text{cm}^2 \text{ s}^{-1})$$

In general, these are relations that apply over a wide range of molecular weight and in theta solvent a_D is always equal to 0.5 and in the range 0.5-0.6 in non-theta solvents for linear polymers²³. The Kirkwood-Riseman theory for linear polymers predicted that a_D in θ condition decreases monotonically from 1 to 0.5 with the increasing molecular weight.

The a_D values obtained for the hyperbranched polyester are lower compared to linear polymers, possibly because the higher segment density of the hyperbranched polymer, but a theoretical treatment for branched polymers has been not developed so far.

The concentration dependence of the diffusion constant, k_D , can also be analysed in function of the thermodynamic and hydrodynamic properties of polymer according to the equation 43(4.1).

$$43(4.1) \quad k_D = 2A_2M - k_s - \nu$$

Where k_s is a friction term defined in 44(4.1).

$$44(4.1) \quad k_s = k_0 \left(\frac{4\pi N_A}{3} \right) \frac{R_h^3}{M}$$

Where ν is the partial specific volume of the polymer in the solution ($0.75 \text{ cm}^3 \text{ g}^{-1}$ for the hyperbranched polyester). The molar mass dependence of k_D was studied in chloroform by the double log plot as shown in figure 15(4.1), while in THF such a plot was not possible because the negative k_D .

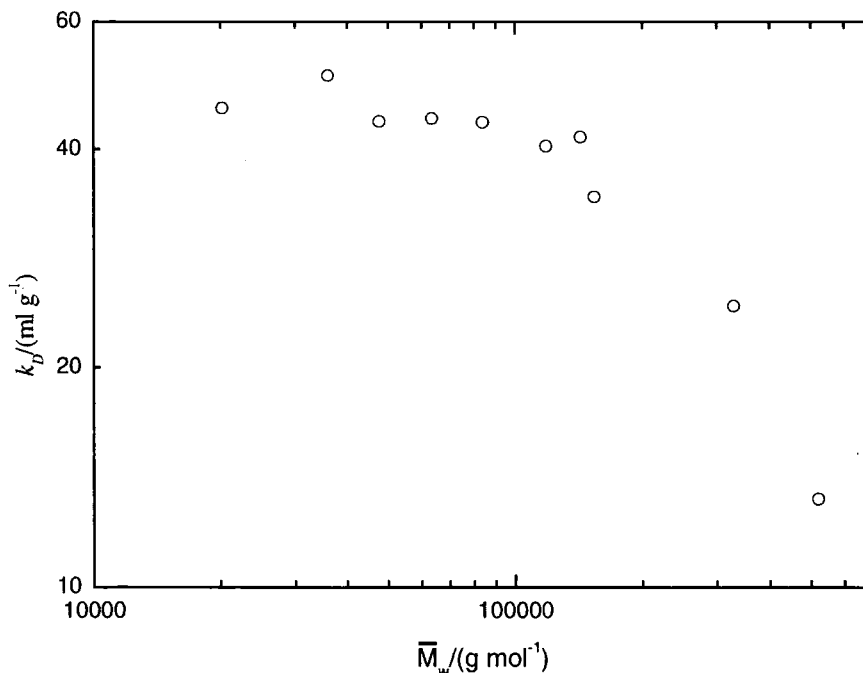


Figure 15(4.1). k_D versus \bar{M}_w : hyperbranched fractions in chloroform.

The value of k_s and k_0 calculated by equation 43(4.1) and 44(4.1) are reported in table 3a(4.1) for the chloroform and in table 3b(4.1) for the THF solutions.

Table 3a(4.1). *Calculated values of k_s and k_0 in chloroform.*

Sample	k_s (ml g ⁻¹)	k_0
1	100.40	2.79
2	198.12	13.52
3	171.21	7.85
4	149.13	8.71
5	165.04	11.77
6	128.07	4.38
7	52.94	1.89
8	68.84	3.08
9	29.29	3.34
10	10.63	0.87

Table 3b(4.1). *Calculated values of k_s and k_0 in THF.*

Sample	k_s (ml g ⁻¹)	k_0
1	-122	-8.5
2	-303	-22.4
3	-26	-2.8
4	-91	-5.1
5	30	4.3
6	-199	-15.8
8	-82	-5.9
9	-64	-5.0
10	-37	-3.2

Only in chloroform is a molar mass dependence of the k_s evident (figure 16(4.1)) but k_0 in both the solvents and k_s in THF showed no molar mass dependence.

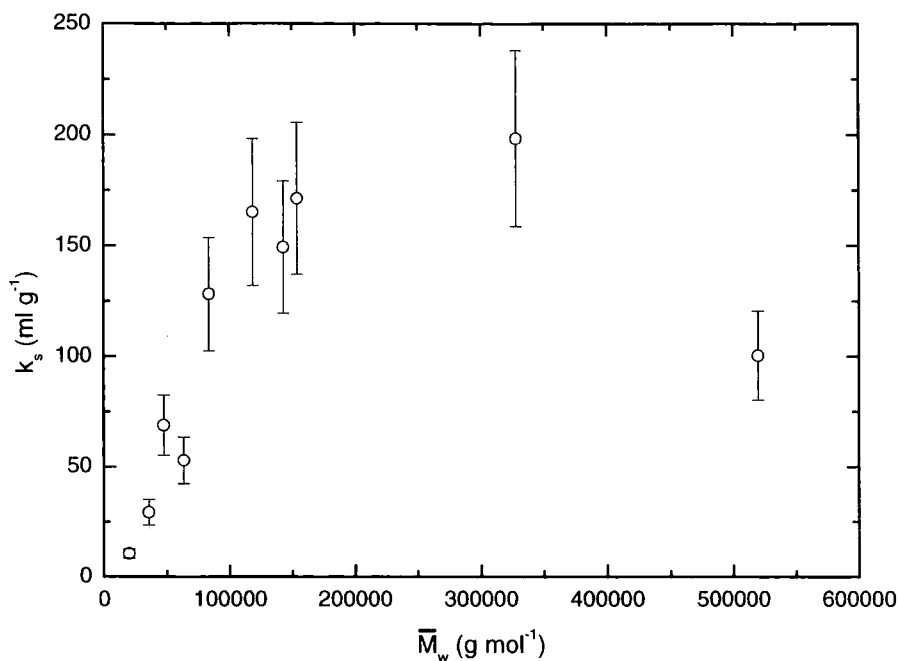


Figure 16(4.1). k_s versus \bar{M}_w : hyperbranched fractions in chloroform

In chloroform, for some of the fractions the values of k_s obtained are comparable to the data presented by Roovers and Martin²² for regular stars, but our data are rather scattered throughout the molecular weight range studied probably due to the effect of polydispersity. In THF the situation is not different, but fraction 5 gave an unexpected positive value for k_s and k_0 .

The average value of k_0 for linear polybutadiene in cyclohexane is about 5.2, while for 18-arm star polybutadienes the value was 7.3, close to the value 7.16 calculated by Pyun and Fixmann²⁴ for hard spheres in good solvent.

Negative value of k_s and k_0 are not common because is very difficult to obtain data for the second virial coefficient below the θ temperature. However, Cotts and Selser²⁵ found negative k_s and k_0 in their work on poly (α -methylstyrene) in θ and sub- θ solvents.

The ρ_b parameter

Another relevant structure parameter is the ratio between the radius of gyration and the hydrodynamic radius, ρ_b . The value of the ρ_b parameter is related to segment density in the macromolecule and for a fractal structure should be independent of the molar mass. The plots of ρ_b versus the weight average molecular weight are shown in figure 17a(4.1) and 17b(4.1) for chloroform and THF solution respectively.

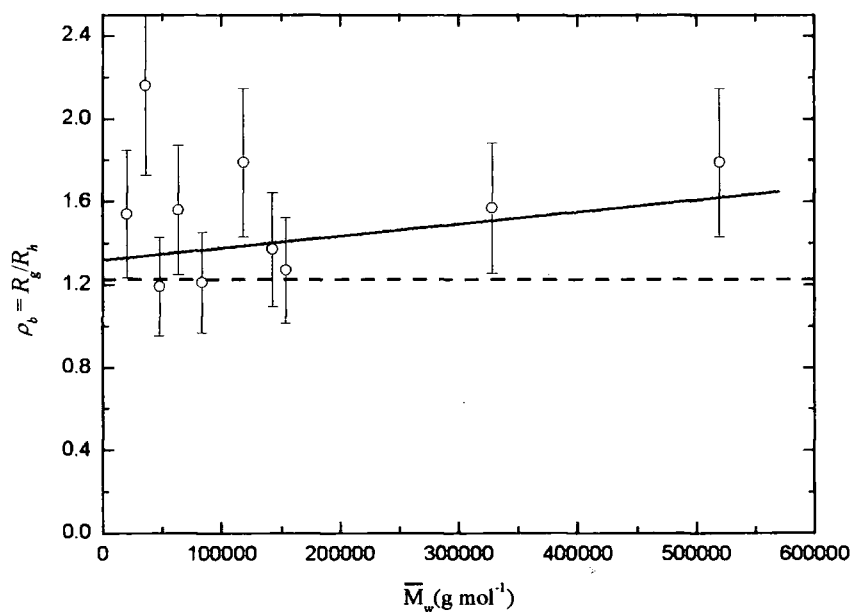


Figure 17a(4.1). ρ_b versus \bar{M}_w (full line) in chloroform; theoretical trend for hyperbranched polymers (dash line).

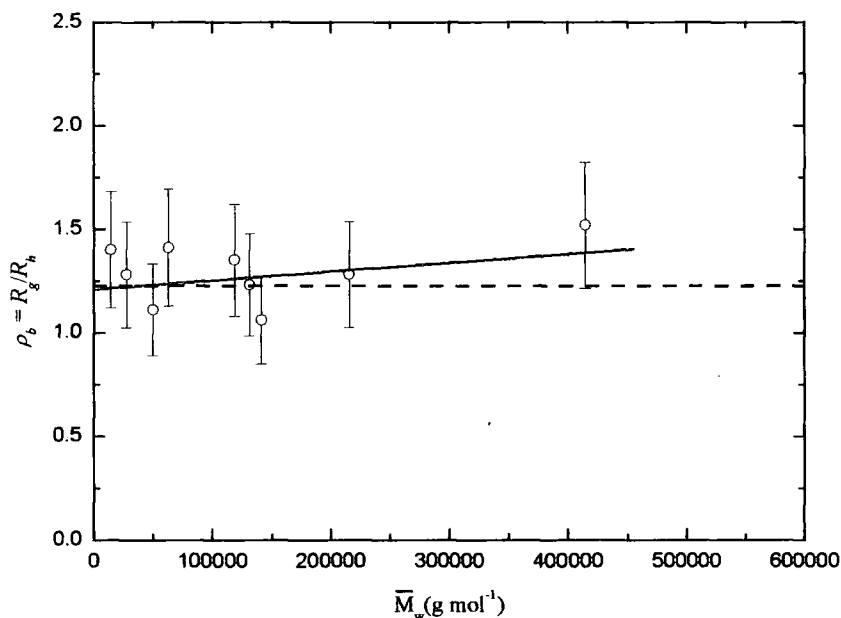


Figure 17b(4.1). ρ_b versus \bar{M}_w (full line) in THF; theoretical trend for hyperbranched polymers (dash line).

In chloroform there appears to be a weak dependence of ρ_b with the molar mass but this is almost non-existent in THF solution. The average values obtained are $\rho_b = 1.3 \pm 0.1$ in chloroform and $\rho_b = 1.21 \pm 0.07$ in THF that can be considered in good agreement with the theoretically predicted value for hyperbranched structure of $\rho_b = 1.22^{11}$.

Model calculations have shown that the ratio $\rho_b = R_g/R_h$ decreases with branching for monodisperse clusters and increases with polydispersity, so in the actual branched system the effect of branching on ρ_b is partially compensated by the effect of polydispersity. For randomly branched systems the two effects are fully balanced and the ρ_b parameter is not molar mass dependent. Since the measurements on starch fractions gave considerably lower values of ρ_b compared to theory, this could indicate that the influence of polydispersity is less important than the effect of branching and that the decrease of ρ_b indicates increased number of branching points per molecule. In general, the value of ρ_b should decrease with increased branching; so the constant value of ρ_b in the hyperbranched fractions studied here also confirm the result found for the

degree of branching by NMR, i.e. the degree of branching is the same for the all fractions.

For poly (vinyl acetates)²⁶ prepared by emulsion free radical polymerisation a value of $\rho_b = 1.84$ was found at a low monomer conversion and $\rho_b = 1.70$ and $\rho_b = 0.55$ for high degrees of conversion. The decrease of ρ_b with the increasing molecular weight, in this case, is an indication that the branching process is not fully random and this deviation from randomness may be related on the chain transfer mechanism that shows some similarities to AB₂-type polycondensation.

Regular 4-armed star polymers with a uniform arm length gave $\rho_b = 1.333$ in θ conditions and a value of 1.534 was found for the same polymer with polydisperse arms. Huber and Burchard²⁷ studied a series of 12-arm star polystyrenes with molecular weight between 5×10^4 to 1.69×10^6 g mol⁻¹ and the values of ρ_b decreases with increasing molecular weight from 1.56 to 0.89 in a θ solvent and in general, for star branched polymers with different number of arms, an increase of the number of arms accompanied by a weak increase of polydispersity is an essential reason for obtaining lower ρ_b values.

The generalised ratios

In a solvent in which the mean forces between segments are repulsive, polymer chains cannot interpenetrate each other and this means that in such a solvent there appear correlations between the relative position and conformations of a pair of chains that tend to overlap²³. The effect that these correlations exert on the thermodynamic behaviour of very dilute solution is measured by the second virial coefficient and it should depend on the strength of segment-segment interaction and on the chain length of the polymer. The excluded volume strength, β , is normally related to the second virial coefficient by a dimensionless quantity h defined in the following equation:

$$45(4.1) \quad h = \frac{2A_2M_0}{N_A\beta}$$

Where M_0 is the molecular weight of the monomer. Unfortunately β is not directly measurable, thus experimentalists prefer the dimensionless quantity, Ψ , penetration or interpenetration function defined by equation 46(4.1).

$$46(4.1) \quad \Psi = \frac{A_2 \overline{M_w}^2}{4\pi^{3/2} N_A R_g^3}$$

The interpenetration function should be a universal function of the expansion factor for the radius of gyration, α_s , describing the excluded volume effect and can be tested experimentally. The physical parameters in the interpenetration function can be obtained by static light scattering experiments but in our case it was not possible to have the experimental α_s and the approximations for its calculation that we can find in literature³ have been developed for linear polymers only. If we consider the expansion factor as proportional to the relative number of branched units, n_w , in the polymer fractions, then figure 18(4.1) shows the trend of Ψ with n_w .

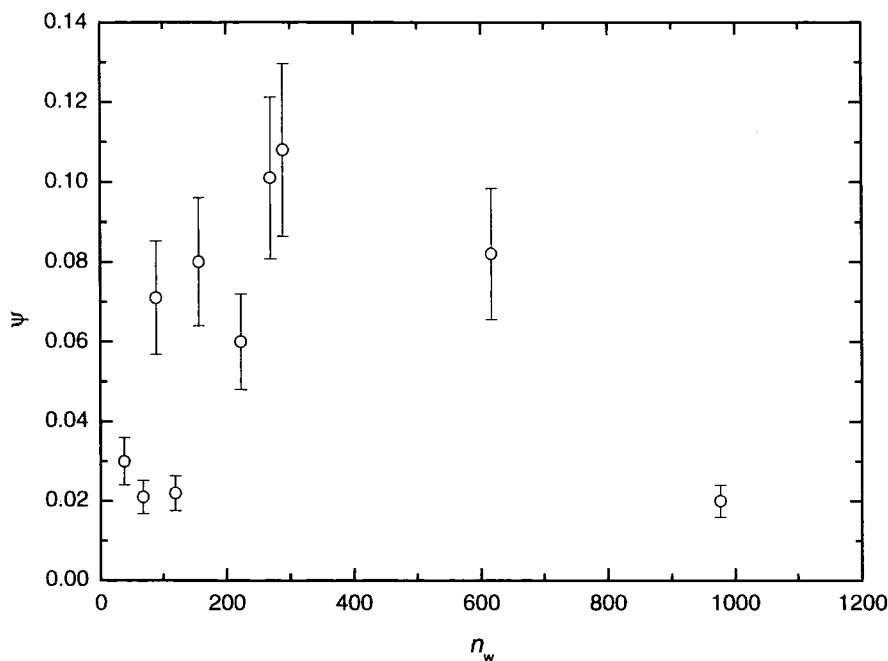


Figure 18(4.1). Ψ versus n_w ; hyperbranched fractions in chloroform.

The majority of the fractions showed an increase of the penetration function from 0.02 to 0.12 but the two fractions with the highest molecular weight are clearly not part of the trend with the others and not in agreement with the expected asymptotic behaviour¹¹. This is due the very low value of the second virial coefficient obtained even in a good solvent like chloroform for these fractions and also because their polydispersity is larger than the other fractions.

Another ratio considered more sensitive to the increased segment density has been introduced and is defined as follows.

$$47(4.1) \quad V_{A_2, \eta} = \frac{A_2 \overline{M}_w}{[\eta]}$$

This function is normally plotted against the number of arms f for the star polymers and produces an asymptotic plot. In our situation the $V_{A_2, \eta}$ function plotted against n_w is shown in figure 19(4.1). Again an asymptotic tendency is not observed because of the low values of A_2 obtained for the two highest molecular weight fractions.

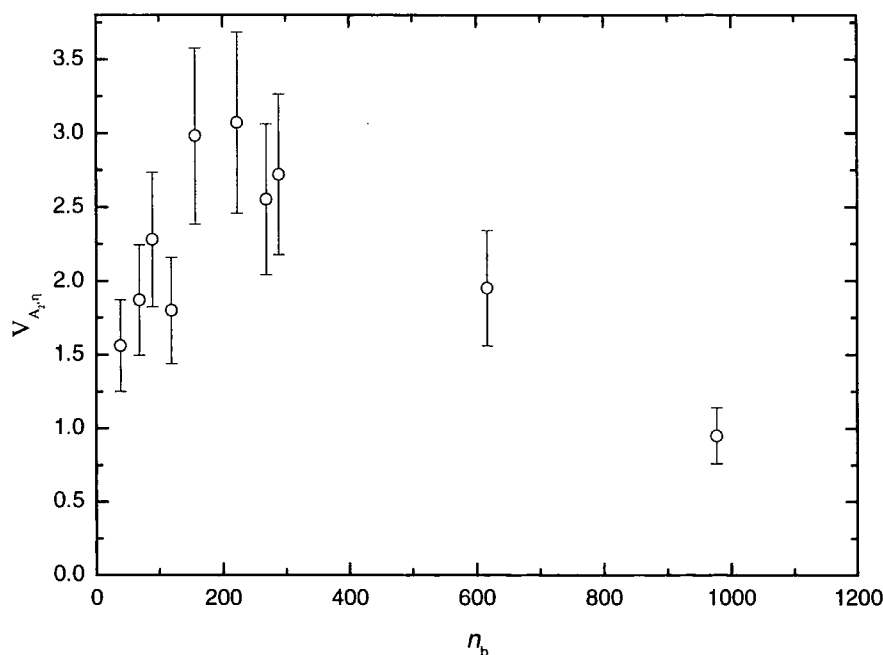


Figure 19(4.1). $V_{A_2, \eta}$ versus n_w ; hyperbranched fractions in chloroform.

As observed for other branched polymers, branching reduces the second virial coefficient in good solvents and the theta temperature. A correspondence between the intrinsic viscosity and the second virial coefficient, valid for hard spheres in solution, holds in good solvent and this correspondence improves with decreasing branching density. This finding explains the fact that the very high number of branched units in the two highest molecular weight fractions of the hyperbranched polyester has reduced the values of the second virial coefficient. The asymptotic value of $V_{A_2 \eta}$ found for hard spheres is 1.6 and for linear chains a value of 1.10 was derived from calculations, for star branched molecules the value varies from 1.52 for 4-arms to 1.73 for 6-arms.

For the hyperbranched polymer studied here the $V_{A_2, \eta}$ values increase from 1.5 to about 3 for the first eight fractions and then for the two highest molecular weight fractions the value decreases. It appears from the penetration and the $V_{A_2, \eta}$ functions that the high branching density of the hyperbranched systems decreases the sensitivity of the generalised ratios and that new theories able to include the peculiar behaviour of the branched systems are needed. There is a region in which the relative number of branched units increases the penetration function, but over a certain limit the polymer-solvent interaction plays a more important role than branching.

References

1. Turner, S. and B. Voit, *Macromolecules*, 1994. **27**: p. 1611.
2. Ioan, C.E., T. Aberle, and W. Burchard, *Macromolecules*, 1999. **32**: p. 7444.
3. Yamakawa, H., *Modern Theory of Polymer Solutions*. 1971, New York: Harper and Row.
4. Zimm, B.H. and W.H. Stockmayer, *J. Chem. Phys.*, 1949. **17**(12): p. 1301.
5. Schaeffgen, J. and P. Flory, *J. Am. Chem Soc.*, 1948. **70**: p. 2709.
6. Stockmayer, W. and M. Fixman, *J. Polym Sci. C*, 1963. **1**: p. 137.
7. Brandrup, J., E.H. Immergut, and E.A. Grulke, *Polymer Handbook*. 1999: John Wiley & Sons, Inc.
8. Ganazzoli, F. and R.L. Ferla, *J. Chem. Phys.*, 2000. **113**(20): p. 9288.
9. Zimm, B. and R. Kilb, *J. Polym. Sci.: Part B: Polym. Phys.* 1996. **34**: p. 1367.
10. Van Krevelen, D.W., *Properties of Polymers*. 1997, Oxford: Elsevier.
11. Burchard, W., *Adv. Polym. Sci.* 1999. **143**: p. 113.
12. Daoud, M. and J. Joanny, *Journal de Physique*, 1981. **42**: p. 1359-1371.
13. Scherrenberg, R. and B. Coussens, *Macromolecules*, 1998. **31**: p. 456.
14. Daoud, M., F. Family, and G. Jannik, *J. Phys. Lett.*, 1984. **45**: p. L199.
15. Hanselmann, R. and W. Burchard, *Macromolecules*, 1996. **29**: p. 3277.
16. Bauer, J. and W. Burchard, *Macromolecules*, 1993. **26**: p. 3103.
17. Galinsky, G. and W. Burchard, *Macromolecules*, 1995. **28**: p. 2363.
18. Flory, P., *Principles of Polymer Chemistry*. 1953: Cornell University Press, Ithaca, NY.
19. Tong, Z., *Polym. J.*, 1983. **15**: p. 835.
20. Tanako, N., *Polym. J.*, 1985. **17**: p. 1123.
21. Bauer, J., P. Lang, and W. Burchard, *Macromolecules*, 1991. **24**: p. 2634.
22. Roovers, J. and J.E. Martin, *J. Polym Sci.: Part B: Polym. Phys.* 1989. **27**: p. 2513.
23. Fujita, H., *Polymer Solutions*. 1990: Elsevier.
24. Pyun, C.W. and M. Fixman, *J. Chem. Phys.*, 1964. **41**(4): p. 937-944.
25. Cotts, P.M. and J.C. Selser, *Macromolecules*, 1990. **23**: p. 2050.
26. Burchard, W., M. Schmidt, and W.H. Stockmayer, *Macromolecules*, 1980. **13**: p. 1265.
27. Huber, K., W. Burchard, and L.J. Fetters, *Macromolecules*, 1984. **17**: p. 541.

4.2 Semi-dilute solutions

When the available volume per polymer molecule calculated from the concentration of the solution approaches the volume of the molecules, molecules start to overlap. In other words, the spatial extent of a molecule is expressed in terms of the radius of gyration and the solution divided into spherical volumes, each containing a polymer molecule, when the sphere radius approaches equals twice the radius of gyration, the spheres will be in contact and this concentration is given by;

$$1(4.2) \quad c^* \approx \frac{M}{N_A R_g^3}$$

c^* identifies the overlap concentration and the beginning of the semi-dilute regime that is still somewhat dilute and normally does not exceed 10 % w/v.

In the dilute regime the osmotic pressure depends on molecular weight enabling its calculation and the absence of the intermolecular interactions allows the evaluation of the radius of gyration and second virial coefficient. Above the c^* , due to the entangled nature of the solution, the solvent activity and osmotic pressure no longer depend on the molecular size but rather on some length set by the distance between entanglement points. De Gennes¹ introduced the term overlap concentration for c^* since linear chains may be visualized as interpenetrating until they eventually become entangled. At c^* a change in the properties of the polymer is expected. Although the picture of chain overlap becomes problematic for branched structures, branched chains and hyperbranched macromolecules can interpenetrate each other in a manner similar to the linear chains. Several definition of c^* exist and a definition of c specific for branched polymers has yet to be given. For flexible linear chains the following conventions are accepted².

$$2(4.2) \quad c^*_{[\eta]} = \frac{1}{[\eta]} \quad (\text{g ml}^{-1})$$

$$3(4.2) \quad c^*_{R_g} = \frac{\overline{M_w}}{4\pi/3 N_A R_g^3} \quad (\text{g ml}^{-1})$$

$$4(4.2) \quad c^*_{A_2} = \frac{1}{A_2 M_w} \quad (\text{g ml}^{-1}) \quad (\text{good solvent})$$

Equation 2(4.2) is for flexible coils and in the case of hard spheres the right hand side has to be replaced by $2.5/[\eta]$. The dimensions of the coils are used in the equations 3(4.2) and equation 4(4.2) uses the thermodynamic interactions. The three relationships for the overlap concentration are assumed to be proportional to each other in the case of the linear chains but this is not true for the branched materials. For the hyperbranched polyester the calculation of the overlap concentration in THF solution by equation 3(4.2) was used because equation 2(4.2) gives incorrect results due to the lower intrinsic viscosity of the hyperbranched polymer solutions and 4(4.2) is not applicable because THF is a poor solvent for the polymer. There is only a weak dependence of the c^* on the molecular weight of the hyperbranched polyester (Figure 1(4.2)). In general c^* is circa $3 \times 10^{-2} \text{ g ml}^{-1}$ except for the last fraction which has a very low molecular weight.

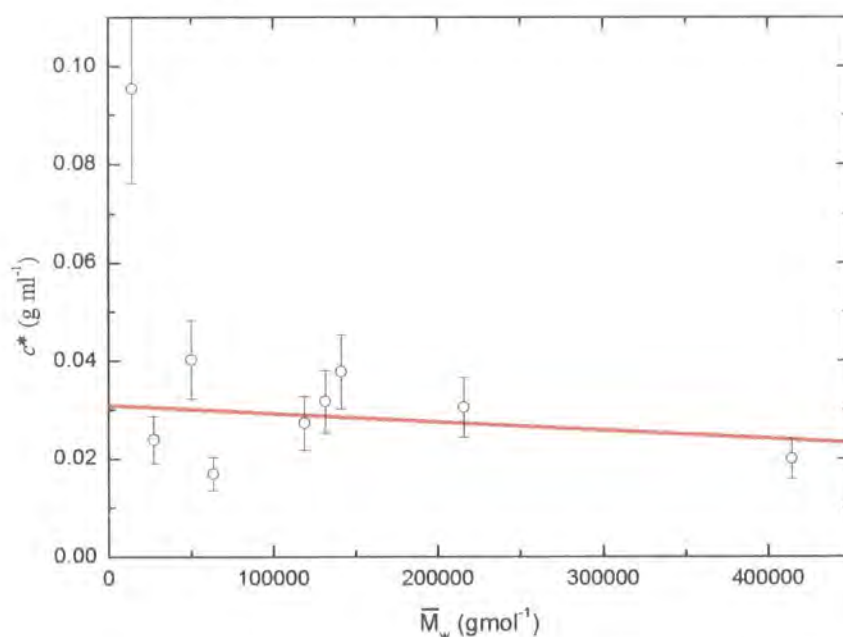


Figure 1(4.2). Molar mass dependence of c^* in THF calculated from equation 3(4.2); hyperbranched fractions.

In the semidilute regime the angular dependence of the scattered light is now also a function of the concentration and the Kc/R_θ expression given in the common virial expansion, has to include the higher virial coefficients. These are normally related to A_2 by the following equations.

$$\mathbf{5a(4.2)} \quad A_3 \overline{M}_w c^2 = g_A (A_2 \overline{M}_w c)^2$$

$$\mathbf{5b(4.2)} \quad A_4 \overline{M}_w c^2 = h_A (A_2 \overline{M}_w c)^3$$

Where the coefficient g_A and h_A are structure dependent. For hard spheres A_3 and A_4 are both positive and in the case of flexible linear chains only A_3 is known with value of 0.277 in good solvent. The semi-dilute regime for the hyperbranched fractions in THF solution has been studied by small angle neutron scattering and the results will be discussed in the following sections.

SANS experiments in the semi-dilute regime

The physical parameters obtainable from SANS data are the radius of gyration, weight average molecular weight, virial coefficients and information about the polymer shape in solution. As mentioned in section 3.9, SANS experiments were carried out in deuterated THF, in a concentration range between 2% w/v and 5% w/v corresponding to the semi-dilute regime. The choice of concentration range is defined by the need for good scattering intensity and good statistics in data acquisition. The first plot of interest is the comparison of the differential scattering cross sections for different concentrations of the same fraction (Figure 1(4.2)). Error bars are not included in the following graphs for clarity.

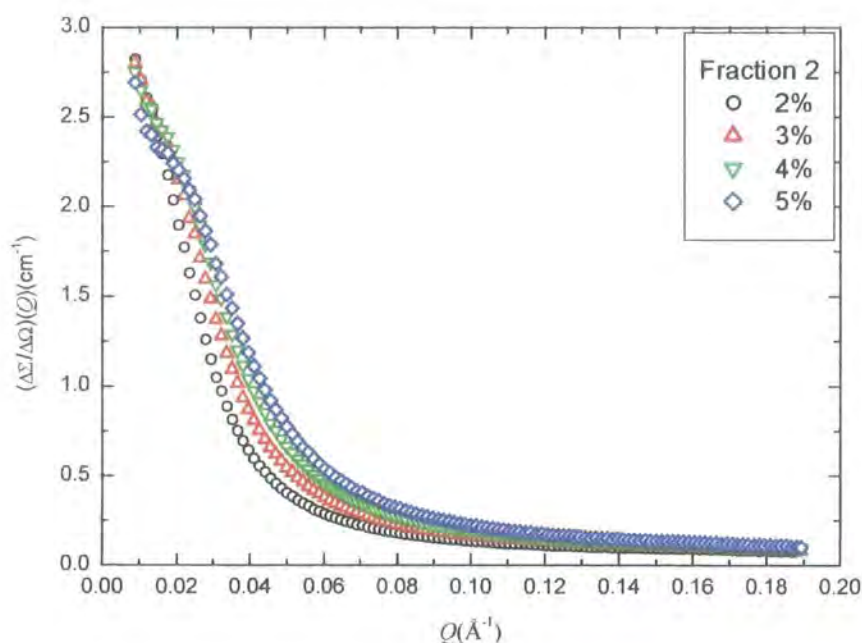


Figure 1(4.2). Concentration dependence of the cross section: fraction 2, D22 data.

It is possible to see an increase of the scattering intensity in the intermediate Q region, while the curves overlay in the very low Q range due to detector and counting imperfections. The cross section curves do not approach zero because of incoherent scattering due to the hydrogenated polymer and the amount of the incoherent scattering is higher in the case of the spectra collected by D22 than in the case of LOQ (Figure 2(4.2)) probably because the different sensitivity of the detectors used in the two instruments.

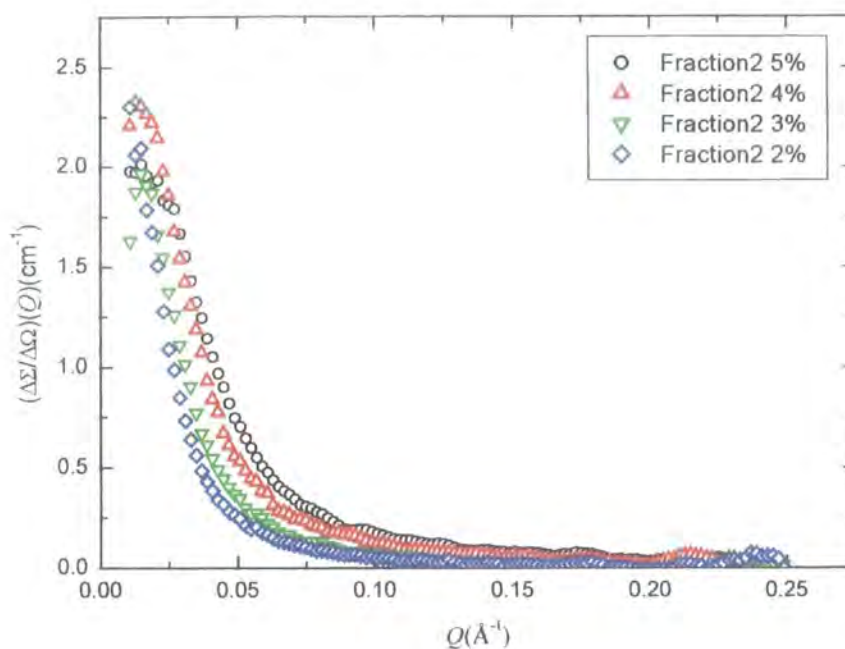


Figure 2(4.2). Concentration dependence of the cross section: fraction 2, LOQ data.

The incoherent scattering was accurately subtracted prior to data fitting and calculation of any physical parameters.

A comparison of different fractions of the polymer at the same concentration indicates that the cross section of the hyperbranched fractions increases with the increasing molecular weight as shown in figure 3(4.2).

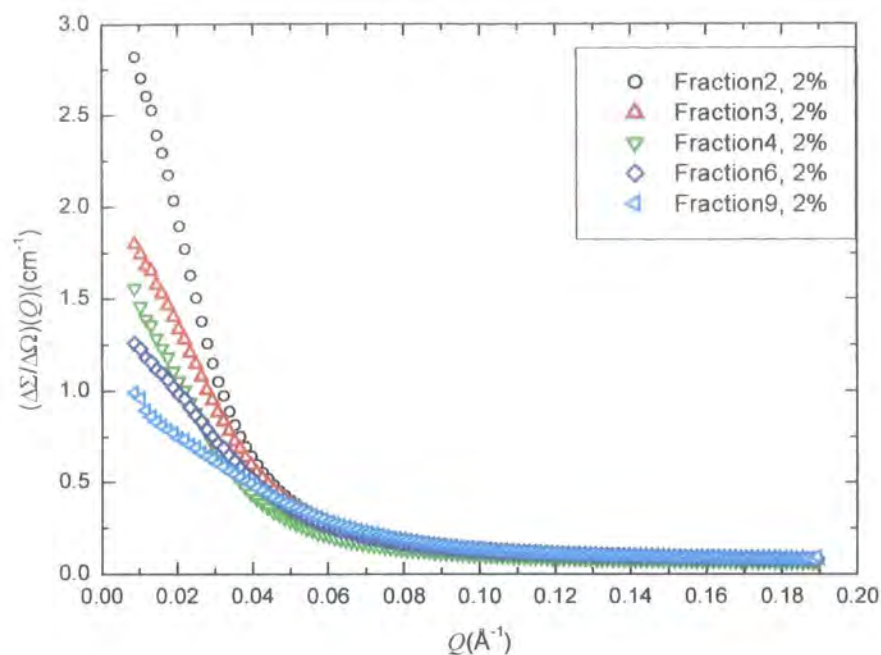


Figure 3(4.2). *Molecular weight dependence of the cross section through the hyperbranched fractions: D22 data.*

As mentioned in section 2.8, the different regions of Q can give different information about the polymer in solution. The first region to be analysed is the low Q -range. In this scattering regime the information gained is the overall dimensions, the molecular weight and the virial coefficients. The most popular method for the investigation of this Q regime is the Zimm plot. This is a typical method for the dilute regime, but is still applicable in the semi-dilute regime. A second method for obtaining molecular weight and radius of gyration is fitting the scattering profiles with a specific form factor for AB_2 polycondensation polymers and a third approach is to use a Kratky plot to extract information about the polymer in solution.

Zimm plot analysis

The method relies on the same concepts adopted in the static light scattering experiments and for SANS the approximation is:

$$6(4.2) \quad \frac{1}{\frac{\Delta\Sigma}{\Delta\Omega}(Q)} \approx \frac{1}{NV^2(\Delta\rho)^2} \left[1 + \frac{(QR_g)^2}{3} \right]$$

Where N and V are the number and volume of the scatterers and $(\Delta\rho)^2$ is the contrast. The plot of $[\Delta\Sigma/\Delta\Omega(Q)]^{-1}$ versus Q^2 should be linear in the low Q^2 range (Figure 4(4.2)) and, by a linear regression fit, the slope and intercept are related to physical parameters as defined in equation 7 (4.2) and 8(4.2).

$$7(4.2) \quad \text{Intercept} = \frac{1}{M_w} \cdot \frac{N_A \cdot \delta}{c \cdot (\Delta\rho)^2}$$

$$8(4.2) \quad \text{Slope} = \frac{R_g^2}{3} \cdot \text{Intercept}$$

The cross section curves were analysed in the low Q -range by the Zimm method to obtain the molecular weight, the radius of gyration and the virial coefficients. In figure 5(4.2) only the extrapolation lines to zero concentration and zero angles are shown for clarity. The details of the results for each fraction are given in table 1a(4.2) for the data collected by the LOQ and 1b(4.2) for the D22 data.

The details of all Zimm plot calculations can be find in Appendix SANS.

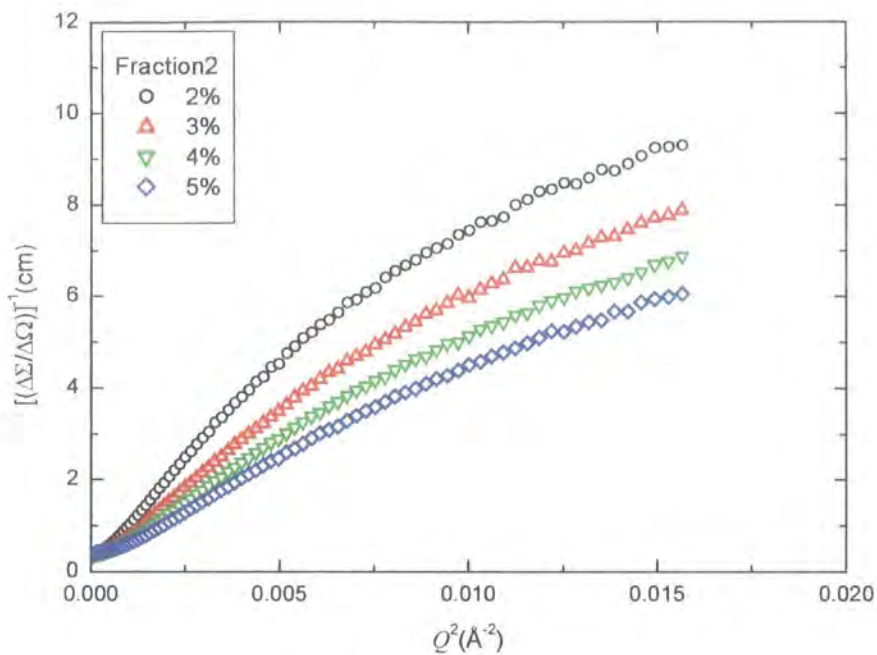


Figure 4(4.2). Scattering data plotted according to the Zimm method.

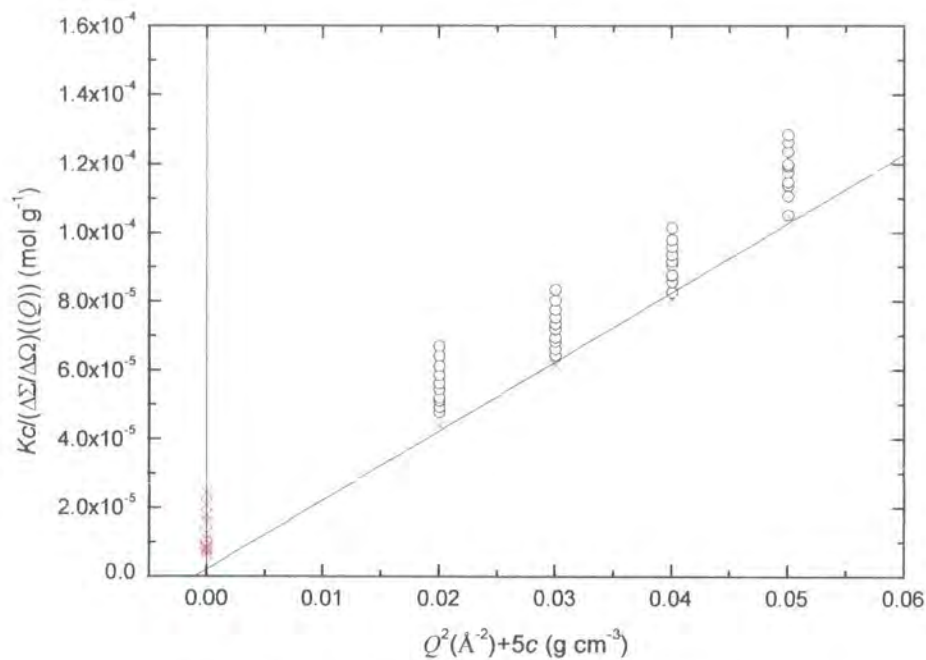


Figure 5(4.2). Example of Zimm plot; hyperbranched fraction2

Table 1a(4.2). Zimm plot results; hyperbranched fractions; LOQ data.

Sample	\bar{M}_w (g mol ⁻¹)	R_g (nm)	$\sum_{i=2}^n A_i$ (cm ³ mol g ⁻²)
1	352 700	11.8	2.1×10^{-4}
2	219 200	9.1	3.1×10^{-4}
3	124 500	8.0	3.6×10^{-4}
4	110 400	8.2	2.0×10^{-4}
5	115 600	7.7	3.0×10^{-4}
6	70 000	7.7	1.4×10^{-4}
7	90 100	5.7	3.8×10^{-4}
8	67 000	5.5	4.3×10^{-4}
9	40 200	4.6	4.2×10^{-4}
10	23 400	2.8	2.4×10^{-4}

Table 1a(4.2). Zimm plot results for the hyperbranched fractions; D22 data.

Sample	\bar{M}_w (g mol ⁻¹)	R_g (nm)	$\sum_{i=2}^n A_i$ (cm ³ mol g ⁻²)
2	199 800	8.6	2.2×10^{-4}
3	118 900	6.7	2.5×10^{-4}
4	107 500	7.9	2.1×10^{-4}
5	111 500	6.1	2.8×10^{-4}
6	83 700	5.8	2.7×10^{-4}
8	70 600	5.7	2.6×10^{-4}
9	58 550	4.8	2.3×10^{-4}
10	39 800	4.7	1.8×10^{-4}

The data obtained by the Zimm plot analysis with the two instruments are in agreement within a 10% error on the \overline{M}_w and the R_g and 15% on the virial coefficient. The term

$\sum_{i=2}^n A_i$ includes the contribution of the other virial coefficients that must be taken into account in semi-dilute regime and it is positive because the higher virial coefficients are normally positive and possibly because the polymer-solvent interaction in D-THF is different. The radii of gyration are in general smaller compared to the ones obtained in the dilute regime by static light scattering because of the expected screening effect. The molar mass dependence of the radius of gyration is shown in Figure 6(4.2).

In all these calculations the density used to calculate the scattering length density of the hyperbranched polyester is the one reported in the polymer handbook for amorphous polyethylene terephthalate³ (1.33 g cm⁻³). This may be incorrect for the hyperbranched polyester and thus some errors in the molecular weight may be evident.

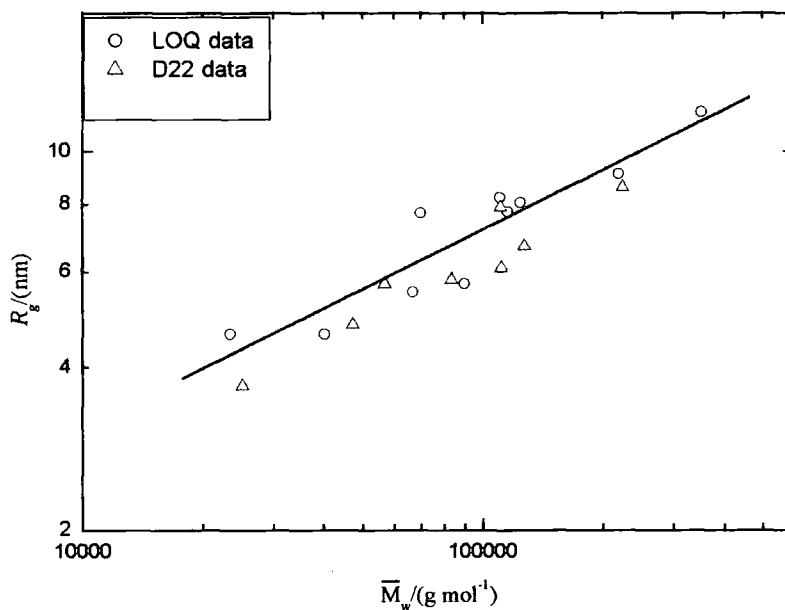


Figure 6(4.2). \overline{M}_w versus R_g : hyperbranched fractions.

The results obtained by the least square linear fits are given in equation 9(4.2).

$$9(4.2) \quad R_g = (0.1 \pm 0.03) \overline{M}_w^{(0.37 \pm 0.05)} \quad (\text{nm})$$

The exponent is comparable to the ones obtained by static light scattering even though the radii of gyration are smaller in the semi-dilute regime due to the concentration screening effect.

Influence of deuterated solvent

Strazielle and Benoit⁴ showed that the interaction of hydrogenated polymers with deuterated solvents is not the same as for protonated solvent. For this reason a few static light scattering experiments have been carried out in deuterated THF and the results compared with the second virial coefficient in protonated THF are shown in table 2(4.2).

Table 2(4.2). Comparison of A_2 ($\text{cm}^3 \text{ mol g}^{-2}$) in D-THF and THF; hyperbranched polyester.

Sample	A_2 (THF)	A_2 (D-THF)
2	-6.8×10^{-4}	-2.1×10^{-4}
5	-0.5×10^{-4}	2.8×10^{-4}
8	-11.9×10^{-4}	1.1×10^{-4}

In all the experiments more positive values of the second virial coefficient were obtained in D-THF showing that the thermodynamic properties in deuterated solvent are different. Strazielle and Benoit demonstrated in the case of deuterated and protonated polystyrene that a shift of the θ temperature depending on whether the solvent was deuterated or protonated occur. No data are available on the possible different polymer-solvent interactions of linear polyesters or branched systems in deuterated solvent, but the data in table 2(4.2) suggest that D-THF is a better solvent for the hyperbranched polyester. Further investigations are needed to understand fully the effect of deuterated solvents.

Form factor analysis

Branched polymers often have a huge molecular weight polydispersity and for very high molecular weight, if the branching density exceeds a certain minimum value, the particle form factor becomes insensitive to the exact branching density. Using fractionated hyperbranched samples permitted the calculation of radii of gyration and weight average molecular weights by fitting the scattering curves with the particle form factor that Burchard⁵ proposed for the AB₂ polycondensate defined in the equation 10(4.2).

$$10(4.2) \quad P(Q) = \left(1 + \frac{(QR_g)^2}{6} \right)^{-2}$$

The fitting of the cross section profiles collected by the two different instruments was carried out with the help of Origin 6.0 software, by using equation 11(4.2).

$$11(4.2) \quad \frac{\Delta\Sigma}{\Delta\Omega}(Q) = A \times \left(1 + \frac{(QR_g)^2}{6} \right)^{-2} + B$$

Where B is the background and A is a coefficient that includes instrumental and physical parameters. Typical curve fits, where the adjustable fitting parameters were A , R_g and B , are shown in figure 7a(4.2) to 7f(4.2).

The details of all form factor calculations can be found in Appendix SANS.

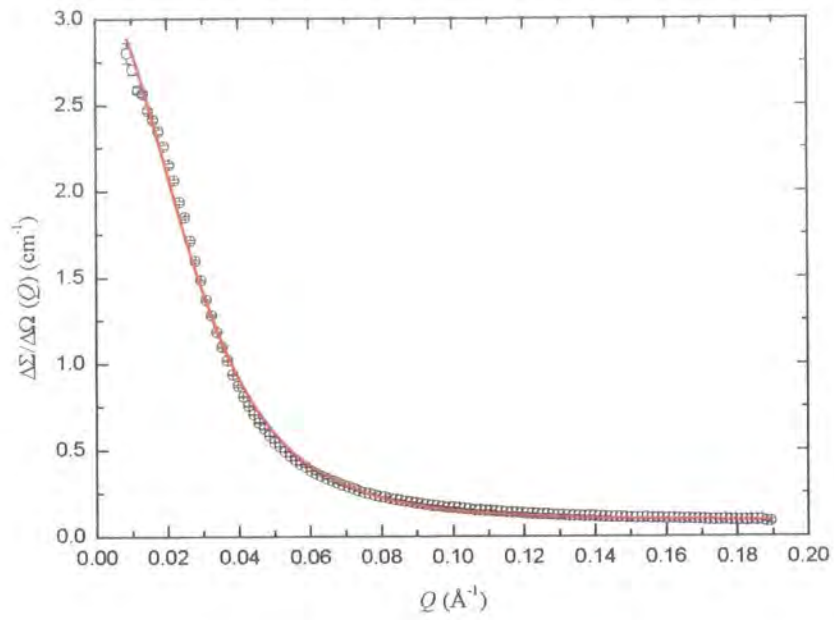


Figure 7a(4.2). Curve fit for the fraction 2 (3% w/v); D22 data.

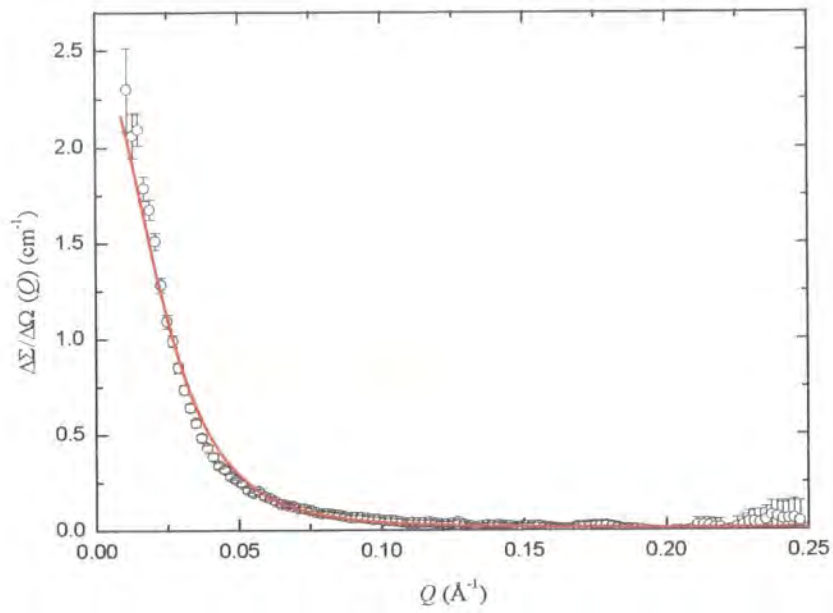


Figure 7b(4.2). Curve fit for the fraction 2 (3% w/v); LOQ data.

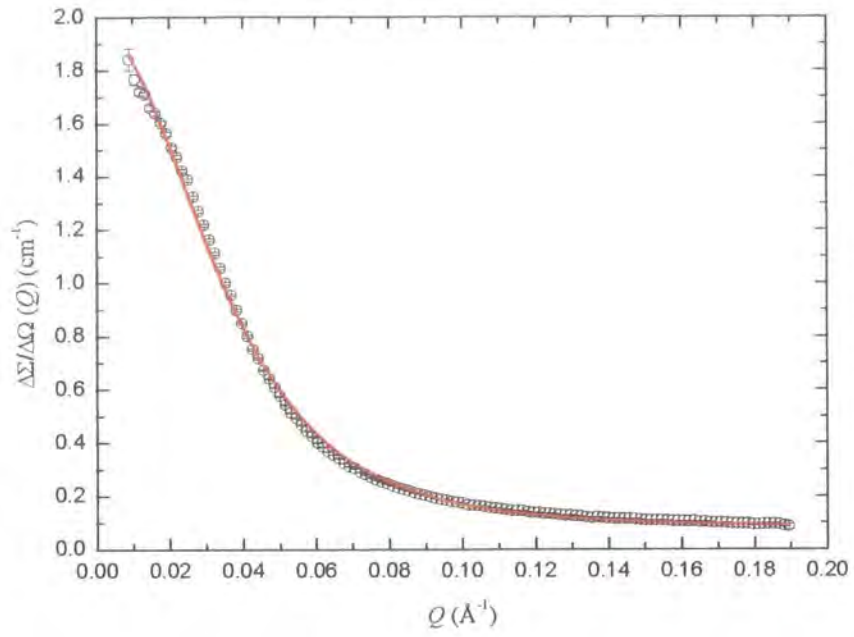


Figure 7c(4.2). Curve fit for the fraction 5 (3% w/v); D22 data.

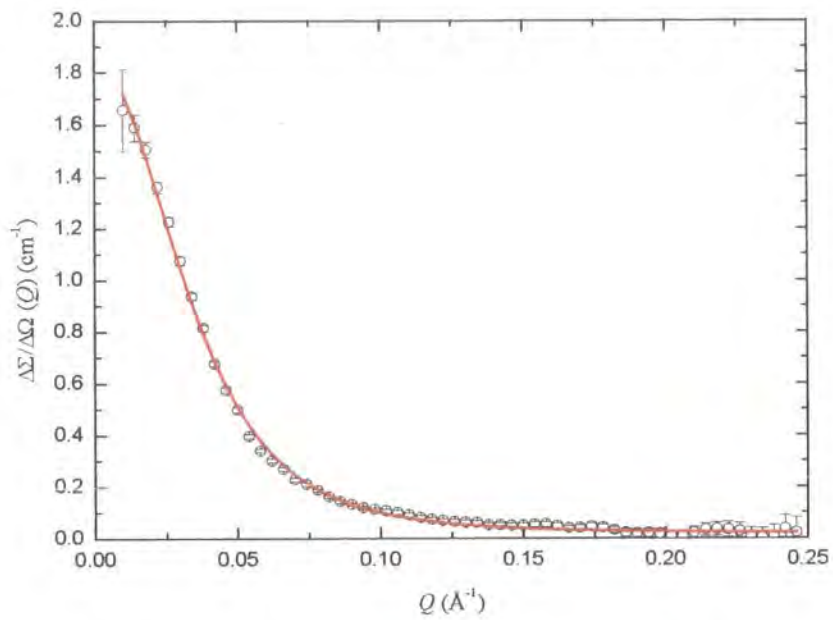


Figure 7d(4.2). Curve fit for the fraction 5 (3% w/v); LOQ data.

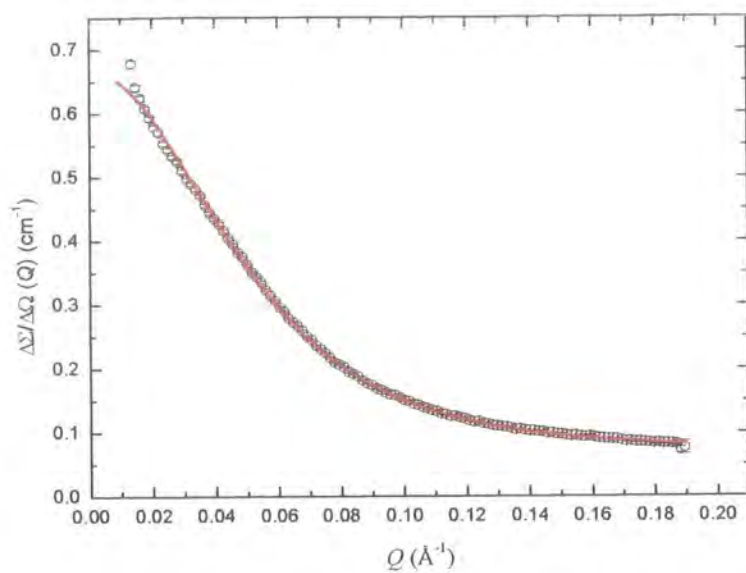


Figure 7e(4.2). Curve fit for the fraction 10 (3% w/v); D22 data.

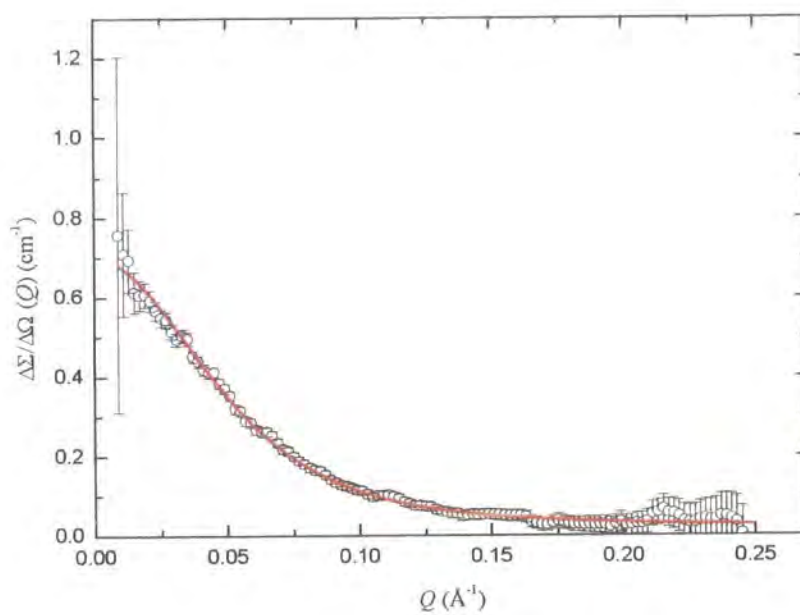


Figure 7f(4.2). Curve fit for the fraction 10 (3% w/v); LOQ data.

The fits to the data are good in most cases, but for some there is a discrepancy between the data and the fitted curve in the very low Q range. This behaviour can be attributed to some extent to the limits of the area detector. The values of the mean square radius of gyration for different concentrations obtained have been extrapolated to zero concentration for each fraction. The constant A in the fitting function includes information about the molecular weight of the polymers because;

$$12(4.2) \quad A = NV^2(\Delta\rho)^2 \frac{1}{\phi}$$

Where N is the number of scattering particles, V is the volume, ϕ is the detector efficiency and $(\Delta\rho)^2$ is the contrast. It is possible to rewrite NV^2 as in 13(4.2).

$$13(4.2) \quad NV^2 = \frac{c\overline{M}_w}{N_A\delta^2}$$

Where c is the concentration, N_A is Avogadro's number and δ is the polymer density. Since the detector efficiency is allowed to be 1 by using a calibrant (H-PS/D-PS blend or H₂O), the substitution of equation 12(4.2) into equation 13(4.2) gives:

$$14(4.1.2) \quad \overline{M}_w = \frac{A \cdot N_A \cdot \delta^2}{c \cdot (\Delta\rho)^2}$$

The results are collected in table 3a(4.2) for the LOQ data and in table 3b(4.2) for the D22 data.

Table 3a(4.2). *Form factor results; hyperbranched fractions, LOQ data.*

Sample	\bar{M}_w (g mol ⁻¹)	R_g (nm)
1	307 000	10.2
2	201 800	9.9
3	101 500	7.2
4	97 900	7.7
5	107 250	6.8
6	74 000	6.5
7	68 560	4.8
8	60 500	4.8
9	41 300	4.6
10	23 500	3.5

Table 3b(4.2). *Form factor results; hyperbranched fractions, D22 data.*

Sample	\bar{M}_w (g mol ⁻¹)	R_g (nm)
2	218 804	8.4
3	124 840	6.8
4	101 967	7.4
5	113 774	6.2
6	78 151	5.9
8	57 109	5.3
9	45 074	4.6
10	22 625	3.8

The molecular weights obtained by SANS appear in good agreement with those measured by classical light scattering.

The results obtained by the two instruments are in good agreement within a 10% experimental error and the molar mass dependence of the radii of gyration is shown in figure 8(4.2).

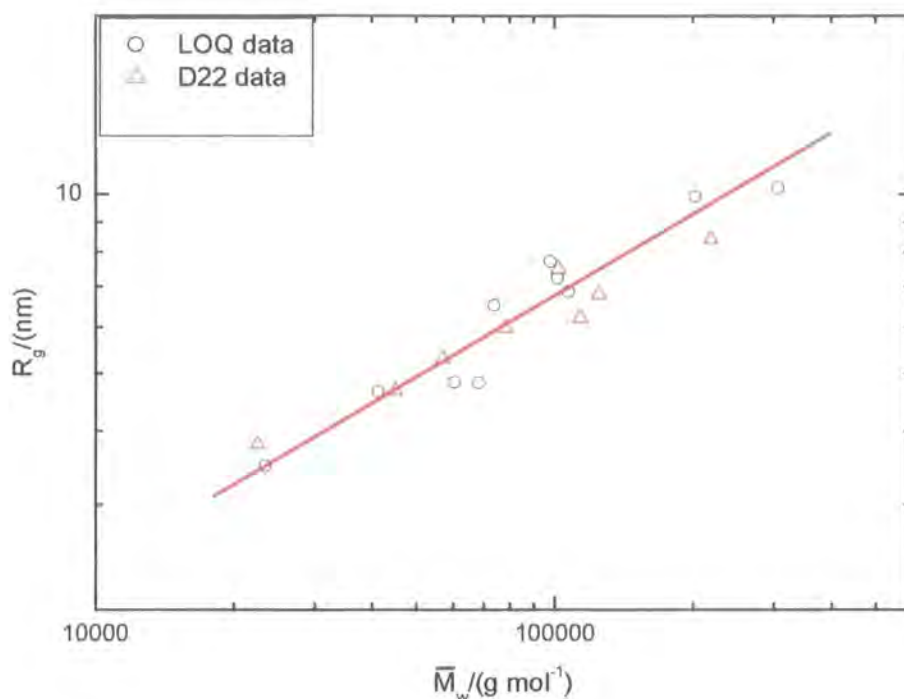


Figure 8(4.2). \bar{M}_w versus R_g : hyperbranched fractions.

The least squared linear regression gave in this case the relationship 15(4.2).

$$15(4.2) \quad R_g = (0.04 \pm 0.02) \bar{M}_w^{(0.44 \pm 0.05)} \text{ (nm)}$$

The exponent obtained is larger than that obtained with the Zimm plot but within experimental error. This difference is probably due to bigger errors (15%) in the calculation of the radii of gyration, propagated from the non-linear fit.

Kratky analysis

The plot of $[Q^2 (\Delta\Sigma/\Delta\Omega)]$ versus Q is known as a Kratky plot and the shape of the curve is characteristic of the type of polymer under investigation. The curves of the Kratky plot for Gaussian segment distribution asymptotically approach a plateau with increasing Q , but deviation from asymptotic behaviour arise from the local order of segments following a non-Gaussian distribution. The effect of branching is displayed more markedly in the Kratky plot⁵ because a maximum precedes the asymptotic region and is the most characteristic feature of branched polymers as mentioned in section 2.8. This maximum becomes more pronounced in star polymers, with increasing number of arms, f , and reaches a limit for star polymers with a very large number of rays and for AB_f polycondensates. In this case the mean square radius of gyration can be estimated from the position of the maximum in the Q^2 scale using equation 17(4.2).

$$17(4.2) \quad \langle s^2 \rangle = \frac{6}{Q_{\max}^2}$$

The typical shape of the Kratky plot for the form factor for the AB_f polycondensate (equation 10(4.2)) is shown in figure 9(4.2).

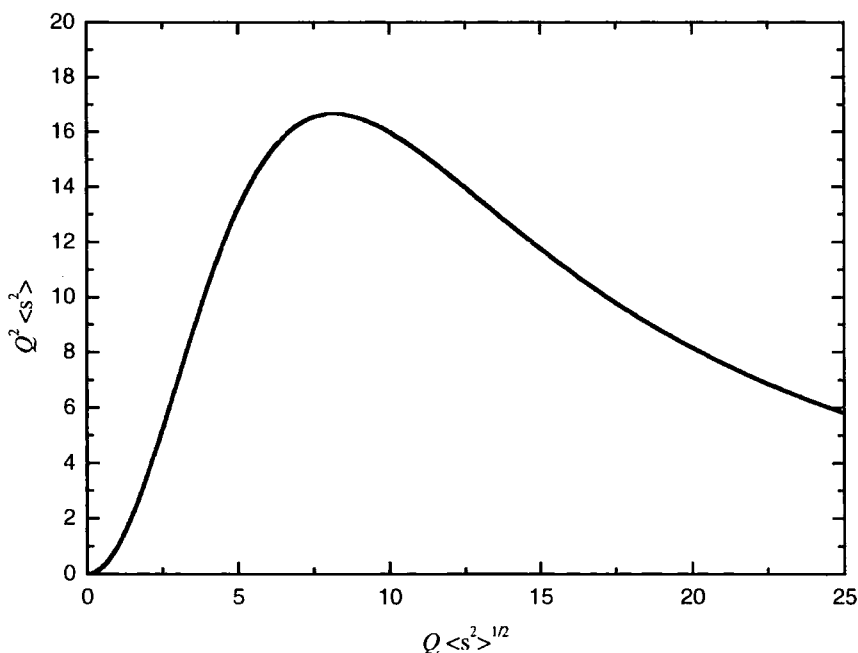


Figure 9(4.2). Kratky plot of the form factor for AB_f polycondensate.

The radii of gyration have been calculated using Kratky plot and the Burchard form factor, equation 17(4.2). As in the other analyses the R_g values obtained were extrapolated to zero concentration.

Kratky plots for different concentrations for one of the hyperbranched polyester fraction are shown in figure 10a(4.2) and the same plot for three different fractions in figure 10b(4.2). The exact value of Q_{\max} was obtained by numerical differentiation of the data plotted in this way. The details of all Kratky plot calculations can be found in Appendix SANS.

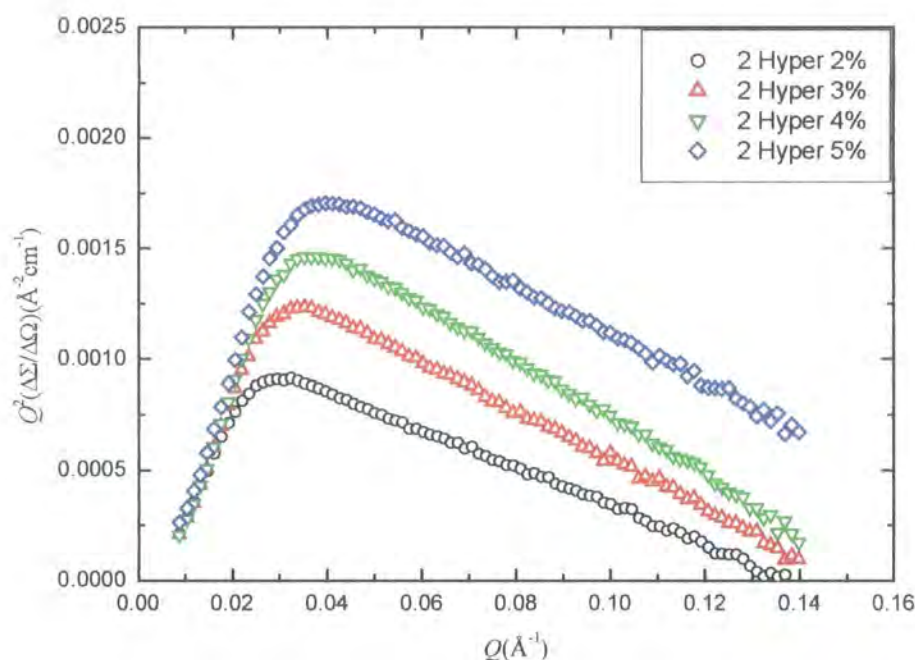


Figure 10a(4.2). Concentration dependence of Kratky curves; fraction 2.

There is evidently a shift of the maximum with the concentration that is attributed to the screening effect of the radius of gyration with increasing concentration. The shift of the maximum for different fractions merely reflects the change in size of the molecules with change in molecular weight.

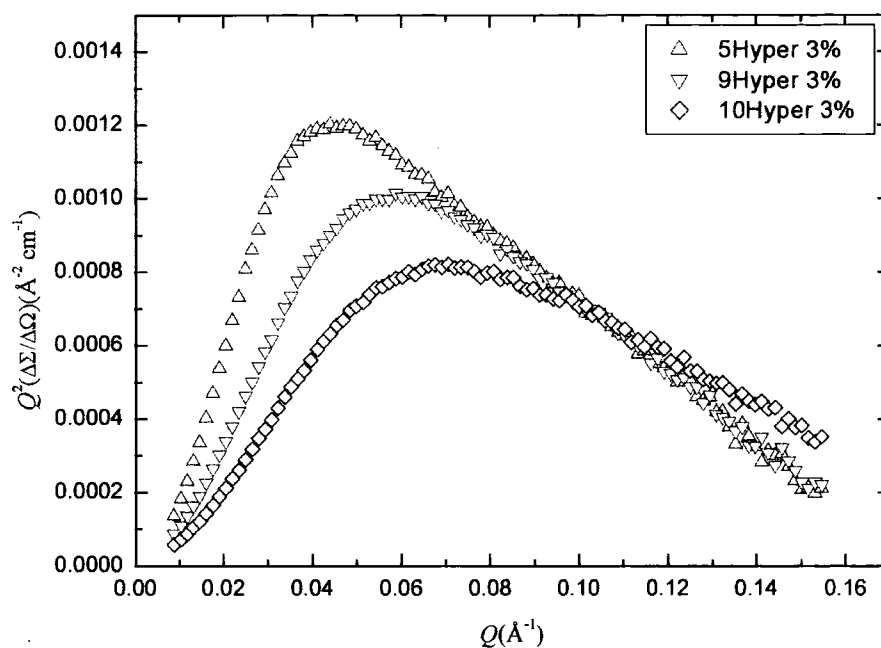


Figure 10(4.2). Q_{max} shift throughout the fractions.

The values of radii of gyration obtained are given in table 4a(4.2) and 4b(4.2).

Table 4a(4.2). R_g by the Kratky plot;

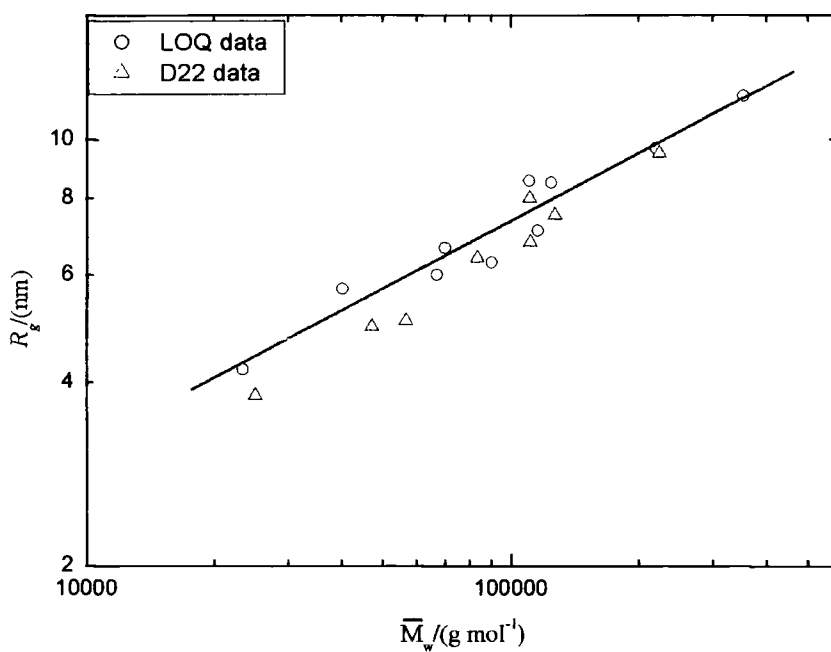
LOQ data.

Sample	R_g (nm)
1	10.6
2	9.6
3	8.4
4	8.5
5	7.0
6	6.6
7	6.2
8	6.0
9	5.7
10	4.6

Table 4a(4.2). R_g by the Kratky plot;*D22 data.*

Sample	R_g (nm)
2	9.5
3	7.5
4	8.0
5	6.7
6	6.3
8	5.0
9	4.9
10	3.8

Kratky plot analysis does not provide molecular weight; hence the molecular weights obtained by Zimm plot analysis have been used. The double log plot is shown in figure 11(4.2).

**Figure 11(4.1.1).** \bar{M}_w versus R_g ; hyperbranched fractions.

The molar mass dependence of the radius of gyration is given in the equation 18 (4.2).

$$18(4.2) \quad R_g = (0.1 \pm 0.05) \overline{M}_w^{(0.37 \pm 0.04)} \text{ (nm)}$$

The exponents found are in good agreement with the ones obtained by the Zimm plot and comparable with the form factor fitting results.

The a_{Rg} exponents from molecular weight dependence of R_g by the Zimm plot, form factor and Kratky plot method are comparable with each other and they will be discussed later in this section in comparison with results extracted from the intermediate Q -range.

Intermediate Q -range

The intermediate Q -range holds information about the shape of polymer particles in solution and the excluded volume effect. The double log plot of the scattering profile (Figure 12(4.2)) provides a means of establishing the various Q -dependencies of the scattering curve.

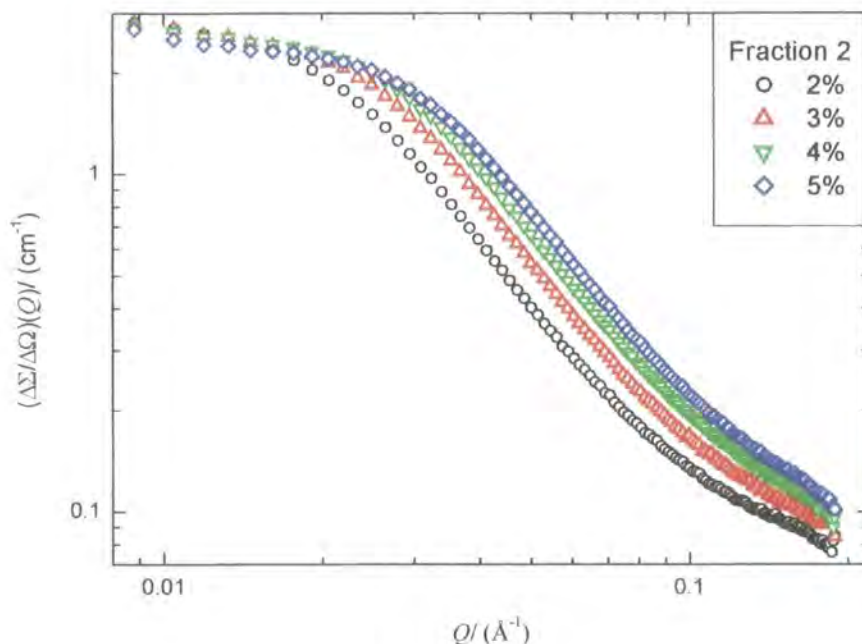


Figure 12(4.2). Double log plot for different concentrations of fraction 2.

Double log plots of each hyperbranched fraction at different concentrations were analysed by linear least squares fitting in the intermediate Q -range. Examples of linear fits are shown in figures 13a(4.2) and 13b(4.2). The better data statistics obtained by D22 provided fits with smaller uncertainties.

The details of all linear fit calculations can be found in Appendix SANS.

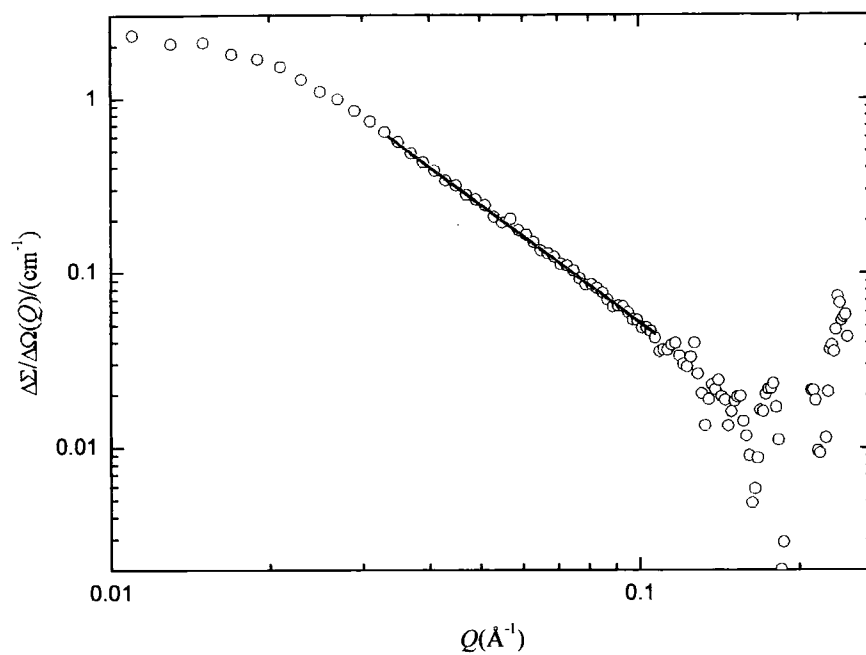


Figure 13a(4.1.4). Intermediate Q -range analysis; fraction 2, LOQ data.

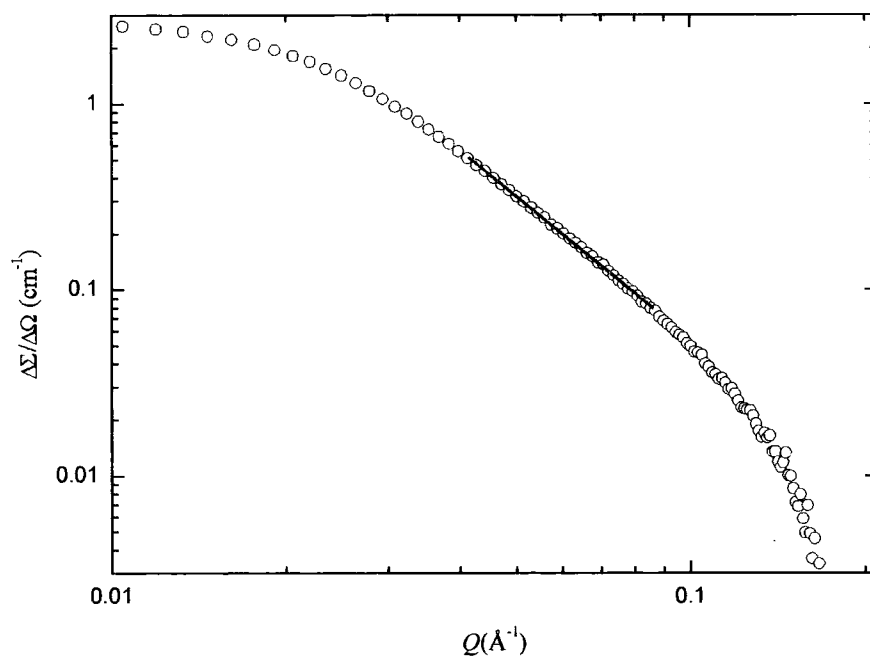


Figure 13b(4.1.4). Intermediate Q -range analysis; fraction 2, D22 data.

An average value of the slope was calculated for each fraction and given in table 5a(4.2) and 5b(4.2).

Table 5a(4.2). Slope for hyperbranched fractions;

LOQ data.

Sample	Slope
1	-2.52
2	-2.45
3	-2.50
4	-2.45
5	-2.57
6	-2.47
7	-2.52
8	-2.49
9	-2.46
10	-2.29

Table 5b(4.2). Slope for hyperbranched fractions;

D22 data.

Sample	Slope
2	-2.45
3	-2.45
4	-2.49
5	-2.45
6	-2.50
8	-2.49
9	-2.46
10	-2.45

Taking into account the all fractions an average slope of 2.4 ± 0.1 from the LOQ data and 2.5 ± 0.1 from the D22 data was obtained.

The intermediate Q-range is often also known as Porod regime and it is used to probe dimensional scale that are small compared to the size of the object, but large compared to the local atomic structure. Scattering curves are often similar in the Porod regime for widely different materials because the length scales are too long to depend on the specific chemical constituents and too short to depend on size or mass. In this region, geometric parameters related to the structure of the scattering particles can be measured and again a method similar to the fractal dimension analysis can be used for interpretation ⁶.

As described in section 4.1, fractal objects lack the rotational and translational symmetry characteristic of regular objects, but they show a particular type of symmetry called self-similarity that it is evident from the power-law relationships between the structural parameters. The reason for intimate relation between power laws and fractal objects is due to the lack of any integer power law for the length scale of fractals because self-similar objects look the same under all magnification.

Since power-law functions are intimately associated with self-similarity, the scattering profiles also obey a power-law.

$$19(4.2) \quad I \approx Q^{-x}$$

The results obtained from the analysis of the intermediate Q-range scattering cross sections of the hyperbranched fractions can be discussed within the assumption of the fractal dimension. The first issue of interest is the information about the surface of the particle. In addition to mass-fractal objects where the power law is of the type $M \approx R^{d_f}$ there are also certain rough surfaces that can be described in terms of fractal dimension in which the relationship is of type $S \approx R^{d_f^s}$ where d_f^s is surface fractal dimension and S is a surface. For ordinary compact objects, the surface area scales as the square of the radius so $d_f^s = 2$ and for objects with highly irregular surfaces area it is possible that the radius scales to a power larger than 2, so in general d_f^s is between 2 and 3. In the case of mass fractal clusters the surface area scales with the mass since the object is entirely surface and $d_f^s = d_f$. This requirement is reasonable since scattering is

produced from fluctuations and for a two-phase system, all fluctuations arise at the interface between the two phases; therefore the total scattered intensity is proportional to the surface area and so combining the equations, the general relationship obtained is:

$$20(4.2) \quad I \approx Q^{(d_f^s - 2d_f)}$$

For ordinary compact objects $d_f = 3$ therefore.

$$21(4.2) \quad I \approx Q^{(-6 + d_f^s)}$$

For a mass fractal object, $d_f^s = d_f$, so that equation 20(4.2) can be written as:

$$22(4.2) \quad I(Q) \approx Q^{-d_f}$$

If $d_f^s = 2$ and $I \sim Q^{-4}$, the exponent is characteristic of an object with a sharp smooth surfaces. If the surface is fractally rough, d_f^s lies between 2 and 3, while the signature of a compact object with a fractally rough surface is a power-law scattering profile with a slope between 3 and 4. The slope obtained by the intermediate Q -range analysis can be now understood in terms of a fractal dimension. The value of about 2.5 verifies equation 20(4.2) and from equation 22(4.2) it appears that the hyperbranched polymer is a mass fractal object with a rough surface. The exponents obtained by the double log plot of the radii of gyration and the molecular weight can also be interpreted in terms of the fractal dimension and compared with the exponents obtained by the analysis of the intermediate Q -range. The linearity of the double log plots do not cover a decade in Q as is generally recommended, but the good agreement with the exponent obtained by the molar mass dependence of the radius of gyration is encouraging for the interpretation of the data by the fractal analysis.

The average fractal dimension for the hyperbranched fractions calculated through the molar mass dependence of the radius of gyration was $d_f = 2.7 \pm 0.3$ from the Zimm plot, $d_f = 2.5 \pm 0.3$ from the form factor fitting and $d_f = 2.6 \pm 0.3$ from the Kratky plot. The values are in good agreement within error. Since the Zimm and Kratky analyses are based on approximations, the value found by the form factor fitting can be considered

more representative of the real geometry of the hyperbranched polymer and it is also in very good agreement with the power law verified by the equation 22(4.2).

In the percolation model a certain number of bonds are thrown on N sites of a finite three-dimensional lattice. Two bonds, which are nearest neighbours, are considered connected and by this procedure a cluster is defined as an ensemble of connected bonds where p is the ratio of the total number of bonds thrown on to N . At the threshold, characterised by p_c , a giant cluster will exist and its fractal dimension has been calculated equal to 2.5⁷.

Similar results were observed for glycogen and amylopectin⁸ where a fractal dimension of 2.3 and 2.8 was found respectively. In this polymeric systems a change in dimension was found almost exactly at overlap concentration, but the increase was less evident in the case of amylopectin than for glycogen probably because of the higher branching density of glycogen.

The fractal dimension obtained for the hyperbranched polyester in semi-dilute is typical of other hyperbranched systems and also agrees with the fractal dimension of the infinite cluster of percolation theory.

References

1. de Gennes, P., *Scaling Concepts in Polymer Physics*. 1979: Cornell University Press Ithaca NY.
2. Galinsky, G. and W. Burchard, *Macromolecules*, 1996. **29**: p. 1498-1506.
3. Thompson, A.B. and D.W. Woods, *Nature*, 1955. **176**: p. 78.
4. Strazielle, C. and H. Benoit, *Macromolecules*, 1975. **8**: p. 203-205.
5. Burchard, W., *Macromolecules*, 1977. **10**(5): p. 919-927.
6. Schaefer, D., *Mat. Res. Soc. Symp. Proc.* 1987. **79**: p. 47-58.
7. Adam, M., M. Delsanti, and D. Durand, *J. Phys.*, 1987. **48**: p. 1809.
8. Ioan, C.E., T. Aberle, and W. Burchard, *Macromolecules*, 1999. **32**: p. 8655-8662.

Chapter 5

Conclusions and Future work

A complete analysis of the solution properties of hyperbranched polyester fractions has been presented. The solution fractionation of the hyperbranched polymer based on poly dimethyl 5-(4 hydroxybutoxy) isophthalate was successfully carried out and from an initial polymer with an approximate polydispersity of 7, fractions with a polydispersity from 4.4 to 1.2 over a range of molecular weight from $5 \times 10^3 \text{ g mol}^{-1}$ to $4 \times 10^5 \text{ g mol}^{-1}$ have been obtained. This fractionation opens new possibilities in the hyperbranched polymer field because the major difference to their monodisperse analogues, i.e. dendrimers is removed facilitating better comparison of properties. A linear analogue of the hyperbranched polyester was also synthesised and samples of different molecular weight were obtained using a transesterification reaction. The degree of branching obtained by quantitative carbon NMR appears to be the same throughout the fractions and equals 0.5. The assignment of the NMR signals is based on reasonable assumptions for the mobility of the terminal, linear and branched sub-units in solution, but possibly a more detailed study of the mobility of the subunits in solution is needed.

The first part of the research dealt with the study of dilute solutions where physical parameters have been obtained using size exclusion chromatography, viscometry and light scattering techniques. The second part was strictly in the semi-dilute regime and was studied by small-angle neutron scattering. Dilute solution properties were investigated in chloroform and in THF solutions, while D-THF was the solvent for the semi-dilute regime.

For both solvents linear Mark-Houwink-Sakurada plots were obtained with exponents $a_{[\eta]}$ of 0.39 ± 0.05 and 0.36 ± 0.05 for chloroform and THF solutions respectively as commonly found for hyperbranched polymers. Huggins constants obtained for the hyperbranched polyester gave an average value of 0.35 ± 0.1 in chloroform and 1.2 ± 0.5 in THF. Assuming the same considerations as for linear polymers, the value of k_H suggest chloroform as a good solvent and THF a poor solvent. This hypothesis was confirmed by the second virial coefficients that were clearly positive for chloroform solutions and negative for THF solutions. The A_2 value in chloroform follows a typical

linear molar mass dependence with an exponent of 0.6 ± 0.1 as already found for other randomly branched systems like hyperbranched polycyanurate¹.

The linear polyester was insoluble in THF, but gave $a_{[\eta]}$ of about 0.5 in chloroform, suggesting θ conditions. Because of its poor solubility, the only reliable data were collected by SEC using chloroform as eluting solvent, where the extreme dilution of the solutions does not cause any precipitation or aggregation phenomenon. Although subject to large errors it was possible to obtain the unperturbed dimensions for this linear polyester and these were comparable with other linear polyesters².

By the use of the Mark-Houwink-Sakurada coefficients of the linear polyester in chloroform, the intrinsic viscosity for the linear analogues of the hyperbranched polymer fractions was calculated and the branching factor g' obtained. The application of the Zimm-Stockmayer³ formula for the theoretical branching factor for AB_2 polycondensate, and the use of the degree of branching obtained from NMR spectroscopy allowed a scaling law of the type $g' = \langle g_3(m) \rangle^{1/4}$ to be obtained and from the relationship between the two branching factors a value of 0.8 ± 0.1 for the cubed ratio of viscosity expansion factors was obtained.

Using considerations introduced by Zimm and Kilb⁴, a modified version of the Stockmayer-Fixman⁵ equation for highly branched polymer has been proposed and applied to the hyperbranched polyester viscosity data giving a value for the unperturbed radii. This new equation needs to be tested in other hyperbranched and branched systems.

The molar mass dependence of the radii of gyration showed similar exponents in both solvents, the radii of gyration in THF solution being slightly smaller than those in chloroform because of the screening effect due to the poorer polymer-solvent interaction. The molar mass dependence of the radii of gyration has also been interpreted by fractal dimension analysis. For the hyperbranched polyester the exponents obtained gave a fractal dimension $d_f = 2.5 \pm 0.3$ in chloroform and $d_f = 2.4 \pm 0.3$ in THF.

Burchard⁶ has found the same relationship in terms of fractal dimension for potato and waxy corn starch and Bauer, studying polycyanurates, found no difference between the fractal dimension in a good solvent ($d_f = 2.44$) and the calculated value ($d_f = 2.5$) for the non-swollen cluster. The fractal dimension found for the hyperbranched polyester can

be considered typical of a partially swollen spherical particle, but it is not clear, so far, what is the effect of the polymer-solvent interaction on the fractal geometry.

The exponents for the molar mass dependence of the hydrodynamic radius in chloroform and THF is 0.35 ± 0.05 , thus the hyperbranched polyester has the same hydrodynamic behaviour in the two solvents. It is not clear why the hydrodynamic radius has a different molar mass dependence of the radius of gyration, but it is a situation already found by Galinsky and Burchard⁶ for starch fractions and the effect of the polydispersity and the possibility that this type of macromolecule is able to change shape was proposed. Certainly branched molecules can be considered as sphere-like but the hydrodynamic properties cannot be directly compared with those of hard spheres since spheres have a smooth and well-defined surface, whereas highly branched macromolecules will more resemble spheres with a hairy surface.

The values of friction coefficients, k_s and k_o , obtained in chloroform and THF are comparable to the values that Roovers and Martin⁷ found for regular star polymers, but our data are somewhat scattered probably due to the effect of shape irregularity. Another parameter investigated for its sensitivity to the specific type of branching is the ratio of the radius of gyration to the hydrodynamic radius, ρ_b . This parameter is related to segment density in the macromolecule and for a self-similar structure should be independent of the molar mass. For both the solvents ρ_b is weakly dependent on the molar mass and the average values obtained are $\rho_b = 1.3 \pm 0.1$ in chloroform and $\rho_b = 1.21 \pm 0.07$ in THF, in good agreement with the theoretically predicted value of $\rho = 1.22$ for a hyperbranched structure⁸. The thermodynamic radius, R_T , was calculated and the ratio of the latter to the radius of gyration studied as a sensitive measure of branching. The hyperbranched fractions described here gave an average value of $R_T/R_g = 1.6 \pm 0.3$, in agreement with the theoretical value of 1.77 proposed for star polymer with a large number of arms⁷.

Generalised ratios, like the penetration function, have also been analysed as a function of the relative number of branched units, n_w , in the polymer fractions. The majority of the fractions showed an increase of the penetration function from 0.02 to 0.12 but the two fractions with the highest molecular weight are clearly not part of the trend with the others and do not agree with the expected asymptotic behaviour. This is due to the very low value of the second virial coefficient obtained for these fractions even in a good solvent like chloroform and also because the first two fractions have a larger

polydispersity than the other fractions. Another generalised ratio is $V_{A2\eta}$ (see section 4.1), which increase from 1.5 to about 3 for the first eight fractions but for the two highest molecular weight fractions the value decreases. It appears from the penetration and the $V_{A2\eta}$ functions that the high branching density of the hyperbranched systems decreases the sensitivity of these generalised ratios and that new theories to understand the excluded volume effect and take into account the peculiar behaviour of the branched systems are needed.

The overlap concentration, c^* , has been calculated to be about 3% w/v. Consequently the small-angle neutron scattering experiments were in the semi-dilute regime. The physical parameters characteristic of the polymer particles in this solution regime have been first analysed using Zimm plots. A few static light scattering experiments have been carried out in deuterated THF and the second virial coefficient compared with those for solutions in protonated THF. A more positive value of the second virial coefficient was obtained for the solution in deuterated solvent showing that the thermodynamic properties in deuterated solvent are different. A second method for obtaining molecular weight and radius of gyration was the fit of the scattering profiles with the specific form factor for AB_f polycondensates. A third method was the use of the Kratky plot to extract information about the polymer in solution.

The radii of gyration obtained in the semi-dilute regime are slightly smaller than those in the dilute solution because of the concentration screening effect. The molar mass dependence of these radii of gyration gave an average exponent of 0.39 ± 0.05 . The three different methods gave results in good agreement with each other within the experimental error and were discussed in comparison with the analysis of the intermediate Q -range. Since power-law functions are intimately associated with self-similarity, the scattering profiles of self-similar objects also obey a power-law. Taking into account all the fractions, an average slope of 2.4 ± 0.1 from the LOQ data and 2.5 ± 0.1 from the D22 data was obtained. The slope obtained by the intermediate Q -range analysis were in good agreement with the power law found for the molar mass dependence of the radius of gyration and the values suggest the hyperbranched polymer is a mass fractal object with a rough surface.

Although some of the theoretical approaches developed for linear polymer can also be used for highly branched polymers, there are no theories that explain completely the problem of the excluded volume effect in these densely branched systems. The chemical

structure of the hyperbranched and dendrimers is responsible for different behaviour in solution compared to their linear analogue, but this fact does not help in the definition of a fully comprehensive theory about highly branched polymers. The classical techniques such as static and dynamic light scattering and small-angle scattering are able to make evident the principal differences between the branched systems and their linear analogue, but the need for a regular hyperbranched model polymer that can be studied to establish formally the physical behaviour of highly branched and hyperbranched systems is crucial. Solution fractionation of hyperbranched systems as set out here is one step on this path but polydispersity has a strong influence on the properties and solution behaviour of this type of polymer and the possibility of synthesising hyperbranched polymer by anionic methods is greatly desirable. This model hyperbranched polymer should be designed in a way in which the amount of branching can be easily determined and a linear analogue that shows good solubility in common organic solvent should also be available.

With the contributions of much more experimental data, new theoretical effort will be stimulated to develop a comprehensive theory of the solution behaviour of hyperbranched systems.

To complete the picture of the configuration of hyperbranched polymers, the concentrated regime would be one of the next aims. This investigation can give information on the concentration screening effect and also about the possibility that these polymer particles can interpenetrate. Mixtures of deuterium labelled and hydrogenous polymers in concentrated solutions can be analysed by neutron scattering techniques and extended to the melt and solid state. Although polyesters in melt react by transesterification reaction, the low glass transition temperature of the hyperbranched polyesters permits the study of the melt state without a significant amount of side reactions.

Massa et al.⁹ investigated the miscibility and thermal behaviour of hyperbranched and linear polyesters blends and they found that in general the hyperbranched polyester is more miscible than its linear analogous.

Much has been reported on the interrelation between molecular morphology and properties of linear polymers, but similar reports for hyperbranched systems are sparse. The mechanical properties of the materials are known to be dependent on both the length-scale of the final morphology and the interfacial adhesion between phases and it is therefore important to understand the static and dynamic processes that control the

strength of the interface, as the morphology develops due to the application of stress in the case of hyperbranched polyesters blends with the linear analogue and other branched or hyperbranched polymers. A range of techniques, including rheology, small-angle light and neutron scattering and electronic microscopy can be used to study the structural evolution in these polymeric systems.

By full comprehension of the dimensions, shape and behaviour in solution, melt and solid state, a complete description of the configurational behaviour can be established.

References

1. Bauer, J. and W. Burchard, *Macromolecules*, 1993. **26**: p. 3103.
2. Brandrup, J., E.H. Immergut, and E.A. Grulke, *Polymer Handbook*. 1999: John Wiley & Sons, Inc.
3. Zimm, B.H. and W.H. Stockmayer, *J. Chem. Phys.*, 1949. **17**(12): p. 1301.
4. Zimm, B. and R. Kilb, *J. Polym. Sci.:Part B: Polym. Phys.* 1996. **34**: p. 1367.
5. Stockmayer, W. and M. Fixman, *J. Polym Sci. C*, 1963. **1**: p. 137.
6. Galinsky, G. and W. Burchard, *Macromolecules*, 1995. **28**: p. 2363.
7. Roovers, J. and J.E. Martin, *J. Polym Sci.: Part B: Polym. Phys.* 1989. **27**: p. 2513.
8. Burchard, W., *Adv. Polym. Sci.* 1999. **143**: p. 113.
9. Massa, D.J., et al., *Macromolecules*, 1995. **28**: p. 3214.

Glossary of symbols**General symbols**

f	functionality number
x_n	chain length
C_∞	characteristic ratio
l	bond length
X_N	degree of polymerisation
Db	degree of branching
c	concentration
c^*	overlap concentration
N_A	Avogadro's number
R	gas constant
G	Free energy
H	enthalpy
S	entropy
T_g	glass transition
T_c	onset crystallisation temperature
T_m	onset melting temperature
θ	theta temperature
p	hydrostatic pressure
K	absolute temperature
R_E	effective radius
$\langle r^2 \rangle$	mean end-to end distance
$\langle s^2 \rangle$	mean squared radius of gyration
R_g	radius of gyration
R_h	hydrodynamic radius
R_T	thermodynamic radius
R_η	viscosity radius
M_0	monomer molecular weight
M	molecular weight
\overline{M}_w	weight average molecular weight
\overline{M}_n	number average molecular weight

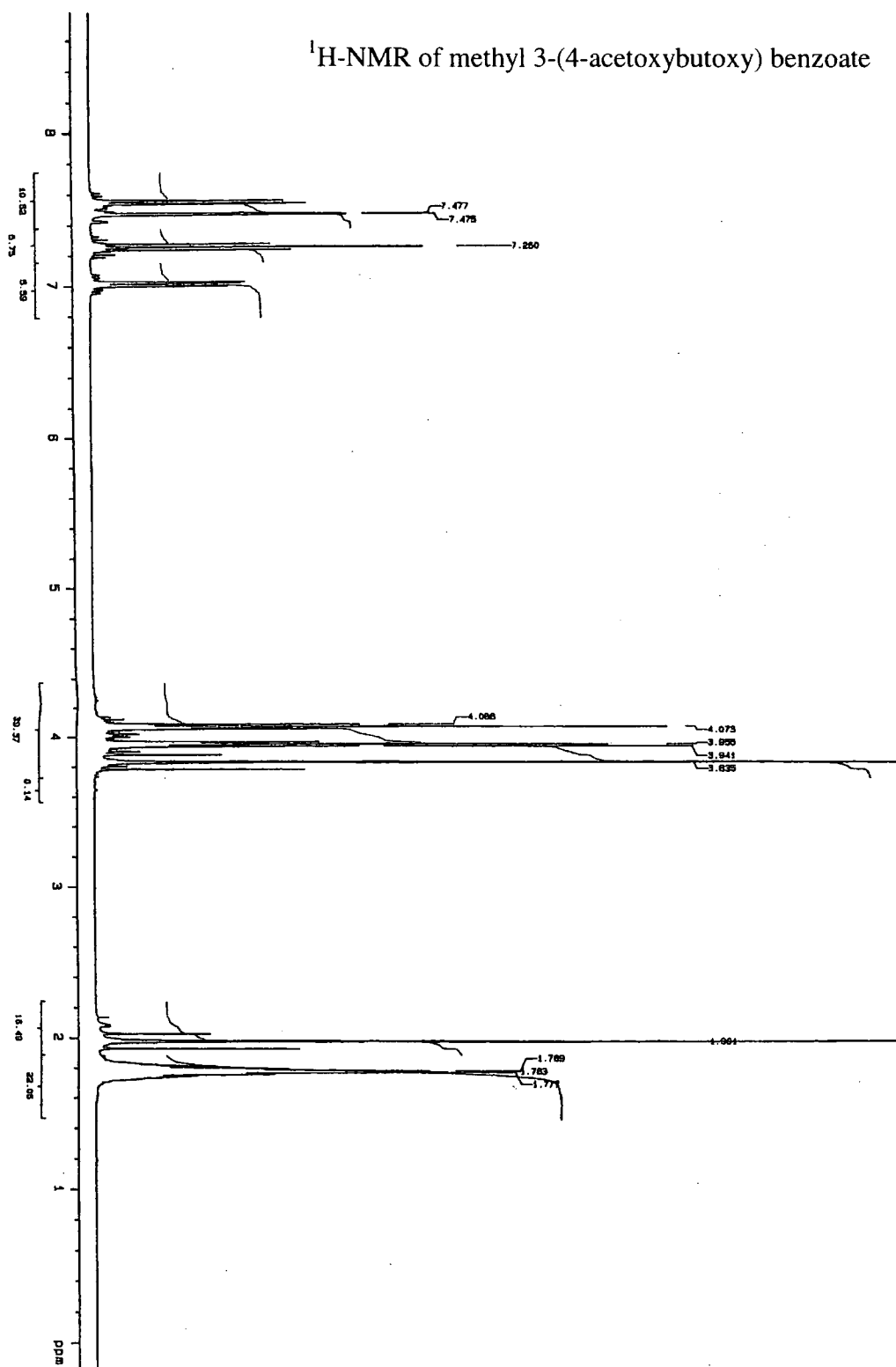
\overline{M}_z	z-average molecular weight
k	Boltzmann's constant
k_H	Huggins constant
k_D	concentration dependence slope of diffusion coefficient
k_s	friction coefficient
g'	viscosity branching factor
g	radius of gyration branching factor
Φ_0	viscosity universal constant
D_t	translational diffusion coefficient
A_2	second virial coefficient
$K_{[\eta]}$	Mark-Houwink constant
K_θ	ideal condition viscosity constant
K_{Rg}	radius of gyration molar mass dependence constant
K_{A2}	second virial coefficient molar mass dependence constant
K_D	diffusion coefficient molar mass dependence constant
a_{Rg}	radius of gyration molar mass dependence exponent
$a_{[\eta]}$	Mark-Houwink exponent
a_{A2}	second virial coefficient molar mass dependence exponent
n_w, m	average number of branched units
d_f	fractal dimension
d_{eff}	effective fractal dimension
d_f^s	surface fractal dimension
n	refractive index
I	scattering intensity
R_θ	Rayleigh ratio
$P(\theta)$	particle scattering factor
Q	scattering vector
Pd	polydispersity
$S(Q)$	interparticle structure factor
B_{inc}	incoherent background
$V_{A_2, \eta}$	generalised ratio for branched polymers

Greek letters

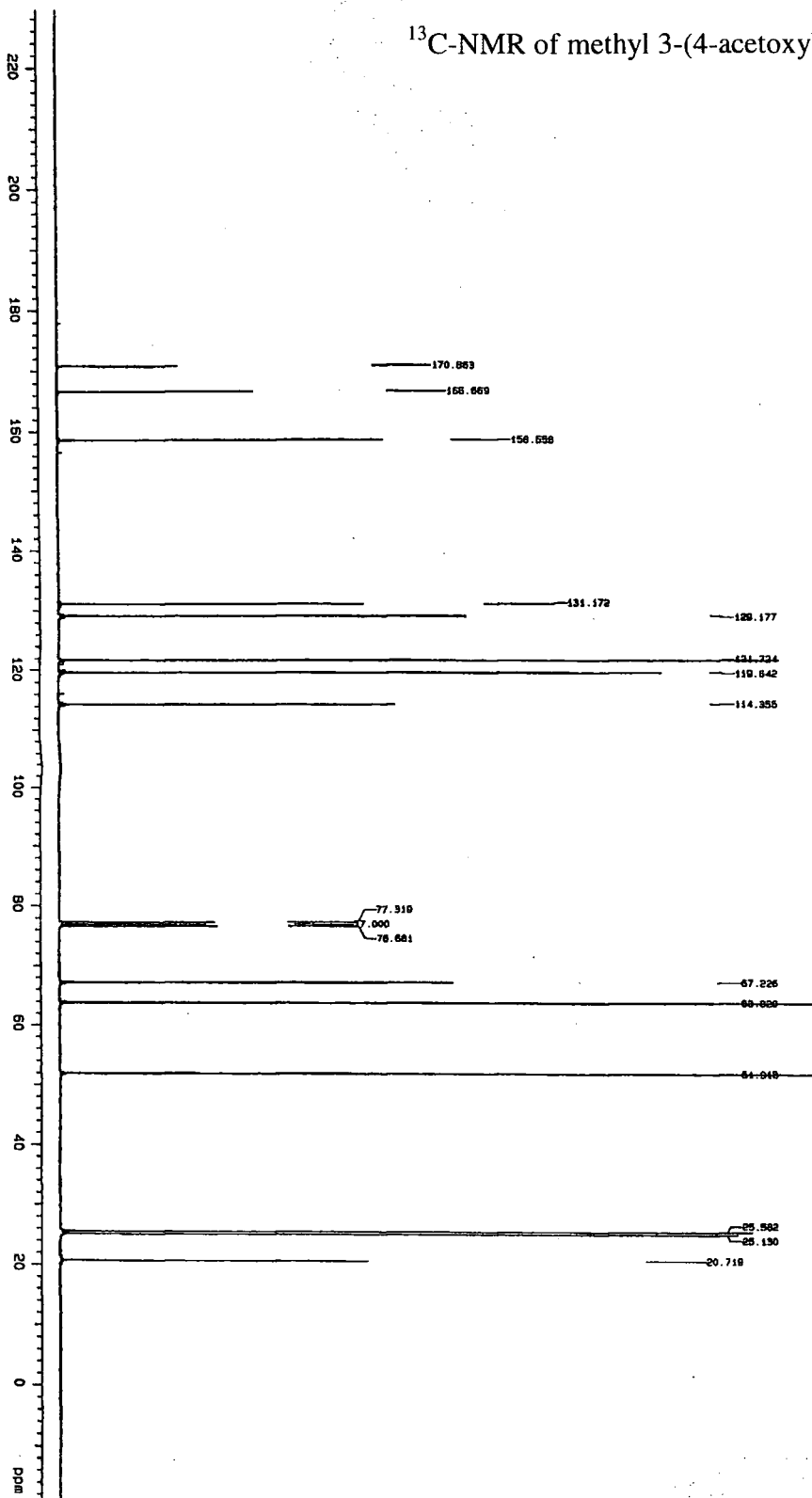
α	probability of reaction
α_η	viscosity expansion factor
α_s	radius of gyration expansion factor
α_p	polarizability
β	excluded volume coefficient
λ	wavelength
δ	density
ϕ	volume fraction
χ	interaction parameter
μ	chemical potential
μ_D	diffusion coefficient molar mass dependence exponent
v	specific volume
π	osmotic pressure
κ	enthalpy parameter
ψ	entropy parameter
η	viscosity
η_{sp}	specific viscosity
η_{rel}	relative viscosity
$(\Delta\rho)^2$	neutron scattering contrast
$\frac{\Delta\Sigma}{\Delta\Omega}$	scattering cross section
τ	polydispersity constant
ρ_b	ratio of radius of gyration and hydrodynamic radius
Ψ	interpenetration function

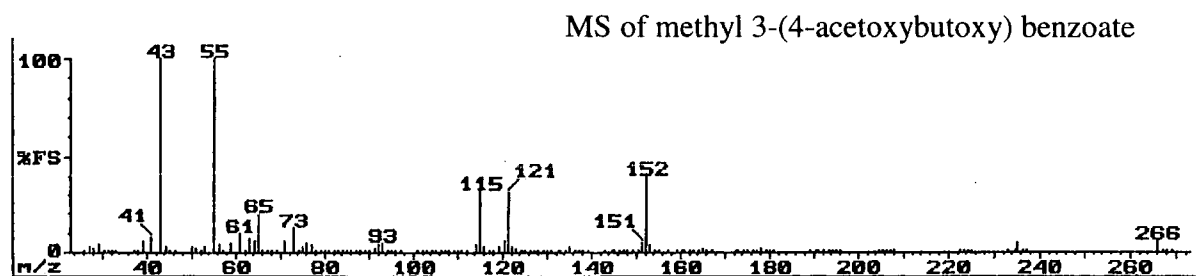
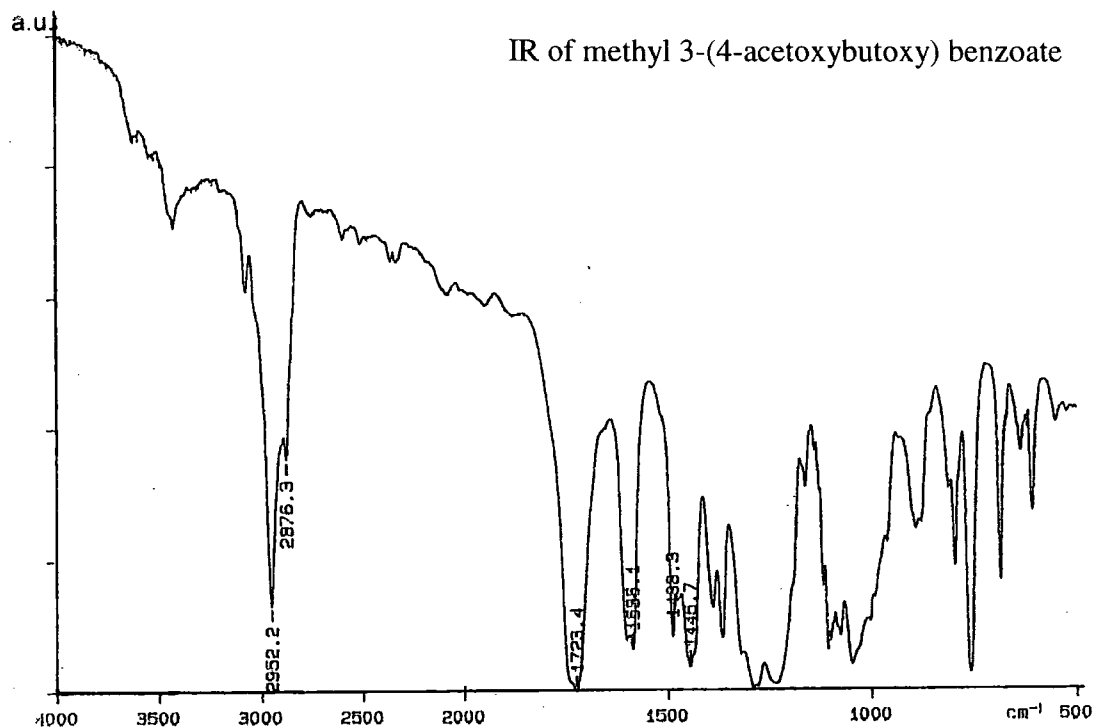
Appendices

Appendix A. NMR, IR, MS spectra for methyl 3-(4-acetoxybutoxy) benzoate



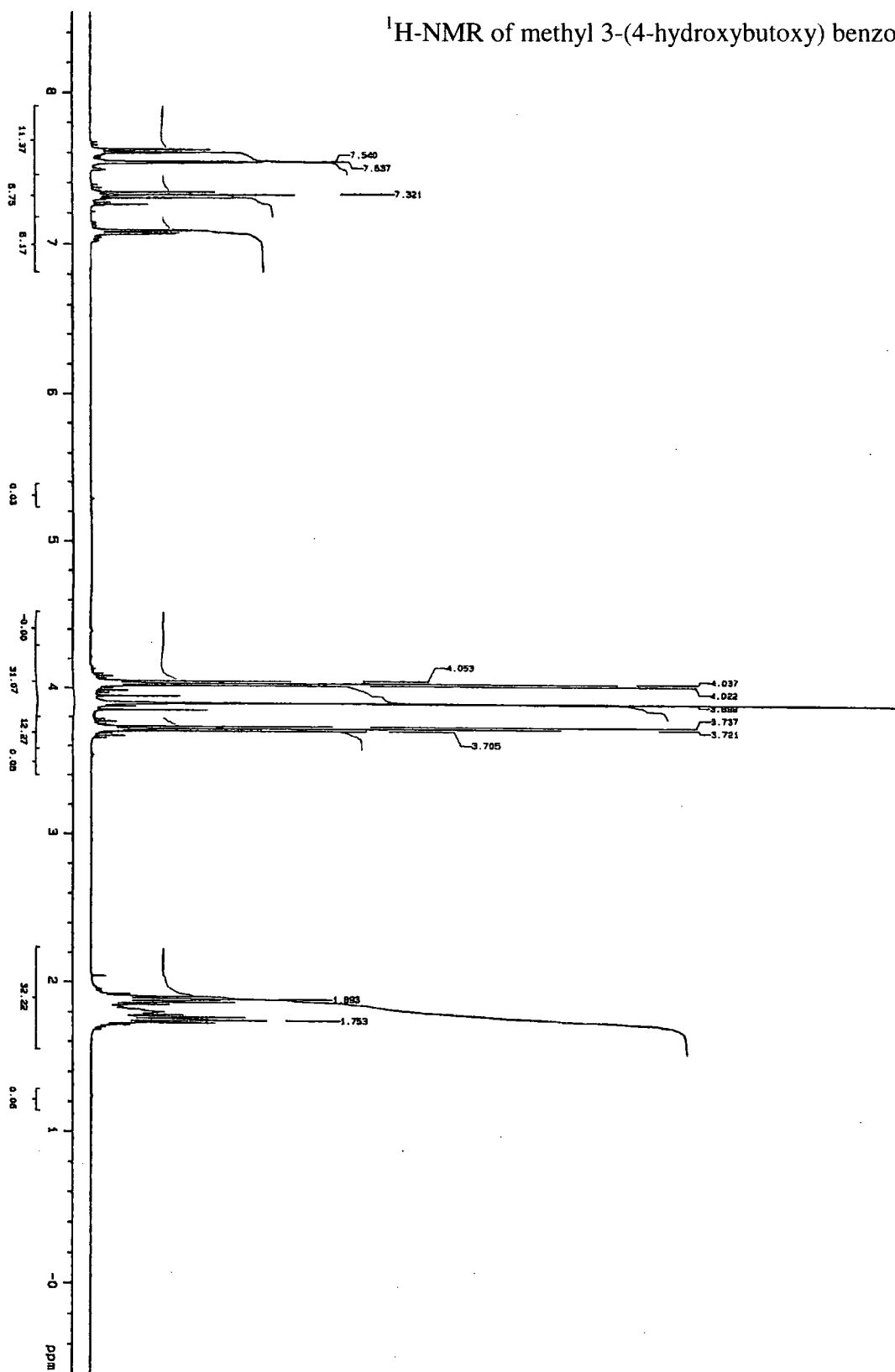
¹³C-NMR of methyl 3-(4-acetoxybutoxy) benzoate

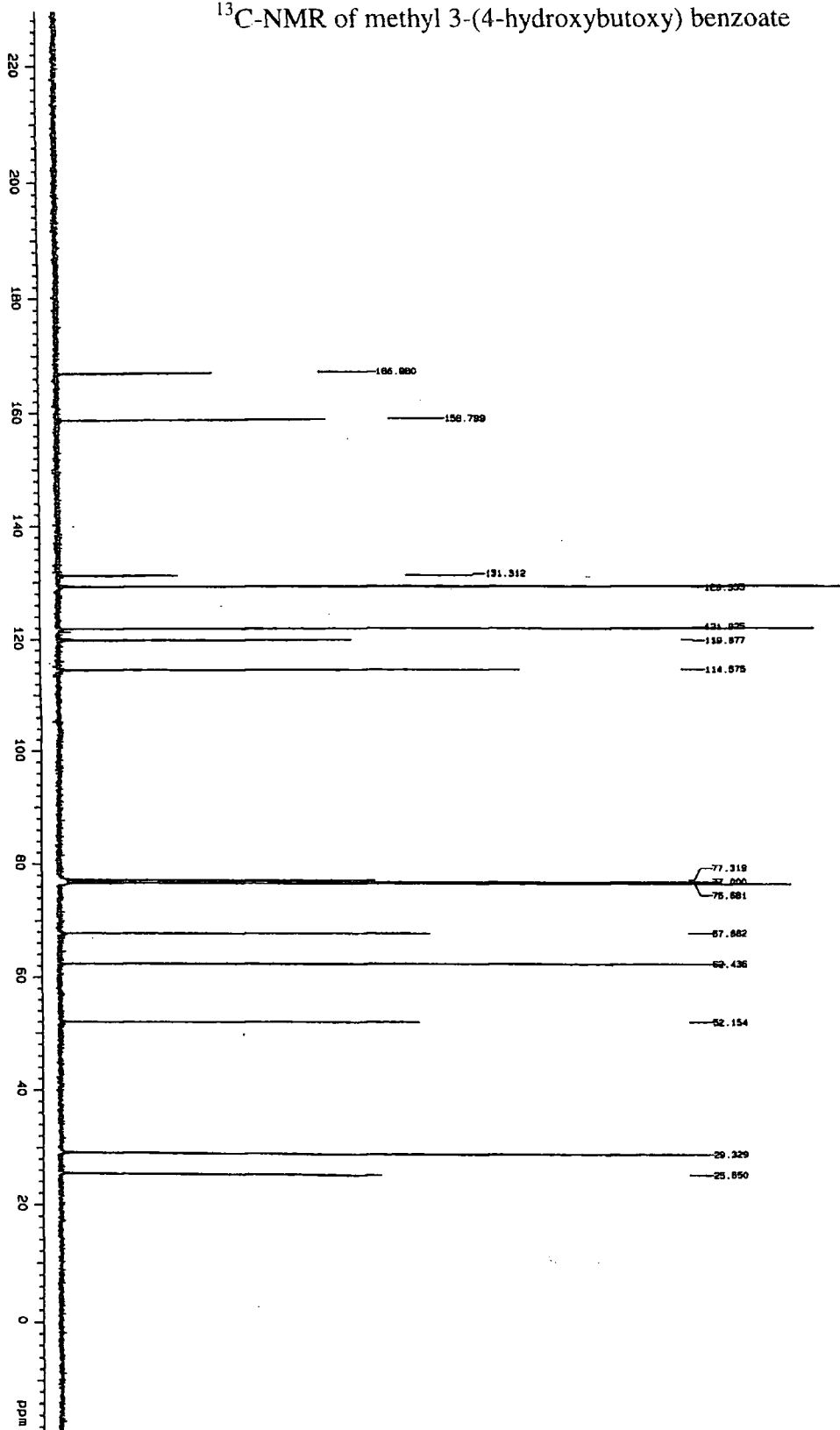


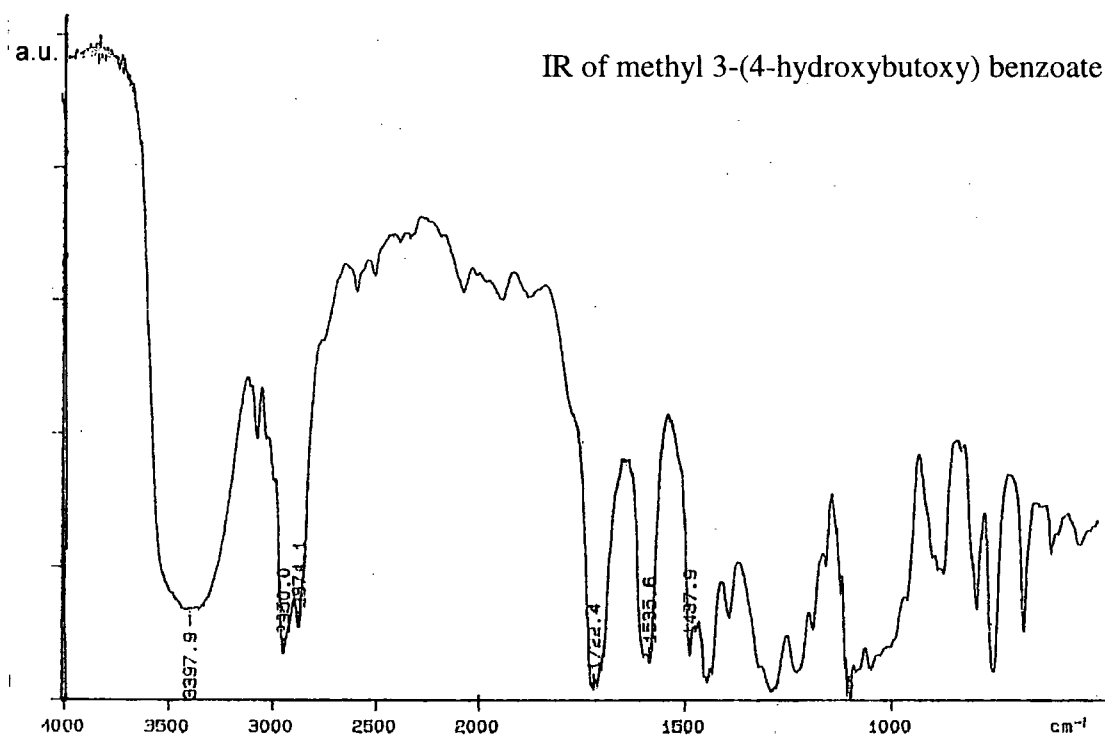


Appendix B. NMR, IR, MS spectra for methyl 3-(4-hydroxybutoxy) benzoate

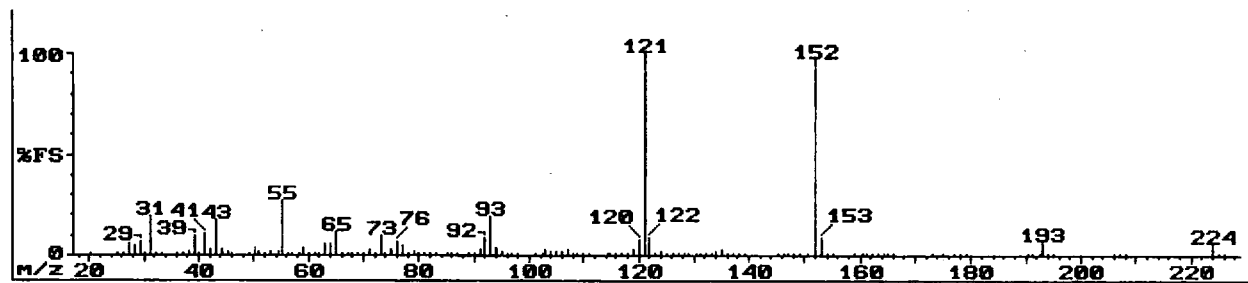
¹H-NMR of methyl 3-(4-hydroxybutoxy) benzoate



^{13}C -NMR of methyl 3-(4-hydroxybutoxy) benzoate



MS of methyl 3-(4-hydroxybutoxy) benzoate



Appendix C. Dynamic light scattering data

Cumulant analysis data; hyperbranched fractions in chloroform.

Sample	c (g l ⁻¹)	K_1	D_c (cm ² s ⁻¹)
Fraction 1	0.799	8170	2.00E-07
	0.999	9165	2.24E-07
	2.999	8836	2.16E-07
Fraction 2	0.796	12601	3.08E-07
	0.996	13600	3.32E-07
	1.992	13828	3.38E-07
	3.984	14058	3.44E-07
Fraction 3	0.993	16590	4.05E-07
	1.986	17065	4.17E-07
	2.979	17484	4.53E-07
	3.973	18271	4.89E-07
Fraction 4	0.999	18470	4.51E-07
	1.999	18638	4.56E-07
	2.998	19693	4.81E-07
	3.998	20550	5.35E-07
Fraction 5	1.999	20481	5.01E-07
	2.999	21683	5.30E-07
	3.999	22404	5.48E-07
	4.999	22821	5.58E-07
Fraction 6	4.004	21545	5.27E-07
	5.005	23945	5.85E-07
	6.006	24050	5.88E-07
	7.007	23974	5.86E-07
Fraction 7	1.943	21857	5.34E-07
	4.856	29015	7.09E-07
	5.828	29468	7.20E-07
Fraction 8	3.023	25136	6.14E-07
	4.031	26583	6.50E-07
	6.046	28182	6.89E-07
Fraction 9	4.022	30806	8.58E-07
	8.043	35851	8.76E-07
	10.054	38644	9.12E-07
Fraction 10	4.015	43986	1.12E-06
	6.023	49816	1.22E-06

	10.038	59862	1.46E-06
--	--------	-------	----------

Cumulant analysis data; hyperbranched fractions in THF.

Sample	c (g l ⁻¹)	K_1	D_c (cm ² s ⁻¹)
Fraction 1	0.396	13752	3.51E-07
	0.595	13391	3.42E-07
	0.793	13645	3.49E-07
	0.992	13266	3.39E-07
Fraction 2	0.402	17239	4.40E-07
	0.603	16888	4.31E-07
	0.805	16724	4.27E-07
	1.006	16541	4.23E-07
Fraction 3	0.505	22941	5.86E-07
	0.792	22693	5.80E-07
	0.991	22422	5.73E-07
	1.189	23185	5.92E-07
Fraction 4	0.619	17418	4.45E-07
	0.786	17379	4.44E-07
	1.054	17250	4.41E-07
	1.221	16323	4.17E-07
Fraction 5	1.597	27165	6.94E-07
	1.996	26272	6.71E-07
	2.395	26180	6.69E-07
Fraction 6	0.585	27183	6.94E-07
	0.790	26790	6.84E-07
	0.996	26805	6.85E-07
	1.391	26838	6.86E-07
Fraction 8	0.806	28010	7.16E-07
	1.008	27787	7.10E-07
	1.209	27736	7.09E-07
	1.411	27405	7.00E-07
Fraction 9	3.999	35459	9.06E-07
	4.999	35414	9.05E-07
	5.952	35222	9.00E-07
Fraction 10	4.018	46143	1.18E-06
	5.023	45919	1.17E-06
	7.032	45340	1.16E-06

Cumulant analysis data; linear fractions in chloroform.

Sample	c (g l ⁻¹)	K_1	D_c (cm ² s ⁻¹)
Linear 1	1.971	9991	2.4E-07
	3.943	8861	2.2E-07
	4.929	6182	1.5E-07
	6.860	5587	1.4E-07
Linear 2	3.047	18051	4.4E-07
	4.064	16491	4.0E-07
	5.004	14756	3.6E-07
	7.005	13958	3.4E-07
Linear 3	7.002	16091	3.9E-07
	8.002	15803	3.9E-07
	10.003	15423	3.8E-07
Linear 4	7.067	23496	5.7E-07
	8.076	22497	5.5E-07
	10.096	17132	4.2E-07

Appendix SANS

Zimm plot results; data collected by LOQ

Sample	$c(\text{g ml}^{-1})$	$\overline{M}_w (\text{g mol}^{-1})$	$R_g(\text{nm})$
Hyper1	0.02018	260500	12.53
	0.03027	115400	7.01
	0.04036	88040	6.77
	0.05044	58040	4.07
Hyper2	0.01955	165600	10.05
	0.02933	68970	5.06
	0.03911	61610	4.38
	0.04888	39040	2.51
Hyper3	0.02009	92500	9.59
	0.03013	54140	4.37
	0.04018	39720	3.55
	0.05022	30310	2.01
Hyper4	0.01976	75410	8.65
	0.02964	55240	2.18
	0.03952	39630	2.46
	0.04939	41060	5.10
Hyper5	0.01964	108900	8.72
	0.02946	69220	6.17
	0.03929	48050	5.04
	0.04911	37160	5.01
Hyper6	0.01990	39600	6.12
	0.02980	43180	2.62
	0.03482	32930	4.76
	0.03980	33640	3.37
Hyper7	0.01986	60870	5.36
	0.02979	46390	4.44
	0.03972	31640	4.74
Hyper8	0.01995	48110	4.64
	0.02992	32640	4.99
	0.03990	27420	4.56
	0.04987	20920	3.83
Hyper9	0.01986	29480	3.50
	0.02978	27120	3.90
	0.03475	22560	3.50
	0.03980	19650	2.48

Hyper10	0.02012	19480	4.54
	0.03019	20630	3.09
	0.03522	16290	2.82
	0.04350	16950	4.35

Zimm plot results; data collected by D22

Sample	$c(\text{g ml}^{-1})$	$\overline{M}_w (\text{g mol}^{-1})$	$R_g(\text{nm})$
Hyper 2	0.02034	146800	7.00
	0.03052	89840	5.14
	0.04069	64200	4.26
	0.05086	48190	3.86
Hyper 3	0.02034	88750	5.65
	0.03052	63580	4.67
	0.04069	48460	3.95
	0.05086	37240	3.8
Hyper 4	0.0197	79830	6.55
	0.02956	68870	5.03
	0.03941	49940	4.05
	0.04926	40760	3.99
Hyper 4b	0.02004	108200	6.32
	0.03006	75650	5.47
	0.04008	55640	4.35
	0.0501	42150	3.10
Hyper 5	0.0197	83120	5.12
	0.02956	59060	4.17
	0.03941	42720	3.45
	0.04926	34670	3.35
Hyper 6	0.0202	60890	4.95
	0.0303	55050	5.08
	0.0404	38300	4.01
	0.0505	30800	4.01
Hyper 8	0.0202	55560	5.18
	0.0303	41820	4.50
	0.0404	34620	4.24
	0.0505	29050	4.11

Hyper 9	0.01977	47630	5.10
	0.02965	37520	4.97
	0.03954	32120	5.03
	0.04942	28340	5.31
Hyper10	0.02026	36330	5.52
	0.03038	24680	5.42
	0.04051	25660	5.55
	0.05064	24620	6.45

Form factor calculation results; data collected by LOQ

Sample	$c(\text{g ml}^{-1})$	$R_g(\text{nm})$	A	$\overline{M}_w(\text{g mol}^{-1})$
Hyper 1	0.02017	8.92	4.41	202221
	0.03026	6.49	3.64	111273
	0.04035	6.44	3.77	86435
	0.05044	5.74	3.9	71532
Hyper 2	0.01955	7.85	2.95	139583
	0.02933	6.27	2.60	82015
	0.03910	5.48	2.95	69793
	0.04888	4.35	2.39	45235
Hyper 3	0.02008	7.24	1.63	75075
	0.03013	5.09	1.97	60490
	0.04017	4.77	1.94	44677
	0.05022	3.74	1.89	34820
Hyper 4	0.01975	7.17	1.45	67904
	0.02963	4.30	2.04	63688
	0.03951	4.71	1.98	46361
	0.04939	4.66	2.12	39711
Hyper 5	0.01964	5.98	1.69	79602
	0.02946	4.73	1.82	57151
	0.03928	4.38	1.89	44511
	0.04910	4.14	1.73	32594
Hyper 6	0.01989	5.60	0.82	38130
	0.02984	3.64	1.48	45880
	0.03480	4.88	1.22	32417
	0.03979	4.05	1.53	35572
Hyper 7	0.01985	4.74	1.24	57771
	0.02978	3.74	1.30	40378
	0.03971	4.39	1.33	30982
Hyper 8	0.01994	4.32	1.02	47309
	0.02992	4.33	0.98	30302
	0.03989	4.33	1.19	27596
	0.04987	3.68	1.11	20593
Hyper 9	0.01985	4.02	0.67	31221
	0.02978	3.64	0.84	26095
	0.03474	3.68	0.84	22368
	0.03979	3.30	0.92	21390

Hyper 10	0.02012	3.29	0.4	18390
	0.03018	3.14	0.65	19923
	0.03521	3.00	0.63	16551
	0.04024	3.10	0.63	14482

Form factor calculation results; data collected by D22

Sample	$c(\text{g ml}^{-1})$	$R_g(\text{nm})$	A	$\overline{M}_w(\text{g mol}^{-1})$
Hyper 2	0.02034	7.06	3.19	145077
	0.03051	5.88	3.05	92474
	0.04068	5.24	2.94	66854
	0.05086	4.69	2.73	49663
Hyper 3	0.02004	5.84	1.90	87767
	0.03006	5.06	2.07	63897
	0.04008	4.51	2.13	49170
	0.05010	4.17	2.02	37304
Hyper 4	0.01970	6.34	1.61	75881
	0.02955	5.24	2.15	67554
	0.03940	4.53	2.12	49797
	0.04926	4.30	2.14	40288
Hyper 4b	0.01984	6.44	2.30	107258
	0.02976	5.92	2.46	76480
	0.03968	5.19	2.47	57593
	0.04960	4.30	2.38	44396
Hyper 5	0.02046	5.34	1.72	78081
	0.03069	4.66	1.88	56666
	0.04092	4.11	1.83	41369
	0.05116	3.85	1.84	33276
Hyper 6	0.02020	5.11	1.26	57941
	0.03030	4.70	1.67	51238
	0.04040	4.11	1.61	36871
	0.05050	3.85	1.65	30285
Hyper 8	0.01976	4.71	1.08	50780
	0.02965	4.26	1.25	39128
	0.03953	3.91	1.38	32412
	0.04942	3.64	1.44	26997

Hyper 9	0.01995	4.21	0.87	40483
	0.02992	3.87	1.03	31904
	0.03990	3.60	1.16	26896
	0.04988	3.44	1.24	23001
Hyper 10	0.02025	3.70	0.61	27863
	0.03038	3.45	0.62	19093
	0.04051	3.34	0.96	21925
	0.05064	3.34	0.96	17540

Kratky plot calculation results; data collected by LOQ

Sample	$c(\text{g ml}^{-1})$	Q_{max}	$R_g(\text{nm})$
Hyper 1	0.02017	0.026	9.42
	0.03026	0.034	7.20
	0.04035	0.034	7.20
	0.05044	0.038	6.45
Hyper 2	0.01955	0.030	8.16
	0.02933	0.034	7.20
	0.03910	0.035	7.00
	0.04888	0.043	5.70
Hyper 3	0.02008	0.033	7.42
	0.03013	0.037	6.62
	0.04017	0.039	6.28
	0.05022	0.053	4.62
Hyper 4	0.01975	0.033	7.42
	0.02963	0.044	5.57
	0.03951	0.048	5.10
	0.04939	0.050	4.90
Hyper 5	0.01964	0.038	6.45
	0.02946	0.042	5.83
	0.03928	0.046	5.32
	0.04910	0.046	5.32
Hyper 6	0.01989	0.040	6.12
	0.02984	0.049	5.00
	0.03482	0.042	5.83
	0.03979	0.047	5.21
Hyper 7	0.01985	0.042	5.83
	0.02978	0.045	5.44
	0.03971	0.046	5.32
Hyper 8	0.01994	0.046	5.32
	0.02992	0.046	5.32
	0.03989	0.050	4.90
	0.04987	0.054	4.54
Hyper 9	0.01985	0.049	5.00
	0.02978	0.057	4.30
	0.03474	0.058	4.22
	0.03979	0.059	4.15

Hyper 10	0.02012	0.060	4.08
	0.03018	0.067	3.66
	0.03521	0.068	3.60
	0.04024	0.071	3.45

Kratky plot calculation results; data collected by D22

Sample	$c(\text{g ml}^{-1})$	Q_{max}	$R_g(\text{nm})$
Hyper 2	0.02034	0.02946	8.31
	0.03051	0.03389	7.23
	0.04068	0.03682	6.65
	0.05086	0.03976	6.16
Hyper 3	0.02004	0.03682	6.65
	0.03006	0.04124	5.94
	0.04008	0.04566	5.36
	0.05010	0.04715	5.20
Hyper 4	0.01970	0.03535	6.93
	0.02955	0.04124	5.94
	0.03940	0.04715	5.20
	0.04926	0.04862	5.04
Hyper 4b	0.01984	0.03389	7.23
	0.02976	0.03682	6.65
	0.03968	0.04566	5.36
	0.04960	0.04566	5.36
Hyper 5	0.02046	0.03976	6.16
	0.03069	0.04566	5.36
	0.04092	0.04715	5.20
	0.05116	0.05006	4.89
Hyper 6	0.02020	0.04271	5.74
	0.03030	0.04715	5.20
	0.04040	0.05006	4.89
	0.05050	0.05303	4.62
Hyper 8	0.01976	0.05448	4.50
	0.02965	0.05303	4.62
	0.03953	0.06184	3.96
	0.04942	0.06184	3.96

Hyper 9	0.01995	0.05448	4.50
	0.02992	0.05890	4.16
	0.03990	0.06477	3.78
	0.04988	0.06477	3.78
Hyper 10	0.02025	0.06770	3.62
	0.03038	0.06770	3.62
	0.04051	0.07068	3.47
	0.05064	0.07213	3.40

Intermediate Q range analysis results; data collected by LOQ

Sample	c(g ml ⁻¹)	Slope
Hyper 1	0.02017	-2.56
	0.03026	-2.53
	0.04035	-2.51
	0.05044	-2.49
Hyper 2	0.01955	-2.57
	0.02933	-2.53
	0.03910	-2.42
	0.04888	-2.28
Hyper 3	0.02008	-2.47
	0.03013	-2.49
	0.04017	-2.49
	0.05022	-2.56
Hyper 4	0.01975	-2.51
	0.02963	-2.43
	0.03951	-2.43
	0.04939	-2.41
Hyper 5	0.01964	-2.67
	0.02946	-2.57
	0.03928	-2.58
	0.04910	-2.44
Hyper 6	0.01989	-2.61
	0.02984	-2.32
	0.03482	-2.54
	0.03979	-2.39
Hyper 7	0.01985	-2.45
	0.02978	-2.54
	0.03971	-2.57
Hyper 8	0.01994	-2.58
	0.02992	-2.49
	0.03989	-2.48
	0.04987	-2.42
Hyper 9	0.01985	-2.58
	0.02978	-2.53
	0.03474	-2.44
	0.03979	-2.28

Hyper 10	0.02012	-2.41
	0.03018	-2.32
	0.03521	-2.23
	0.04024	-2.20

Intermediate Q range analysis results; data collected by D22

Sample	$c(\text{g ml}^{-1})$	Slope
Hyper 2	0.02034	-2.53
	0.03051	-2.50
	0.04068	-2.40
	0.05086	-2.43
Hyper 3	0.02004	-2.51
	0.03006	-2.51
	0.04008	-2.38
	0.05010	-2.38
Hyper 4	0.01970	-2.57
	0.02955	-2.53
	0.03940	-2.42
	0.04926	-2.42
Hyper 5	0.02046	-2.46
	0.03069	-2.48
	0.04092	-2.49
	0.05116	-2.38
Hyper 6	0.02020	-2.52
	0.03030	-2.64
	0.04040	-2.45
	0.05050	-2.37
Hyper 8	0.01976	-2.46
	0.02965	-2.54
	0.03953	-2.57
	0.04942	-2.40
Hyper 9	0.01995	-2.51
	0.02992	-2.45
	0.03990	-2.45
	0.04988	-2.44

Hyper 10	0.02025	-2.48
	0.03038	-2.47
	0.04051	-2.50
	0.05064	-2.35

Attached CD

The CD contains, in two folders named RALdata and ILLdata, the raw data collected by the LOQ and D22 spectrometers respectively.

The data have been normalised and background subtracted following the specific procedures required for the two instruments.

The different samples are identified by the filename "XhypY" where the two numbers X and Y define the fraction number and the concentration in percentage respectively. This concentration can be transformed in g l^{-1} by comparison with the previous tables.

Example:

2hyp3 \equiv fraction 2, 3% w/v (0.03051 g l^{-1}).

